약학박사학위논문

인간 세포질 aminoacyl-tRNA synthetases의 동적인 상호작용과 효소 활성에 대한 분석법 개발

Assay development for dynamic interactions and catalytic activities of human cytosolic aminoacyl-tRNA synthetases

2020년 8월

서울대학교 대학원

약학과 의약생명과학전공

공 지 원

Abstract

To the best of our knowledge, protein synthesis (translation) is a universal process, which resides in all extant lifeforms. An aminoacyl-tRNA synthetase (ARS) takes a role in the very first step of the translation process; it catalyzes esterification (aminoacylation) of a specific amino acid on its cognate transfer RNAs (tRNAs) to make aminoacylated tRNAs (aminoacyl-tRNAs). The aminoacyl-tRNA delivers the amino acid to the ribosome which catalyzes the translation of a messenger RNA (mRNA) into a polypeptide chain.

The cytoplasmic ARSs are differentially regulated in different species; they have gained additional domains and noncanonical functions throughout evolution, and the largest multi-tRNA synthetase complex (MSC) among the eukaryotes exists in higher eukaryotes, which is comprised of eight ARSs for eight or nine amino acids. Among them, the mammalian MSC is the most complexed one, which is composed of eight cytoplasmic ARSs for nine amino acids, and three scaffold proteins. Consequently, nearly half of the aminoacyl-tRNA efflux becomes concentrated at the MSC. Stable supply of the aminoacyl-tRNA to the ribosome is, therefore, considered to be a major role of the mammalian MSC. Furthermore, the mammalian

MSC also serves as a reservoir for releasable ARSs or scaffold proteins to support the noncanonical functions of them. In part I, a split-luciferase complementation system was applied to investigate the configuration of the MSC in live mammalian cells. Multiplex interconnections between the components of the MSC were simplified into binary protein-protein interactions, and pairwise comparison of the interactions reconstituted a framework that is consistent with previous *in vitro* studies. Reversibility of the split-luciferase reporter binding demonstrated convertible organization of the mammalian MSC, including interferon gamma (IFNɣ)-stimulated glutamyl-prolyl-tRNA synthetase 1 (EPRS1) release, as well as the cooperation with the ribosome bridged by the tRNAs. The cell-based analysis provided an improved understanding of the flexible framework of the mammalian MSC in physiological conditions.

On the other hand, abnormality of the aminoacylation has been implicated in a wide variety of cancer pathologies. The ARSs exist in large excess in cancer cells due to their increased demand for the protein synthesis. Meanwhile, most other translation apparatuses are quantitatively limited. There has been no report for mutations of the ARSs that demonstrate constitutive activity of the aminoacylation; the hyperactivity of the ARSs may disrupt stable association of the MSC.

Hence, interference of the aminoacylation activity is expected to be independent of genotype variation and may not develop drug resistance. In part II, a high-throughput screen (HTS) platform was established to find the mammalian ARS inhibitors. The ARSs of rabbit reticulocyte closely resemble both the individual and complexed structures of human ones. Therefore, an *in vitro* translation system with the rabbit-reticulocyte lysate may predispose active compounds to be readily applicable for mankind. The assay was further validated for identifying familiar translational inhibitors from a pilot screen, such as emetine, proving its suitability for the purpose. Having demonstrated excellent quality control (QC) parameters and reproducibility, it is proven ready for further HTS campaign with large molecular entities.

Keywords: aminoacyl-tRNA synthetase (ARS); mammalian multi-tRNA synthetase complex (MSC); macromolecular complex; ribosome; tRNA; high-throughput screening (HTS); aminoacylation; protein-synthesis inhibitor

Student number: 2013-30500

Contents

Part I

Cell-based analysis of pairwise interactions between the components of the multi-tRNA synthetase complex

Part II

High-throughput screen for protein synthesis inhibitors targeting aminoacyl-tRNA synthetases

List of figures and tables

Part I

Part II

Introduction

Transfer RNA (tRNA) matches a codon triplet in a messenger RNA (mRNA) with an amino acid it codes for. Therefore, charging of tRNA with the cognate amino acid needs to be precise and requires specific enzymes named as aminoacyl-tRNA synthetases (ARSs). There are twenty ARSs for each standard amino acid. As initiating translation of the genetic code, the ARSs are essential for all cellular life.

Most organisms manipulate a citric acid cycle to produce certain amino acids. Even anaerobes and some aerobes at least have the partial citric acid cycles. A major difference between the prokaryotic and eukaryotic citric acid cycles is compartmentalization. When a symbiotic relationship was formed between a mitochondrion and a host cell, the cytoplasm of engulfed aerobic proteobacteria became a cellular compartment of the eukaryotic cell, in which the citric acid cycle takes place (Margulis 1970, Andersson, Zomorodipour et al. 1998, Martijn, Vosseberg et al. 2018). Therefore, in the eukaryotic entity, majority of the amino acids synthesized from the citric acid cycle should come out from the mitochondria to the cytoplasm.

Although the remnant abilities to make certain amino acids vary between species and age, the ARSs retain a footprint which shows an adaptation of the translational machinery of the host cell to the mitochondria. In higher eukaryotes, from insects to humans, a multi-tRNA synthetase complex (MSC) is consisted with eight ARSs and three auxiliary proteins, namely leucyl-tRNA synthetase 1 (LARS1), aspartyl-tRNA synthetase 1 (DARS1), arginyl-tRNA synthetase 1 (RARS1), lysyl-tRNA synthetase 1 (KARS1), methionyl-tRNA synthetase 1 (MARS1), isoleucyl-tRNA synthetase 1 (IARS1), glutaminyl-tRNA synthetase 1 (QARS1), glutamyl-prolyl-tRNA synthetase 1 (EPRS1), aminoacyl-tRNA synthetase complex-interacting multifunctional protein 1 (AIMP1), aminoacyl-tRNA synthetase complex-interacting multifunctional protein 2 (AIMP2), and eukaryotic translation elongation factor 1 epsilon 1 (EEF1E1) (Kerjan, Cerini et al. 1994). In nematodes, there is a reduced form of MSC which has additional valyl-tRNA synthetase 1 (VARS1) and lacks DARS1 and EEF1E1 (Havrylenko, Legouis et al. 2011). Unicellular eukaryotes, such as yeast, *African Trypanosomes*, and *Apicomplexan*, have the simpler forms of MSC with the single scaffold protein, AIMP1 (Simos, Segref et al. 1996, Cestari, Kalidas et al. 2013, van Rooyen, Murat et al. 2014). Surprisingly, most amino acids that correspond to the ARSs constituting all the eukaryotic

MSCs are derived from two intermediates of the citric acid cycle, α-ketoglutarate and oxaloacetate (Eswarappa and Fox 2013). Exceptions in the multicellular organisms, l-leucine and l-valine, are biosynthesized from pyruvate which is consequently transported into the mitochondria and oxidized to form acetyl-CoA or carboxylated to form oxaloacetate, to be involved the citric acid cycle. One more exception is l-tyrosine in *Toxoplasma gondii* which has a unique dual-activity amino-acid hydroxylase. L-phenylalanine to l-tyrosine, and l-tyrosine to levodopa metabolisms are intertwined in *T. gondii* because, unlike other species, the single phenylalanine-tyrosine hydroxylase has similar catalytic efficiency with both substrates (Gaskell, Smith et al. 2009). As l-tyrosine is further reduced to the products that feed into the citric acid cycle (Flydal and Martinez 2013), the parasite may needed a separate source for detecting the availability of l-tyrosine. Both the sensing of availabilities and reduction of diffusion of the amino acids by the MSC in close proximity of the mitochondria should have been beneficial to the eukaryotic entity; the number of ARSs and scaffold proteins involved in the MSC have been gradually increased during the unicellular to multicellular transition in the evolution.

On the other hand, durability of the MSC organization remains as an unanswered question. Especially in mammals, there are plenty of evidences that the ARSs have gained the novel functions by fragment creation or additional new domains (Guo and Schimmel 2013). And the MSC-consisting ARSs have been found in various cellular compartments and they showed the nontranslational functions. EPRS1 is dissociated from the MSC by interferon gamma (IFNγ)-induced phosphorylation and becomes a member of IFNγ-activated inhibitor of translation (GAIT) complex which binds GAIT element in 3’ UTR of certain mRNAs to block their translation (Sampath, Mazumder et al. 2004). L-glutamine modulates QARS1 to interact with apoptosis signal-regulating kinase 1 (ASK1) to inhibit ASK1-induced apoptosis (Ko, Kim et al. 2001). LARS1 senses presence of l-leucine to regulate lysosomal localization and activation of mammalian target of rapamycin complex 1 (mTORC1) (Han, Jeong et al. 2012). KARS1 is translocated not only to the plasma membrane by laminin, but also to the extracellular space under the starvation (Kim, Lee et al. 2014, Kim, Kim et al. 2017). The auxiliary proteins of the mammalian MSC also facilitate the expanded functions, suggesting that even the scaffold of the MSC does not persist. Truncated forms of AIMP1 act as cytokines in the extracellular space (Schwarz, Kandel et al. 1999, Park, Park et al. 2002, Murray, Heng et al. 2004). AIMP2 promotes ubiquitination of FUSE-binding protein (FBP) to downregulate transcription of c-*myc* (Kim, Park et al. 2003). EEF1E1 enters the nucleus under DNA damage and activates ataxia telangiectasia mutated (ATM) and ATM and Rad3-related (ATR) protein kinases to modulate p53 (Park, Kang et al. 2005).

For the MSC, there are three possible ways to support the diverse functions of the individual components. Firstly, if the MSC organization is ever-present throughout the cellular lifespan, the MSC could rearrange itself into another forms when each component is absent. Alternatively, the MSC could be completely disrupted by the leaving of its constituents and recomposed upon return or synthesis of them. The last option is that the MSC assembly could be occurred by the need of the protein synthesis, and it might not exist constantly. Thus far, there is no evidence supporting any of the hypothesis. In the first part of this research (part I), a split-luciferase complementation system was applied to monitor the dynamic interactions between the MSC components in the live mammalian cells to find an evidence.

According to structure of catalytic sites, the individual ARSs are classified into two categories: class I and II. Class I ARSs have Rossmann fold which is characterized by a five-stranded β-sheet parallelly interconnected by α-helices. Class II ARSs adapt a six- or seven-stranded β-sheet antiparallelly flanked by α-helices (Ribas de Pouplana and Schimmel 2001). Since both architectures have the highly-conserved sequence motifs, the differences are more noticeable between the classes than the species (Beuning and Musier-Forsyth 2001). Still, the small variances between the species have been tackled as therapeutic targets and validated for multiple diseases.

The microorganismal ARSs have been well studied for infectious diseases to block the translational activity of the pathogens. Most antibiotics blocking the ARSs resemble adenosine triphosphate (ATP) or aminoacyl-adenylate (aa-AMP) intermediate molecules of the aminoacylation reaction. For example, cladosporin for *Plasmodium falciparum* lysyl-tRNA synthetase (KARS) and Chem 1781 for *Trypanosoma cruzi* histidyl-tRNA synthetase (HARS) mimic the partial structure of ATP (Teng, Hilgers et al. 2013, Fang, Han et al. 2015). On the other hand, the aa-AMP analogs, namely quinazoline for bacterial threonyl-tRNA synthetase (TARS), microcin C for bacterial aspartyl-tRNA synthetase (DARS), agrocin 84 for *Agrobacterium tumefaciens* leucyl-tRNA synthetase (LARS), and mupirocin for isoleucyl-tRNA synthetase (IARS) of Gram-positive bacteria, form the largest group of ARS inhibitors (Silvian, Wang et al. 1999, Reader, Ordoukhanian et al. 2005, Vondenhoff, Dubiley et al.

2011, Koh, Siddaramaiah et al. 2015).

In contrast, the less species-selective compounds have been used to target human ARSs and related diseases, such as malaria and cancer. For instance, febrifugine derivatives have powerful antimalarial potency along with adverse side effects (Kikuchi, Tasaka et al. 2002). Halofuginone, a halogenated derivative of febrifugine with reduced toxicity, is an amino acid-tRNA dual site inhibitor which subdues the translational activity of prolyl-tRNA synthetase (PARS) in mammalian system *in vitro* (Keller, Zocco et al. 2012, Zhou, Sun et al. 2013). Additionally, halofuginone induces amino acid response *in vivo*, blocks T_H17 cell differentiation and melanoma metastasis, and enhances autophagy in colorectal cancer (Sundrud, Koralov et al. 2009, Juarez, Mohammad et al. 2012, Chen, Gong et al. 2017). Borrelidin is another example of the ARS inhibition for the wide range of species. Interestingly, borrelidin shares no structure similarity with ATP or aa-AMP, while it has sub-nanomolar affinity to most bacterial and eukaryotic TARSs (Fang, Yu et al. 2015). Nonetheless, it has been showed anticancer activity for oral, hepatocellular, and pancreatic cancers (Sidhu, Miller et al. 2015, Gao, Jiang et al. 2017, Jeong, Kim et al. 2018[1]). Recently, a liposomal formulation of borrelidin is developed to enhance the therapeutic efficacy by overcoming its liver toxicity as the natural form (Jeong, Kim et al. 2018[2]).

On the other hand, amino acid analogs mildly affect the ARSs compared to the small molecules. Moreover, they could bring a synergy such as amino acid deprivation which benefits the cancer therapies. L-histidinol inhibits the protein synthesis of cultured mammalian cells at relatively high concentration (0.1-0.5 mM) by inducing l-histidine deprivation (Vaughan and Hansen 1973, Litt and Weiser 1978). And it reverses drug resistance of cancer cells in protein-synthesis dependent manner, and protects normal cells from multiple anticancer drugs, including cisplatinum (Warrington, Fang et al. 1996). For another example, resveratrol is a widely used health supplement, which extends lifespan not only by antidiabetic and anticancer effects, but also by protective activities for cardiovascular system and brain (Howitz, Bitterman et al. 2003, Baur, Pearson et al. 2006, Milne, Lambert et al. 2007). Among multiple targets of resveratrol, namely quinone reductase 2, transthyretin, leukotriene A4 hydrolase, troponin C, sirtuin 1, 3, and 5, peroxisome proliferator-activated receptor, methionine adenosyltransferase, estrogen receptor, and tyrosyl-tRNA synthetase 1 (YARS1), YARS1 is catalytically nullified and redirected to a nuclear function with poly(ADP-ribose) polymerase 1 (PARP1) by a tyrosine-like phenolic ring of resveratrol

(Klabunde, Petrassi et al. 2000, Buryanovskyy, Fu et al. 2004, Davies, Mamat et al. 2009, Pineda-Sanabria, Robertson et al. 2011, Gertz, Nguyen et al. 2012, Nguyen, Gertz et al. 2013, Shafqat, Muniz et al. 2013, Calleri, Pochetti et al. 2014, Nwachukwu, Srinivasan et al. 2014, Sajish and Schimmel 2015).

Other human ARSs are also involved in the cancer pathologies. Highly expressed ARSs correlate with short-term survival of cancer patients: the overexpression of glycyl-tRNA synthetase 1 (GARS1) in papillary thyroid carcinoma, KARS1 in breast cancer, and MARS1 in non-small cell lung cancer have been reported (Scandurro, Weldon et al. 2001, Park, Kim et al. 2005, Kim, Jung et al. 2017, Uhlen, Zhang et al. 2017, Kwon, Fox et al. 2019). Furthermore, the catalytic activities of the ARSs are increased in cancer cells. The catalytic activity of MARS1 is heightened in colon tumor by four fold compared to adjacent normal tissue (Kushner, Boll et al. 1976). In myeloid leukemia, phenylalanyl-tRNA synthetase 1 (FARS1) activity is elevated (Rodova, Ankilova et al. 1999).

To broaden the availabilities of novel human ARS inhibitors for the cancer therapeutics, a large-scale drug-screening campaign is needed. In the second part of this research (part II), an *in vitro* translation system was optimized for high-throughput screening (HTS) on a 384-well scale, and it demonstrated potential application to the human ARSs.

Part I

Cell-based analysis of pairwise interactions between the components of the multi-tRNA synthetase complex

Graphical abstract

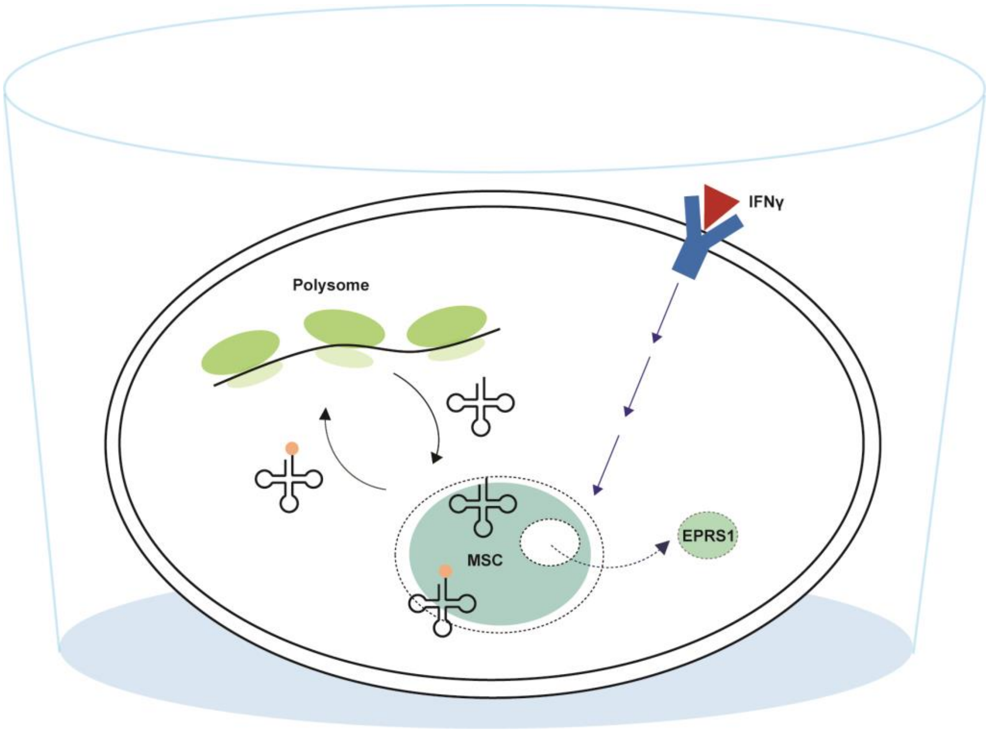

Highlights

- Full framework of a multi-tRNA synthetase complex (MSC) has hardly been addressed.
- Reporters for monitoring binary protein-protein interactions successfully incorporated into the endogenous MSC.
- Pairwise comparison of the reporter interactions reconstituted the entire framework of the MSC.
- Dynamic rearrangements of the MSC were assessed by the reporters in physiological conditions.
- The cell-based analysis complemented the structure of the MSC derived from *in vitro* assays by a context of aminoacyl-tRNA supply network.

Introduction

The multi-tRNA synthetase complex (MSC) is a macromolecular complex, the framework for which has not yet been completely defined. In mammals, the MSC is comprised of eight cytoplasmic aminoacyl-tRNA synthetases (ARSs) and three auxiliary proteins, namely aspartyl-tRNA synthetase 1 (DARS1), glutamyl-prolyl-tRNA synthetase 1 (EPRS1), isoleucyl-tRNA synthetase 1 (IARS1), lysyl-tRNA synthetase 1 (KARS1), leucyl-tRNA synthetase 1 (LARS1), methionyl-tRNA synthetase 1 (MARS1), glutaminyl-tRNA synthetase 1 (QARS1), arginyl-tRNA synthetase 1 (RARS1), aminoacyl-tRNA synthetase complex-interacting multifunctional protein 1 (AIMP1), aminoacyl-tRNA synthetase complex-interacting multifunctional protein 2 (AIMP2), and eukaryotic translation elongation factor 1 epsilon 1 (EEF1E1). Thus far, parts of the MSC structure have been resolved by *in vitro* techniques, and the suggested models are dynamic rather than stable. For instance, KARS1 forms a tetramer with a dimeric AIMP2 N-terminus at a unique geometry, $\alpha_2\beta_1:\beta_1\alpha_2$. The subcomplex acquires two different conformations to accommodate retention and release of KARS1 under various stimulations (Guo, Ignatov et al. 2008, Fang, Zhang et al. 2011, Kim, Lee et al. 2014, Hei, Wu et al. 2019). Other examples include binary or tertiary glutathione S-transferase (GST)-homology domain complexes: $EPRS1_{GST}$:$AIMP2_{GST}$, $EPRS1_{GST}$:EEF1E1, $MARS1_{GST}$:EEF1E1, and $EPRS1_{GST}$:$AIMP2_{GST}$:DARS1 (Cho, Maeng et al. 2015, Hahn, Park et al. 2019). These assemblies are considered to be involved in flexible associations with each other to support subcellular translocations of EPRS1, MARS1, and EEF1E1 for their non-translational roles (Sampath, Mazumder et al. 2004, Park, Kang et al. 2005, Kwon, Kang et al. 2011).

Other sub-interactions of the MSC are correlated with substrate tRNAs. When a symmetric subcomplex of the MSC is co-crystallized with the cognate tRNA or an analog, it becomes asymmetric. For example, a prolyl-tRNA synthetase (PARS) homodimer of *Thermus thermophilus* with the cognate tRNA, as well as the human PARS homodimer with halofuginone (the dual-site inhibitor for tRNA and amino acid binding) and ATP, are captured with the asymmetric unit (Yaremchuk, Kriklivyi et al. 2000, Zhou, Sun et al. 2013). Likewise, yeast $tRNA^{Asp}$ functionally interconnects the active-site domain of one monomer and the anticodon-binding region of the other monomer of *Escherichia coli* aspartyl-tRNA synthetase (DARS) homodimer (Moulinier, Eiler et al. 2001).

Furthermore, in humans, C-terminus of QARS1, N-terminus of RARS1, and N-terminus of AIMP1 form a tertiary subcomplex bearing the asymmetric unit, which is able to undergo rigid-body rotational motion to facilitate binding of tRNA (Fu, Kim et al. 2014).

A presumed role of the MSC in translation is enhancement of tRNA-aminoacylation efficiency. In Archaea, the ARSs are copurified as one or two multiprotein complexes. For example, in an archaeal methanogen, *Methanothermobacter thermautotrophicus*, a large complex composed of leucyl-tRNA synthetase (LARS), KARS, PARS, and translation elongation factor 1A (EF1A) as a cofactor, as well as a small complex comprising seryl-tRNA synthetase (SARS) and arginyl-tRNA synthetase (RARS), are identified. Both complexes increase the catalytic reaction of the ARSs compared with that of the free forms (Hausmann, Praetorius-Ibba et al. 2007, Praetorius-Ibba, Hausmann et al. 2007, Godinic-Mikulcic, Jaric et al. 2011). Similarly, the budding yeast *Saccharomyces cerevisiae*, a lower eukaryote, also has two ARS complexes with the cofactors: glutamyl-tRNA synthetase (EARS), methionyl-tRNA synthetase (MARS), and aminoacyl-tRNA synthetase cofactor 1 (ARC1) comprise a tertiary complex, while SARS separately interacts with peroxin 21 (PEX21). Furthermore, the cofactors, ARC1 and PEX21, promote the aminoacylation by forming stable interactions between the ARSs and tRNAs (Simos, Segref et al. 1996, Simos, Sauer et al. 1998, Godinic, Mocibob et al. 2007). In mammals, human valyl-tRNA synthetase 1 (VARS1) forms a complex with heavy form of elongation factor 1 (EF-1H) to enhance the aminoacylation of $tRNA^{Val}$ (Negrutskii, Shalak et al. 1999). The function of the mammalian MSC for the aminoacylation, however, remains to be characterized.

On the other hand, the mammalian MSC is considered to be involved at one end of an aminoacyl-tRNA supply network, i.e. the end at which tRNA receives the cognate amino acid and transits further to the ribosome. In *Rattus norvegicus*, the MSC-incorporated RARS1 is implicated in the delivery of Arg-$tRNA^{Arg}$ to eukaryotic translation elongation factor 1A (eEF1A) to prevent their dissemination into the surrounding cytoplasm (Sivaram and Deutscher 1990). In *Cricetulus griseus*, the MSC-incorporated RARS1 is crucial for normal protein synthesis and cell growth, while exogenous tRNA and free RARS1 are not essential (Stapulionis and Deutscher 1995, Kyriacou and Deutscher 2008). Additionally, one of the scaffold proteins of the MSC, EEF1E1, mediates the transfer of Met-$tRNA_i^{Met}$ from MARS1 to active eukaryotic initiation factor 2 (eIF2) complex for initiation of translation in *Mus musculus* and humans (Kang, Kwon et al. 2012). Moreover, in archaeon *Thermococcus kodakarensis* and humans, the MSCs are associated with the translating ribosome (Kaminska, Havrylenko et al. 2009, David, Netzer et al. 2011, Raina, Elgamal et al. 2012). Therefore, it was hypothesized that the cooperation between the mammalian MSC and the ribosome would affect the organization of the mammalian MSC under physiological conditions. The *in vitro* assays such as X-ray crystallography, small-angle X-ray scattering, and cryogenic electron microscopy may not effectively capture the complete physiological context of the MSC and the ribosome, especially in regards to the aminoacyl-tRNA supply network mediated by the translation elongation and initiation factors. Alternatively, the yeast two-hybrid system is unable to represent the mammalian MSC as the endogenous yeast MSC only shares EARS and MARS with the mammalian MSC. Therefore, a methodical investigation of the mammalian MSC configuration in live mammalian cells using a split-NanoLuc complementation system was performed in this research (Dixon, Schwinn et al. 2016, Laschet, Dupuis et al. 2019).

Materials and methods

Cloning

pBiT1.1-C [TK_LgBiT], pBiT2.1-C [TK_SmBiT], pBiT1.1-N [TK_LgBiT], and pBiT2.1-N [TK_SmBiT] vectors, which are components of NanoBiT PPI MCS starter system (Promega, Madison, WI, USA) were used as backbones for reporter construction. Inserted human genes *(DARS1*, *EPRS1*, *IARS1*, *KARS1*, *LARS1*, *MARS1*, *QARS1*, *RARS1*, *AIMP1*, *AIMP2*, and *EEF1E1*) were obtained from in-house cDNA library. Ten units of BmtI and XhoI restriction enzymes (New England Biolabs, Ipswich, MA, USA) were used to treat each μg of DNA in a 50 μL reaction volume, at 37˚C for 16 hours. Up to 100 ng of the digested vectors and inserts were mixed at a 1:3 molar ratio and incubated with 1 μL of T4 DNA ligase (New England Biolabs) in a 20 μL reaction volume, at 16˚C for 18 hours. After heat inactivation at 65˚C for 10 minutes, the mixtures were transformed into TOP10 chemically competent cells (Invitrogen, Carlsbad, CA, USA).

Cell culture

CHO-K1 cell line (CCL-61, ATCC, Old Town Manassas, VA, USA) was maintained in RPMI-1640 culture media (SH30255.01, GE Healthcare, Chicago, UT, USA) supplemented with 10% fetal bovine serum (FBS, SH30084.03, GE Healthcare). At a density of 8 x 10^3 CHO-K1 cells per well, 0.2 µg of the cloned reporter plasmids (0.1 µg each) were transiently transfected using 0.6 µL TurboFect transfection reagent (Thermo Fisher Scientific, Waltham, MA, USA) in 100 µL 10% FBS-supplemented RPMI-1640 media in a 96-well solid white microplate (3917, Corning Inc., Corning, NY, USA). For siRNA transfection, 10 nM of si-*AIMP1* was transfected with 0.6 µL Lipofectamine RNAiMAX (Invitrogen, Carlsbad, CA, USA) at a density of 5 x 10^3 CHO-K1 cells per well, one day before the reporter plasmid transfection (5’-GAGCTGCGGGTTCGCCGCTTCATGA-3’). Then, 48 hours after the reporter plasmid transfection, luminescence was determined, or the following treatments were performed and luminescence was measured thereafter: IFNγ (R&D Systems, Minneapolis, MN, USA) treatment was performed as previously described (Sampath, Mazumder et al. 2004). Other treatments with 40 ug/mL puromycin (Santa Cruz Biotechnology, Inc., Dallas, TX, USA), 20 ug/mL cycloheximide (MilliporeSigma, Burlington, MA, USA), 10 µM harringtonine (Cayman Chemical

Company, Ann Arbor, MI, USA), and 1 μM emetine (MilliporeSigma) in 10% FBS-supplemented RPMI-1640 media were performed for 5 minutes and 4 hours. All compounds were added to 100 μL of media per well after gentle aspiration of the original media.

Luminescence detection

A mixture of 1.25 μL Nano-Glo live cell substrate (Promega) and 23.75 μL Nano-Glo LCS dilution buffer (Promega) was added to each well in the 96-well solid white microplate containing 100 μL of the media. After gentle tapping for 30 seconds, the plate was further incubated at 37˚C for 10 minutes. Luminescence was measured using GloMax 96 microplate luminometer (Promega), with 0.5-seconds integration.

Size-exclusion chromatography

CHO-K1 cells (5 x 10^8) were lysed in ice-cold buffer containing 50 mM Tris-HCl (pH 7.6), 50 mM NaCl, 1 mM phenylmethylsulfonyl fluoride, and 1 mM dithiothreitol by passing through a 27G x 1/2” needle (Sigma-Aldrich, St. Louis, MO, USA) 20 times. After centrifugation at 21,130 *g* for 30 minutes, at 4°C (Centrifuge 5424 R with Rotor FA-45-24-11, Eppendorf, Hamburg, Germany), cytoplasmic extract (3 mg of protein) was eluted with the Superose 6 increase 10/300 GL column (GE Healthcare) at a flow rate of 0.5 mL/min using ÄKTA pure protein purification system (GE Healthcare). A gel filtration calibration kit for high molecular weights (ovalbumin (43 kDa), conalbumin (76 kDa), aldolase (158 kDa), ferritin (443 kDa), thyroglobulin (669 kDa), and blue dextran 2,000 (>2,000 kDa, for void volume), GE Healthcare) was used as a standard. Among 39 chromatographic fractions collected per minute for 5-24 mL elution volume, 6.5-24 mL fractions were subjected to luminescence detection and 8-21 mL fractions were measured for RNA concentrations thereafter. For the luminescence detection, 134.7 μL of the chromatographic fractions were mixed with 0.3 μL Nano-Glo luciferase assay substrate (N113A (N2410), Promega) and 15 μL Nano-Glo blotting buffer (N242A (N2410), Promega) in the 96-well solid white microplate. The mixtures were incubated at 37°C for 10 minutes before luminescence measurement. For the RNA concentration measurement, 2 μL of the chromatographic fractions were applied to NanoDrop 2000/2000c spectrophotometer (Thermo Fisher Scientific). For immunoblotting, 40 μL of chromatographic fractions were resolved by SDS-PAGE, and target proteins were detected using specific antibodies.

Antibodies

Rabbit polyclonal antibodies for AIMP1 (A304-896A, Bethyl Laboratories, Montgomery, TX, USA), QARS1 (NBP1-89487, Novus Biologicals, Littleton, CO, USA), DARS1 (GTX33145, GeneTex, Irvine, CA, USA), GAPDH (GTX100118, GeneTex), and ribosomal protein L4 (RPL4, GTX112184, GeneTex) were diluted at 1:1,000 and incubated overnight at 4°C for immunoblotting. Other rabbit polyclonal antibodies for EPRS1 (A303-959A, Bethyl Laboratories) and LARS1 (A304-315A, Bethyl Laboratories) were diluted at 1:5,000 and incubated overnight at 4°C for immunoblotting. Mouse monoclonal antibodies for AIMP2 (Choi, Kim et al. 2011) and α-Tubulin (T7064, Sigma-Aldrich) were diluted at 1:1,000. AIMP2 antibody was incubated overnight at 4°C and α-Tubulin antibody was incubated for 1 hours at room temperature for immunoblotting.

X-ray structural data analysis

Protein structures deposited in RCSB PDB database (https://www.rcsb.org/), PDB ID 5IBO (Lovell, Scott et al. To be published), 1IL2 (Moulinier, Eiler et al. 2001), 4HVC (Zhou, Sun et al. 2013), 4BVX (Cho, Maeng et al. 2015), 4DPG (Ofir-Birin, Fang et al. 2013), and 4R3Z (Fu, Kim et al. 2014), were analyzed using the Protein Workshop program (Moreland, Gramada et al. 2005). Distances within the structures were individually measured with the PyMOL 2.3.3 program (Schrodinger, New York, NY, USA) and labeled on the images created using the Protein Workshop program.

Data processing

All heatmaps and graphs were drawn using the GraphPad Prism 8.2.1 program (GraphPad Software, San Diego, CA, USA). Quantification of protein levels detected by the immunoblotting was performed using ImageJ 1.52v program (Schneider, Rasband et al. 2012).

Results

System validation

The split-luciferase complementation systems are based on the structural and functional complementation of the two luciferase fragments via the interaction between target proteins conjugated to each fragment. Generally, the probes have high signal-to-background ratios and their interactions are reversible by small molecules (Azad, Tashakor et al. 2014). The split-NanoLuc complementation tags are specifically engineered from the luciferase of the deep-sea shrimp *Oplophorus gracilirostris* to have a large dissociation constant value (K_D = 190 μM) thereby assuring accurate indication of the target interactions with K_D < 10 μM (Dixon, Schwinn et al. 2016, Laschet, Dupuis et al. 2019). Moreover, the molecular weight of the NanoLuc is relatively low (19 kDa) compared to firefly (61 kDa) or *Renilla* (36 kDa) luciferases. The brightness of the NanoLuc is also 150 times higher than these other two luciferases (Hall, Unch et al. 2012). Therefore, I supposed that the split-NanoLuc complementation system could be incorporated into the MSC due to the small size of the probes, and subsequently report the weak dynamics or indirect interactions within the MSC by the high signal-window.

The two NanoLuc fragments, a large (LgBiT; LB) and small subunit (SmBiT; SB), were tagged to either side of human cytoplasmic AIMP1, AIMP2, EEF1E1, DARS1, EPRS1, IARS1, KARS1, LARS1, MARS1, QARS1, and RARS1 (**Figure 1**). Once the 44 reporter constructs were cloned, all possible binary combinations were evaluated; most of the reporters exhibited luminescence in a partner-dependent manner (**Figure 2-11**). There were few exceptions, however, that showed tag-specific low signals: KARS1-SB and LB-RARS1 emitted a much stronger signal than their counterparts, KARS1-LB and SB-RARS1. Hence, the latter clones were excluded from further analysis. The pairs with the highest luminescence intensity from each binary interaction were then selected and compared to each other on the same 96-well plate to eliminate between-plate variation (**Table 1** and **Figure 12*A***).

To understand whether the expression or luminescent emission of the reporters was perturbed by the untagged endogenous homologues, the relative expression levels of the reporters of AIMP1, AIMP2, and QARS1, and their luminescent signals were measured by knockdown of endogenous AIMP1. For AIMP1:AIMP1 interaction, the relative expression levels of LB-AIMP1 and SB-AIMP1 were increased by 1.2-fold and 1.1-fold, respectively, when the relative expression of endogenous AIMP1 was decreased by 0.4-fold (**Figure 12*B***). At the same time, the luminescent signal from LB-AIMP1:SB-AIMP1 was increased by 1.3-fold (**Figure 12*E***). For AIMP1:AIMP2 interaction, the relative expression level of SB-AIMP1 was decreased by 0.9-fold, while that of LB-AIMP2 remained unchanged during the reduction of endogenous AIMP1 by 0.6-fold (**Figure 12*C***). Meanwhile, the luminescent signal from SB-AIMP1:LB-AIMP2 was increased by 1.4-fold (**Figure 12*F***). For AIMP1:QARS1 interaction, when the relative expression level of endogenous AIMP1 was decreased by 0.4-fold, the relative expression level of LB-AIMP1 was increased by 1.4-fold; however, the sum of SB-QARS1 and endogenous QARS1 expressions was decreased by 0.9-fold (**Figure 12*D***). Meantime, the luminescent signal from LB-AIMP1:SB-QARS1 was increased by 1.5-fold (**Figure 12*G***). There was some ambiguity in the QARS1 expression levels because SB-QARS1 and endogenous QARS1 bands were not well separated to determine the levels of each. Therefore, for AIMP1:AIMP1 and AIMP1:QARS1 interactions, there is a possibility that the heightened luminescent signal was because of the increased expression of the reporters due to the reduction in endogenous AIMP1 levels. However, for AIMP1:AIMP2 interaction, enhanced incorporation of the AIMP1 reporter into the MSC, filling in the vacancy of endogenous AIMP1, would be coupled with incorporation of the AIMP2 reporter and elevate the luminescent signal.

The derived steady-state configuration enabled reconstitution of the sub-interactions that had been analyzed by the *in vitro* assays (black connective lines) and assessment of the spatial-proximities within the MSC (grey connective lines) (**Figure 12*H***). Meanwhile, the only sub-interactions not reconstructed by the system were those with $EPRS1_{GST}$: $EPRS1_{GST}$:$AIMP2_{GST}$(:DARS1) and $EPRS1_{GST}$:EEF1E1. The difference may be attributed to the EARS or WHEP domain of EPRS1, which was not present in the previous studies, or to the flexible association between EPRS1 and the MSC due to the dual localization of EPRS1 in response to interferon gamma (IFNγ) signaling (Sampath, Mazumder et al. 2004) (**Figure 15*E***).

Comparison of the system and the protein structures

X-ray crystallography and small-angle X-ray scattering techniques have enabled elucidation of the partial structures for the MSC. Therefore, validation of the MSC framework derived from the reporter system via the known structures is crucial. Firstly, a maximal distance at which the interaction between the C-terminus of LB and the N-terminus of SB was permitted, was measured. The distance between the N- and C-terminus of LB was ~53 Å, based on the structure of the original protein, the NanoLuc (**Figure 14*A***). When additional linker peptides in the reporter constructs were taken into account, therefore, the marginal distances allowing the interaction between the C-terminus of LB and the N-terminus of SB were ~164 Å for the N-terminus to N-terminus interaction of the target proteins (**Figure 13*B, D***), ~125 Å for the C-terminus to C-terminus interaction of the target proteins (**Figure 13*A, C***), and ~68 and ~221 Å for the N-terminus to C-terminus interactions of the target proteins (**Figure 13*B, C*** and ***A, D***). The contour length per amino acid was estimated as ~4 Å in the approximation (Carrion-Vazquez, Marszalek et al. 1999).

However, a large proportion of the terminus-to-terminus distances measured on the known protein structures was much shorter than the requirements above (**Figure 14*B-D,*** and ***F***), indicating that the difference in luminescent signals from the split-NanoLuc complementation system may originate from steric hindrance within the protein complex. For instance, the luminescent signal from the C-terminus to C-terminus interaction of the DARS1 homodimer was the highest among all the DARS1:DARS1 pairs, since it was the only path at which LB and SB could interact without encountering any steric bulk based on the DARS homodimer structure (**Figure 14*B*** and **5*A***). For another example, the luminescent signal from the interaction between the C-terminus of EEF1E1 and the N-terminus of MARS1 was stronger than that from the interaction between the N-terminus of EEF1E1 to the N-terminus of MARS1 owing to steric hindrance, although the lengths of the paths were very similar to each other (**Figure 14*C*** and **4*G***). An exception was the C-terminus to C-terminus interaction of the EPRS1 homodimer, which had the steric hindrance based on the PARS homodimer structure. Therefore, the minimal participation offered by the N-terminus of EPRS1 in the interaction was likely due to the flexibility of the WHEP domain, not by the steric hindrance (Ray and Fox 2014) (**Figure 14*D*** and **6*A***).

The same notion can be applied to the partial-protein structures that lacked the protein termini. The undetected portion of the N-terminus of KARS1 was ~280 Å (70 amino acids), while that of the C-terminus of KARS1 was ~88 Å (22 amino acids). And the N-terminus of KARS1 preferentially interacted with the N-terminus of AIMP2 as it presented less steric hindrance than did the C-terminus of KARS1 within the crystallized region (**Figure 14*E*** and **3*F***).

Moreover, the undetected portions on the known protein structure could be predicted using the system. In the AIMP1:QARS1:RARS1 structure, only the interaction between the N-terminus of AIMP1 and the N-terminus of RARS1 was observed (**Figure 14*F***). Meanwhile, both interactions between the N-terminus of AIMP1 and the N-terminus of RARS1, as well as the C-terminus of AIMP1 and the N-terminus of RARS1 were favored over other AIMP1:RARS1 pairs in the split-NanoLuc complementation system (**Figure 2*K***). Therefore, the undetected C-terminus of AIMP1 was highly expected to face the same side of the N-terminus of AIMP1. Furthermore, the N-terminus of QARS1 interacted with both the N-terminus of AIMP1 and RARS1, while the C-terminus of QARS1 was not involved in the AIMP1:QARS1 and QARS1:RARS1 interactions in the split-NanoLuc complementation system (**Figure 2*J*** and **11*B***). Hence, the N-terminus of QARS1 was predicted to be on the same side of the N- and C-terminus of AIMP1 and the N-terminus of RARS1.

Incorporation of the reporters into the endogenous MSC

Although the components of the MSC are primarily located within the complex, some exist in their free forms. In the absence of discrimination between the reporter and endogenous proteins in terms of their recruitment into the endogenous MSC, the reporter system is considered adequate to represent the MSC. To verify this presumption, the EPRS1 reporters were paired with each other in every possible combination and subjected to size-exclusion chromatography to compare ratios of the MSC-integrated reporter and the total protein at an elution volume containing the MSC. At the elution volume of 9 mL, the ratios were 321 for the C-terminus to C-terminus interaction, 13 and 10 for the N-terminus to C-terminus interactions, and 4 for the N-terminus to N-terminus interaction (**Figure 15*A*-*D***). For the C-terminus to C-terminus interaction, two peaks of the reporter signal were observed: the major peak was sharp, and near to the expected molecular weight of the MSC (~1.5 Mda) (Rho, Kim et al. 1999, Dias, Renault et al. 2013), indicating successful incorporation of the reporters into the endogenous MSC; while the minor peak was broader than the first, and was located between the molecular weights of the MSC and GAIT complex (~440 kDa) (Sampath, Mazumder et al. 2004) (**Figure 15*A*** and **16).**

Additionally, most of the EPRS1 binary interactions were decreased by prolonged IFNγ treatment, and the system showed corresponding changes of other binary interactions representing the rearrangement of the remaining components in response to EPRS1 release from the MSC (**Figure 15*E***).

tRNA-mediated MSC-ribosome cooperation

To verify the hypothesis that the MSC-ribosome cooperation is bridged by the aminoacyl-tRNA supply network, the system was treated with chemical inhibitors targeting the ribosome. Although the specific targets of the compounds are not the same, they all effectively stall the ribosome. Since the CHO-K1 cell line is resistant to emetine, which has mutations on ribosomal protein S14 (RPS14) (Gupta and Siminovitch 1977, Martin-Nieto and Roufa 1997), emetine was used as a control. Interestingly, puromycin, cycloheximide, and harringtonine reduced the same binary interactions of the system (AIMP1:AIMP1, AIMP1:AIMP2, AIMP1:IARS1, AIMP1:KARS1, AIMP1:MARS1, AIMP2:AIMP2, IARS1:KARS1, IARS1:LARS1, IARS1:MARS1, IARS1:QARS1, KARS1:LARS1, and KARS1:MARS1) to a similar extent (> 0.55-fold decrease) (**Figure 17*A***), and the endogenous MSC showed comparable swelling to the system under puromycin treatment **(Figure 17*B*-*D*)**. Moreover, both LARS1 and ribosomal protein L4 (RPL4) exhibited a fractional shift to a higher molecular weight. Furthermore, rearrangement of RNA distribution was observed simultaneously. RNA was concentrated at the elution volume of 9 mL when the ribosome was translating. In contrast, it was gradually disseminated at the broad fractions, corresponding to prolonged ribosomal inhibition.

Discussion

Among the various protein complexes, the MSC represents a suitable example that undergoes conformational changes to achieve the multiple purposes. As a complex comprised of housekeeping enzymes and cofactors, the primary roles of the MSC are related to protein translation. Additionally, the individual components of the MSC have acquired unique secondary functions, independent of the complex, throughout evolution. The physiological conditions, therefore, are essential to determining the MSC organization. However, these are difficult to analyze by *in vitro* techniques as the supplemental factors that are not directly incorporated into the target-protein interaction do not produce observable effects in the assays. Therefore, a cell-based platform demonstrating the dynamic changes of the MSC is necessary. The luciferase reporter system applied here simplified the multiplex interconnections within the MSC by the sum of binary protein-protein interactions. Further, by analyzing these interactions independently, the system was able to reconstitute the MSC configuration in live cells (**Figure 12**). This is the first report on such a system responding to IFNγ signal, and demonstrating subsequent conformational changes under physiological conditions (**Figure 15**).

Two well-known ribosome inhibitors target tRNA: puromycin mimics the aminoacyl-tRNA to block the P site of the polysome, and cycloheximide prevents binding of the deacylated tRNA to the E site of the polysome (Azzam and Algranati 1973, Schneider-Poetsch, Ju et al. 2010). Harringtonine has an entirely different effect on the monosome, halting it at the initiation codon via an unknown mechanism (Ingolia, Lareau et al. 2011). Interestingly, all of these compounds induced comparable levels of swelling of the MSC, as evidenced by both the size-exclusion chromatography and the cell-based system (**Figure 17**). As shown in **Figure 17*B*-*D***, RNA was redistributed at both higher and lower molecular weight fractions during the ribosomal pause. In the context of functional relationships between the MSC and the ribosome, tRNA is the only common denominator. Therefore, a discontinuance of the aminoacyl-tRNA supply network due to the ribosomal pause would be the primary cause of the observed tRNA dispersion, which is responsible for the coincident enlargements of the MSC and the ribosome. Furthermore, in the mid-molecular weight fractions (11-13 mL) of the immunoblots, a trail of LARS1 band was strengthened by ribosome inhibition. This suggests the existence of a potential subcomplex of the MSC that supports cellular survival under nutrient shortage or other stresses by holding the aminoacyl-tRNAs and enabling their rapid resupply on restoration of normal conditions.

Figures and table

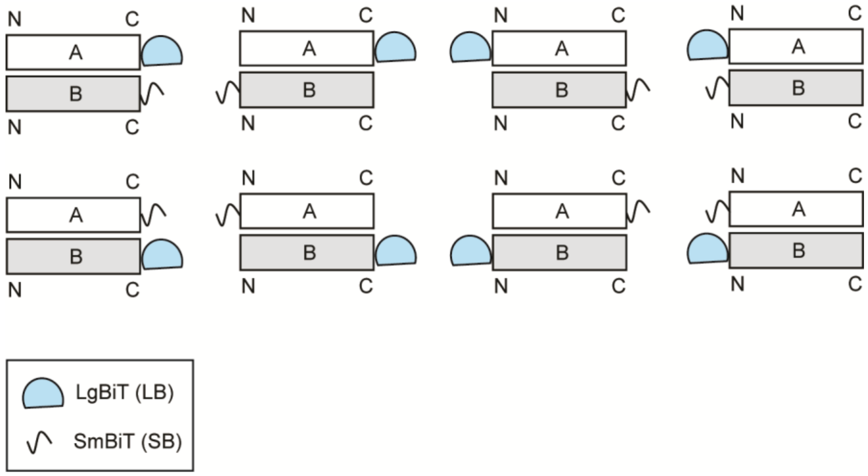

Figure 1 A schematic of the split-NanoLuc complementation reporters.

A

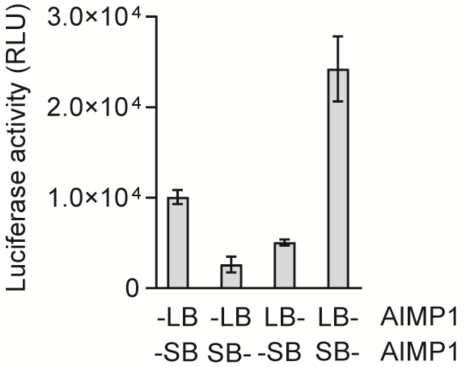
Luciferase activity (RLU)
3.0×10⁴
2.0×10⁴
1.0×10⁴
0
-LB -LB LB- LB- AIMP1
-SB SB- -SB SB- AIMP1

B

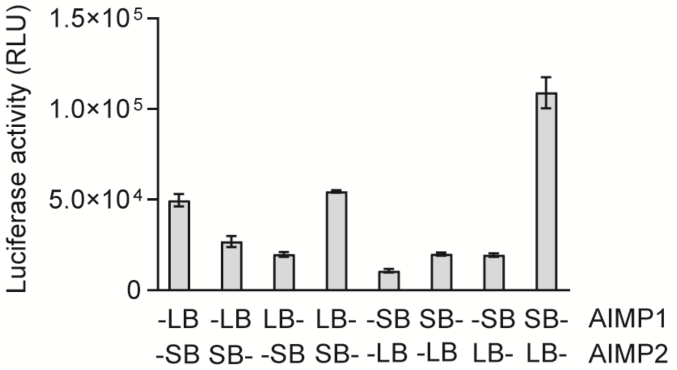
Luciferase activity (RLU)
1.5×10⁵
1.0×10⁵
5.0×10⁴
0
-LB -LB LB- LB- -SB SB- -SB SB- AIMP1
-SB SB- -SB SB- -LB -LB LB- LB- AIMP2

C

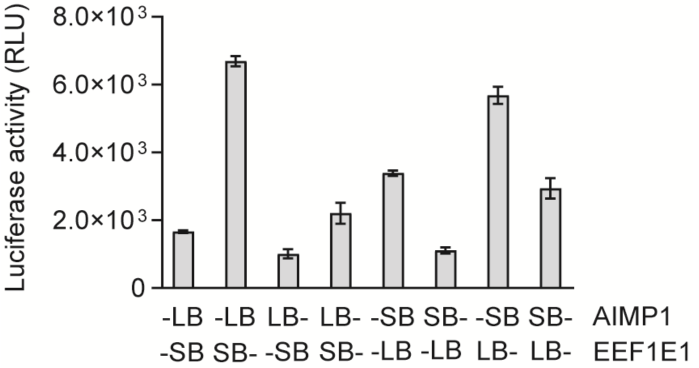
Luciferase activity (RLU)
8.0×10³
6.0×10³
4.0×10³
2.0×10³
0
-LB -LB LB- LB- -SB SB- -SB SB- AIMP1
-SB SB- -SB SB- -LB -LB LB- LB- EEF1E1

D

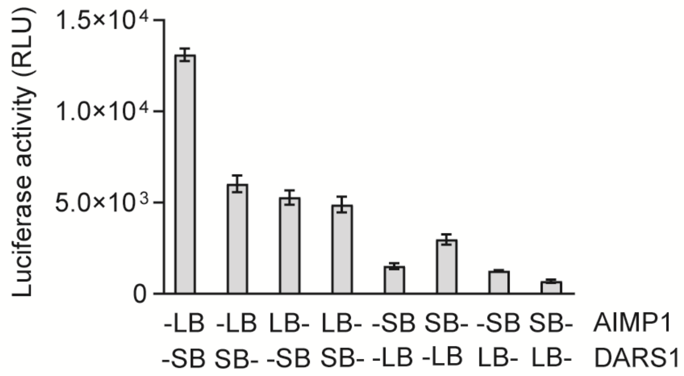
Luciferase activity (RLU)
1.5×10⁴
1.0×10⁴
5.0×10³
0
-LB -LB LB- LB- -SB SB- -SB SB- AIMP1
-SB SB- -SB SB- -LB -LB LB- LB- DARS1

E

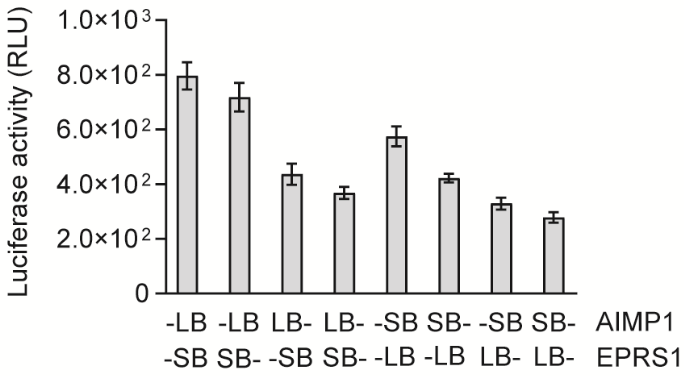
Luciferase activity (RLU)
1.0×10³
8.0×10²
6.0×10²
4.0×10²
2.0×10²
0
-LB -LB LB- LB- -SB SB- -SB SB- AIMP1
-SB SB- -SB SB- -LB -LB LB- LB- EPRS1

F

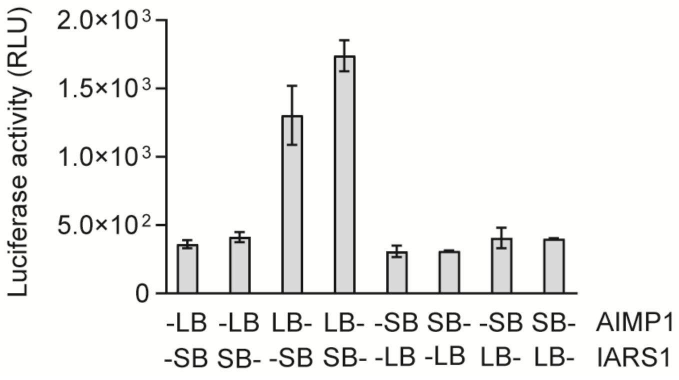
Luciferase activity (RLU)
2.0×10³
1.5×10³
1.0×10³
5.0×10²
0
-LB -LB LB- LB- -SB SB- -SB SB- AIMP1
-SB SB- -SB SB- -LB -LB LB- LB- IARS1

G

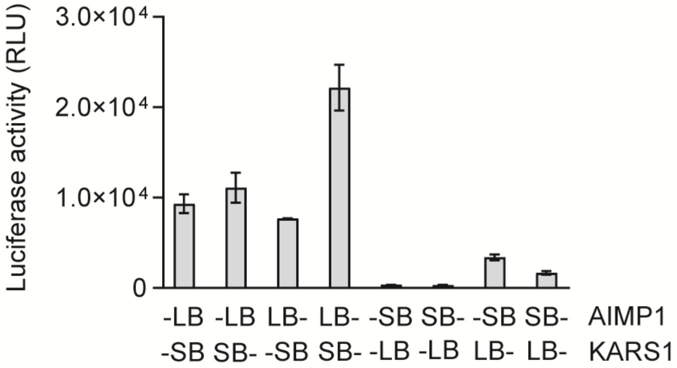
Luciferase activity (RLU)
3.0×10⁴
2.0×10⁴
1.0×10⁴
0
-LB -LB LB- LB- -SB SB- -SB SB- AIMP1
-SB SB- -SB SB- -LB -LB LB- LB- KARS1

H

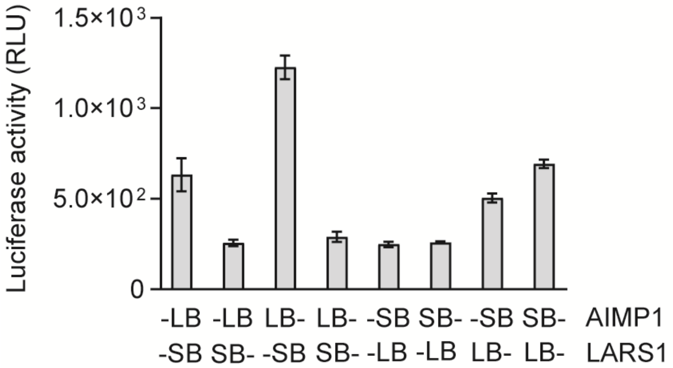
Luciferase activity (RLU)
1.5×10³
1.0×10³
5.0×10²
0
-LB -LB LB- LB- -SB SB- -SB SB- AIMP1
-SB SB- -SB SB- -LB -LB LB- LB- LARS1

I

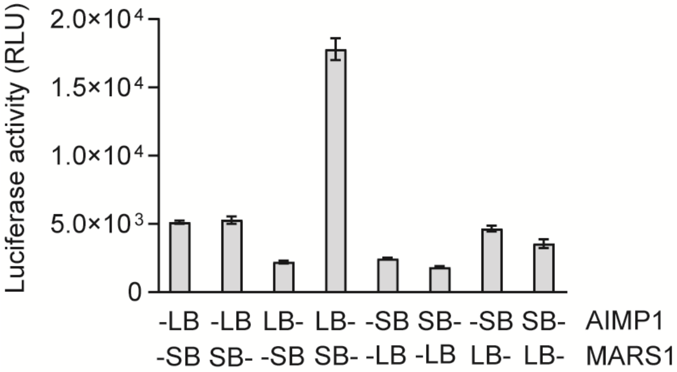
Luciferase activity (RLU)
2.0×10⁴
1.5×10⁴
1.0×10⁴
5.0×10³
0
-LB -LB LB- LB- -SB SB- -SB SB- AIMP1
-SB SB- -SB SB- -LB -LB LB- LB- MARS1

J

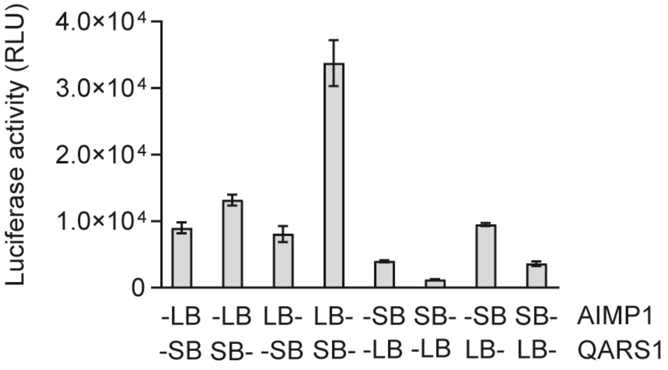
Luciferase activity (RLU)
4.0×10⁴
3.0×10⁴
2.0×10⁴
1.0×10⁴
0
-LB -LB LB- LB- -SB SB- -SB SB- AIMP1
-SB SB- -SB SB- -LB -LB LB- LB- QARS1

K

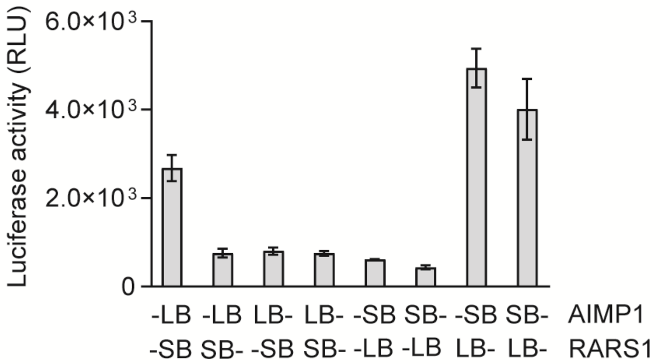
Luciferase activity (RLU)
6.0×10³
4.0×10³
2.0×10³
0
-LB -LB LB- LB- -SB SB- -SB SB- AIMP1
-SB SB- -SB SB- -LB -LB LB- LB- RARS1

Figure 2 Aminoacyl-tRNA synthetase complex-interacting multifunctional protein 1 (AIMP1) binary interactions with the multi-tRNA synthetase complex (MSC) components. (**A**) AIMP1:AIMP1 interaction. (**B**) AIMP1:aminoacyl-tRNA synthetase complex-interacting multifunctional protein 2 (AIMP2) interaction. (**C**) AIMP1:eukaryotic translation elongation factor 1 epsilon 1 (EEF1E1) interaction. (**D**) AIMP1:aspartyl-tRNA synthetase 1 (DARS1) interaction. (**E**) AIMP1: glutamyl-prolyl-tRNA synthetase 1 (EPRS1) interaction. (**F**) AIMP1:isoleucyl-tRNA synthetase 1 (IARS1) interaction. (**G**) AIMP1:lysyl-tRNA synthetase 1 (KARS1) interaction. (**H**) AIMP1:leucyl-tRNA synthetase 1 (LARS1) interaction. (**I**) AIMP1:methionyl-tRNA synthetase 1 (MARS1) interaction. (**J**) AIMP1:glutaminyl-tRNA synthetase 1 (QARS1) interaction. (**K**) AIMP1:arginyl-tRNA synthetase 1 (RARS1) interaction. The experiments were repeated for three times.

A

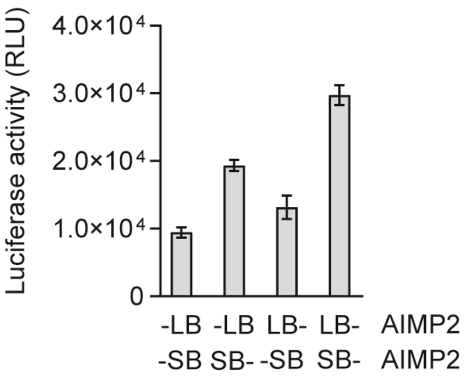
Luciferase activity (RLU)
4.0×10^4
3.0×10^4
2.0×10^4
1.0×10^4
0
-LB -LB LB- LB- AIMP2
-SB SB- -SB SB- AIMP2

B

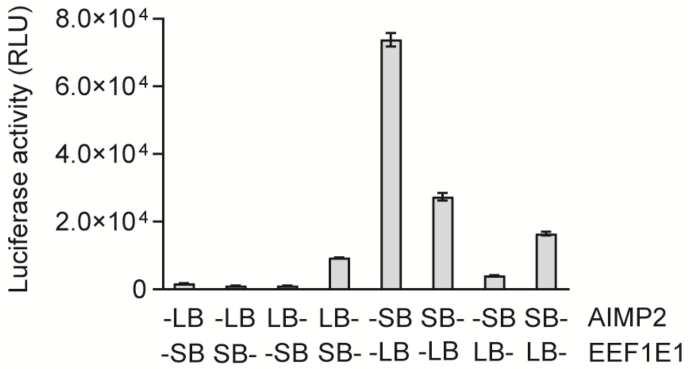
Luciferase activity (RLU)
8.0×10^4
6.0×10^4
4.0×10^4
2.0×10^4
0
-LB -LB LB- LB- -SB SB- -SB SB- AIMP2
-SB SB- -SB SB- -LB -LB LB- LB- EEF1E1

C

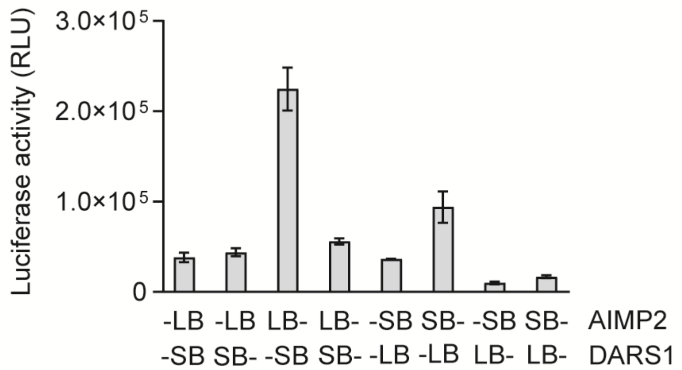
Luciferase activity (RLU)
3.0×10^5
2.0×10^5
1.0×10^5
0
-LB -LB LB- LB- -SB SB- -SB SB- AIMP2
-SB SB- -SB SB- -LB -LB LB- LB- DARS1

D

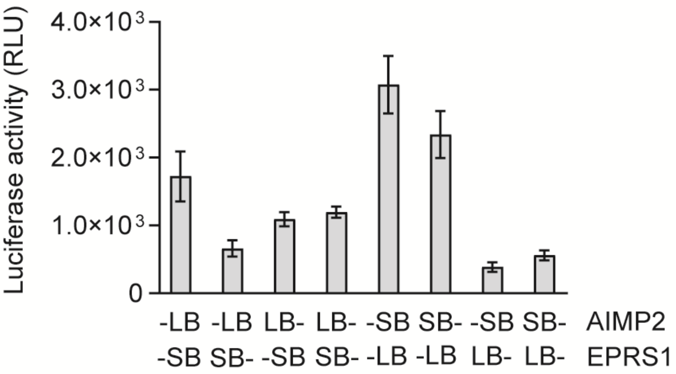
Luciferase activity (RLU)
4.0×10³
3.0×10³
2.0×10³
1.0×10³
0
-LB -LB LB- LB- -SB SB- -SB SB- AIMP2
-SB SB- -SB SB- -LB -LB LB- LB- EPRS1

E

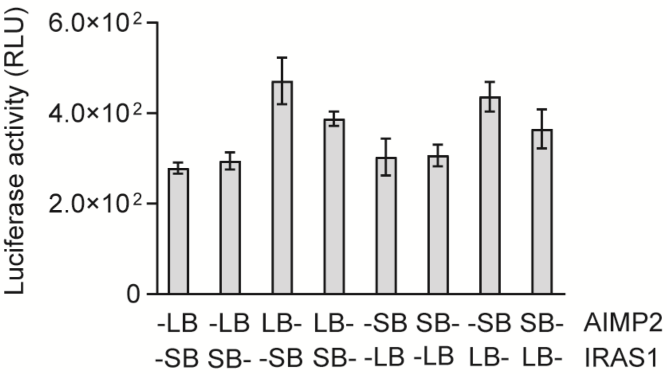
Luciferase activity (RLU)
6.0×10²
4.0×10²
2.0×10²
0
-LB -LB LB- LB- -SB SB- -SB SB- AIMP2
-SB SB- -SB SB- -LB -LB LB- LB- IRAS1

F

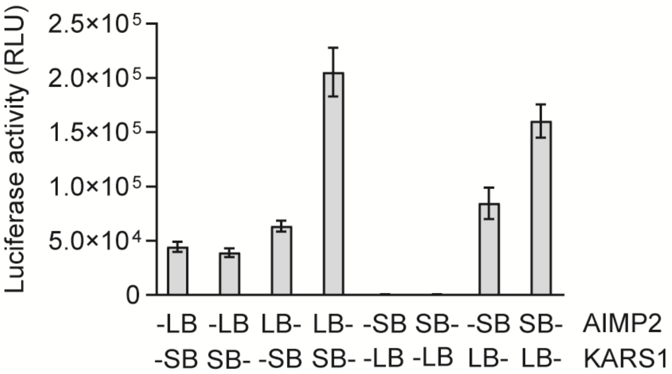
Luciferase activity (RLU)
2.5×10⁵
2.0×10⁵
1.5×10⁵
1.0×10⁵
5.0×10⁴
0
-LB -LB LB- LB- -SB SB- -SB SB- AIMP2
-SB SB- -SB SB- -LB -LB LB- LB- KARS1

G

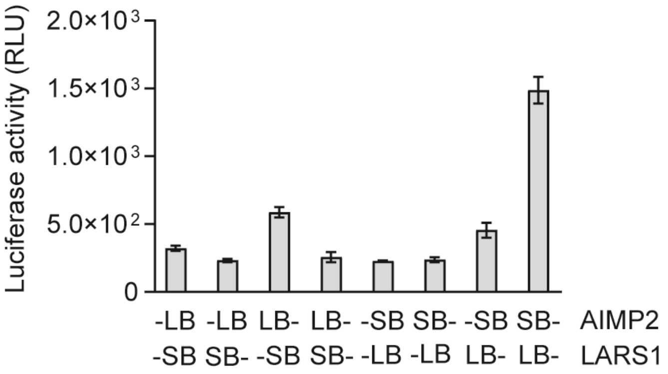
Luciferase activity (RLU)
2.0×10³
1.5×10³
1.0×10³
5.0×10²
0
-LB -LB LB- LB- -SB SB- -SB SB- AIMP2
-SB SB- -SB SB- -LB -LB LB- LB- LARS1

H

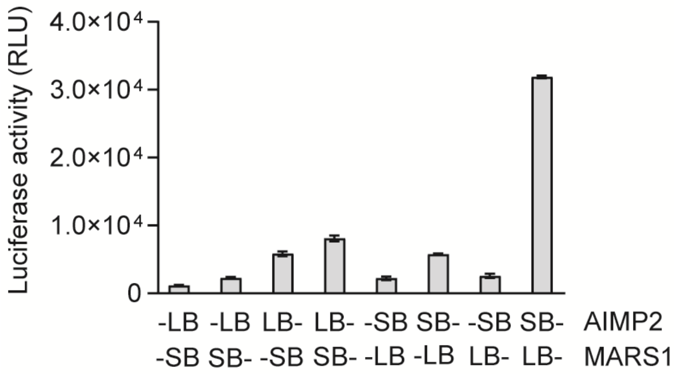
Luciferase activity (RLU)
4.0×10⁴
3.0×10⁴
2.0×10⁴
1.0×10⁴
0
-LB -LB LB- LB- -SB SB- -SB SB- AIMP2
-SB SB- -SB SB- -LB -LB LB- LB- MARS1

I

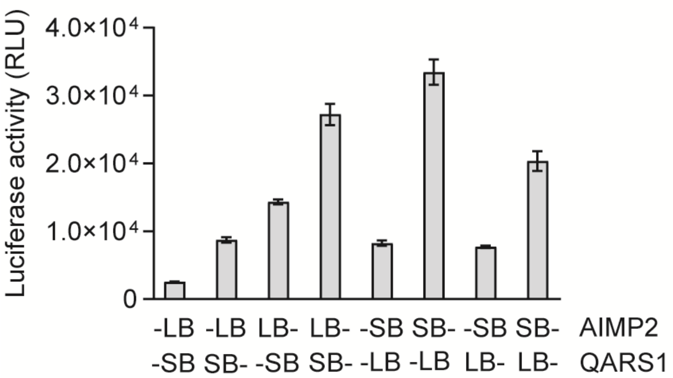
Luciferase activity (RLU)
4.0×10⁴
3.0×10⁴
2.0×10⁴
1.0×10⁴
0
-LB -LB LB- LB- -SB SB- -SB SB- AIMP2
-SB SB- -SB SB- -LB -LB LB- LB- QARS1

J

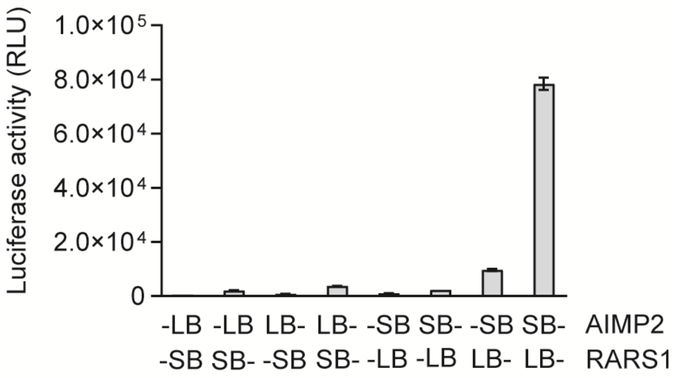

Figure 3 AIMP2 binary interactions with the MSC components. (**A**) AIMP2:AIMP2 interaction. (**B**) AIMP2:EEF1E1 interaction. (**C**) AIMP2:DARS1 interaction. (**D**) AIMP2:EPRS1 interaction. (**E**) AIMP2:IARS1 interaction. (**F**) AIMP2:KARS1 interaction. (**G**) AIMP2:LARS1 interaction. (**H**) AIMP2:MARS1 interaction. (**I**) AIMP2:QARS1 interaction. (**J**) AIMP2:RARS1 interaction. The experiments were repeated for three times.

A

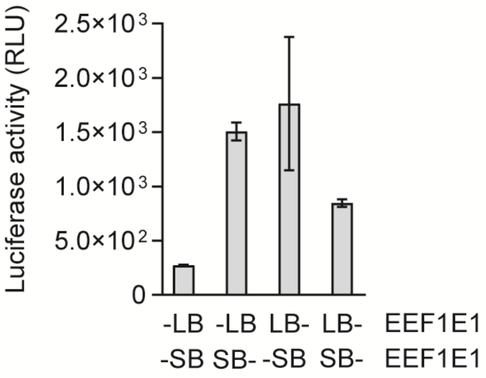

Luciferase activity (RLU)
2.5×10³
2.0×10³
1.5×10³
1.0×10³
5.0×10²
0
-LB -LB LB- LB- EEF1E1
-SB SB- -SB SB- EEF1E1

B

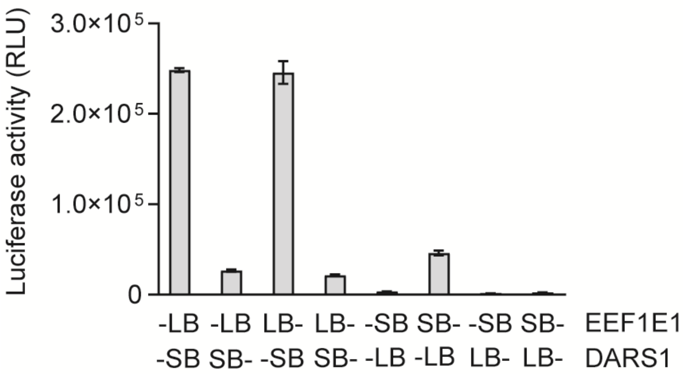

Luciferase activity (RLU)
3.0×10⁵
2.0×10⁵
1.0×10⁵
0
-LB -LB LB- LB- -SB SB- -SB SB- EEF1E1
-SB SB- -SB SB- -LB -LB LB- LB- DARS1

C

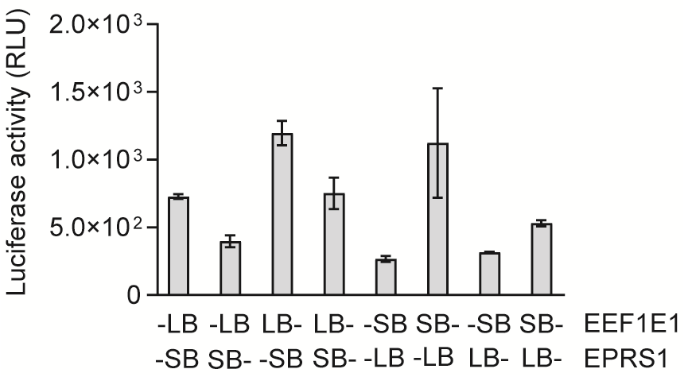

Luciferase activity (RLU)
2.0×10³
1.5×10³
1.0×10³
5.0×10²
0
-LB -LB LB- LB- -SB SB- -SB SB- EEF1E1
-SB SB- -SB SB- -LB -LB LB- LB- EPRS1

D

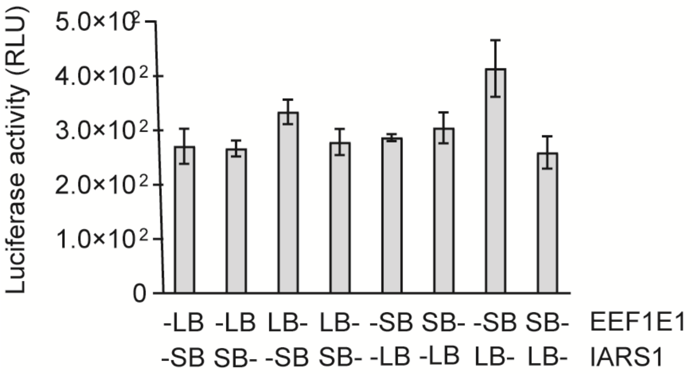
Luciferase activity (RLU)
5.0×10²
4.0×10²
3.0×10²
2.0×10²
1.0×10²
0
-LB -LB LB- LB- -SB SB- -SB SB- EEF1E1
-SB SB- -SB SB- -LB -LB LB- LB- IARS1

E

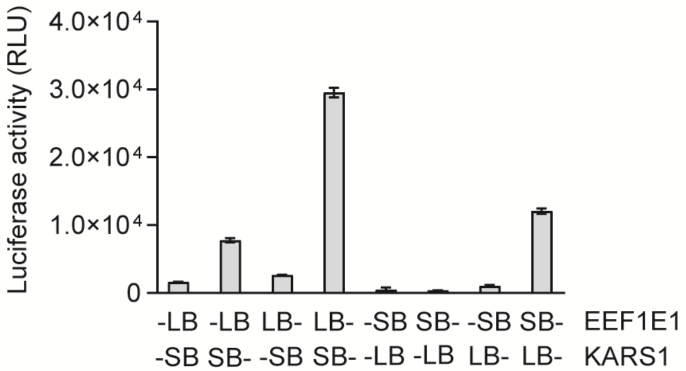
Luciferase activity (RLU)
4.0×10⁴
3.0×10⁴
2.0×10⁴
1.0×10⁴
0
-LB -LB LB- LB- -SB SB- -SB SB- EEF1E1
-SB SB- -SB SB- -LB -LB LB- LB- KARS1

F

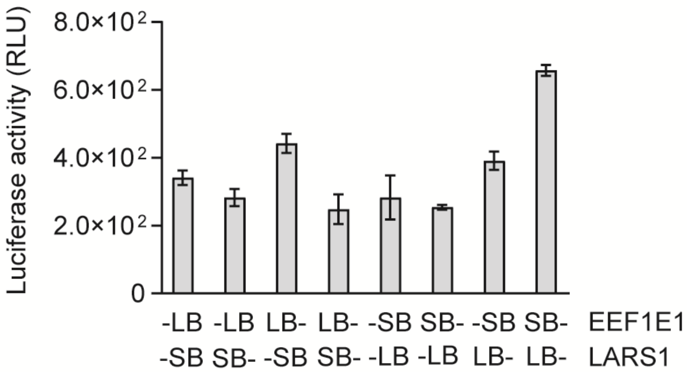
Luciferase activity (RLU)
8.0×10²
6.0×10²
4.0×10²
2.0×10²
0
-LB -LB LB- LB- -SB SB- -SB SB- EEF1E1
-SB SB- -SB SB- -LB -LB LB- LB- LARS1

G

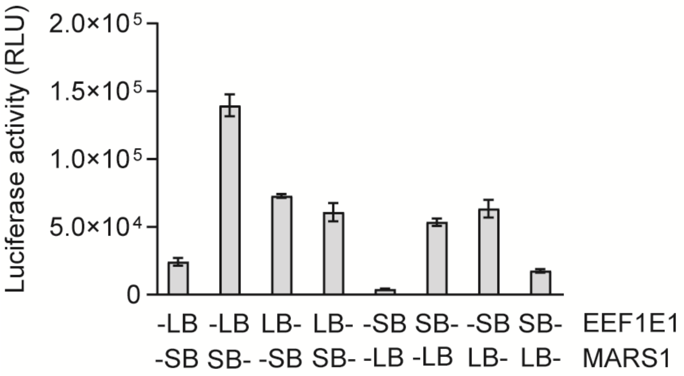
Luciferase activity (RLU)
2.0×10^5
1.5×10^5
1.0×10^5
5.0×10^4
0
-LB -LB LB- LB- -SB SB- -SB SB- EEF1E1
-SB SB- -SB SB- -LB -LB LB- LB- MARS1

H

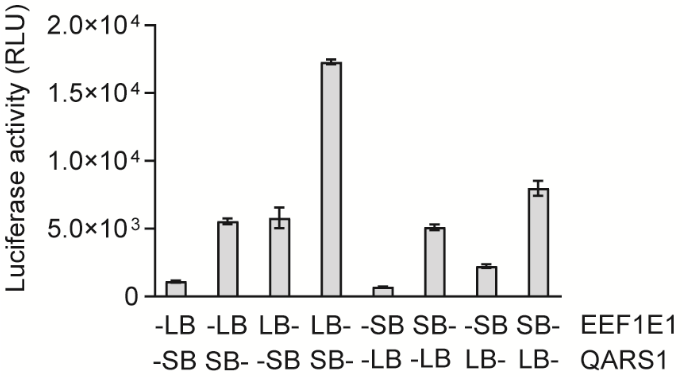
Luciferase activity (RLU)
2.0×10^4
1.5×10^4
1.0×10^4
5.0×10^3
0
-LB -LB LB- LB- -SB SB- -SB SB- EEF1E1
-SB SB- -SB SB- -LB -LB LB- LB- QARS1

I

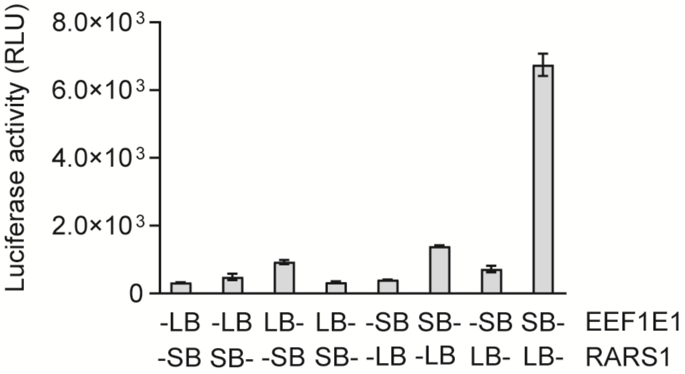
Luciferase activity (RLU)
8.0×10^3
6.0×10^3
4.0×10^3
2.0×10^3
0
-LB -LB LB- LB- -SB SB- -SB SB- EEF1E1
-SB SB- -SB SB- -LB -LB LB- LB- RARS1

Figure 4 EEF1E1 binary interactions with the MSC components. (**A**) EEF1E1:EEF1E1 interaction. (**B**) EEF1E1:DARS1 interaction. (**C**) EEF1E1:EPRS1 interaction. (**D**) EEF1E1:IARS1 interaction. (**E**) EEF1E1:KARS1 interaction. (**F**) EEF1E1:LARS1 interaction. (**G**) EEF1E1:MARS1 interaction. (**H**) EEF1E1:QARS1 interaction. (**I**) EEF1E1:RARS1 interaction. The experiments were repeated for three times.

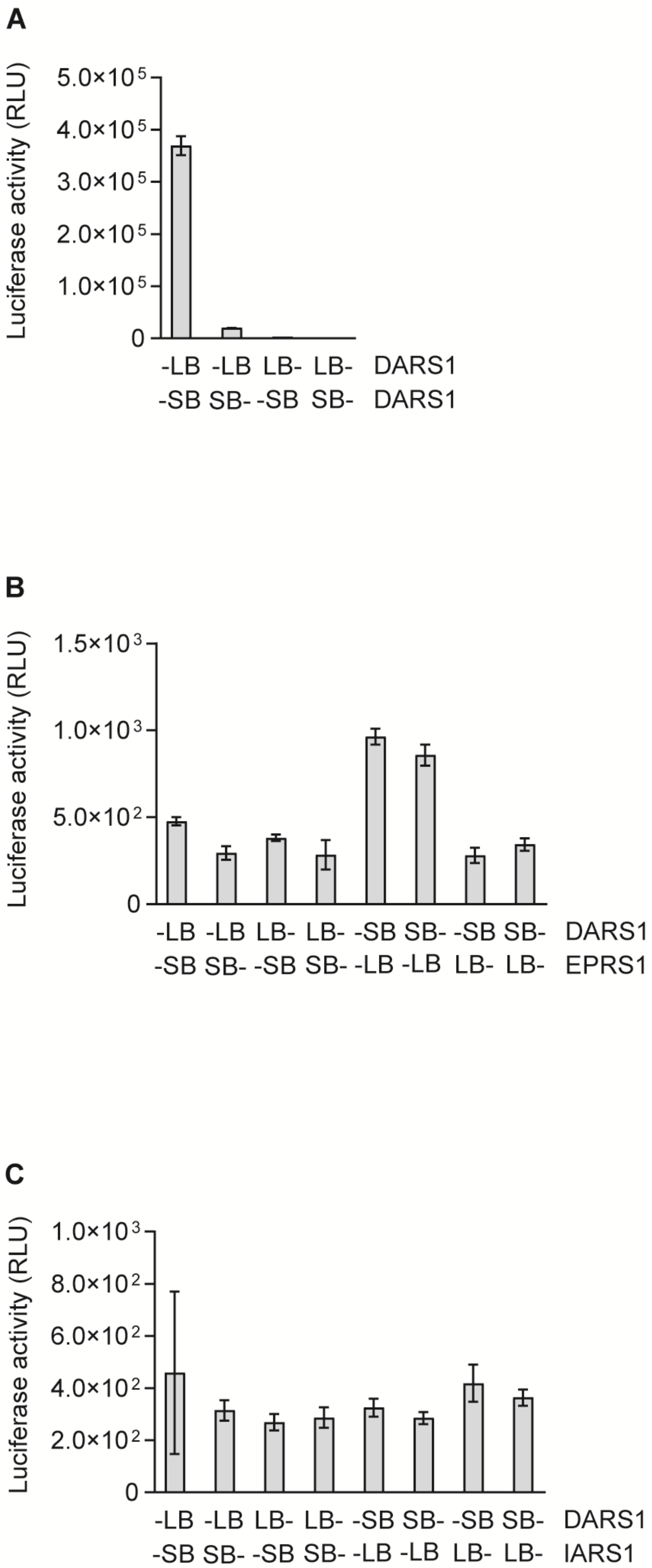
A
Luciferase activity (RLU)
5.0×10^5
4.0×10^5
3.0×10^5
2.0×10^5
1.0×10^5
0
-LB -LB LB- LB- DARS1
-SB SB- -SB SB- DARS1
B
Luciferase activity (RLU)
1.5×10^3
1.0×10^3
5.0×10^2
0
-LB -LB LB- LB- -SB SB- -SB SB- DARS1
-SB SB- -SB SB- -LB -LB LB- LB- EPRS1
C
Luciferase activity (RLU)
1.0×10^3
8.0×10^2
6.0×10^2
4.0×10^2
2.0×10^2
0
-LB -LB LB- LB- -SB SB- -SB SB- DARS1
-SB SB- -SB SB- -LB -LB LB- LB- IARS1

D

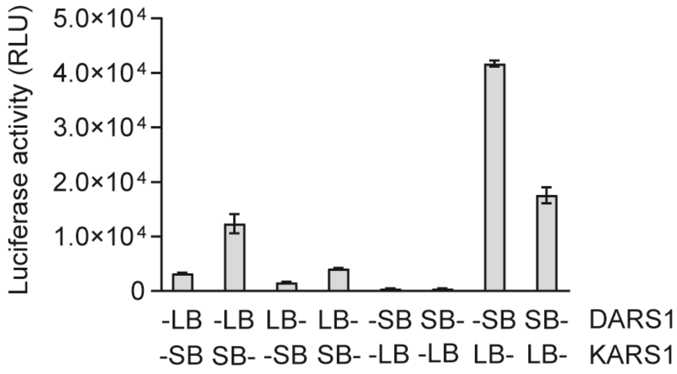
Luciferase activity (RLU)
5.0×10⁴
4.0×10⁴
3.0×10⁴
2.0×10⁴
1.0×10⁴
0
-LB -LB LB- LB- -SB SB- -SB SB- DARS1
-SB SB- -SB SB- -LB -LB LB- LB- KARS1

E

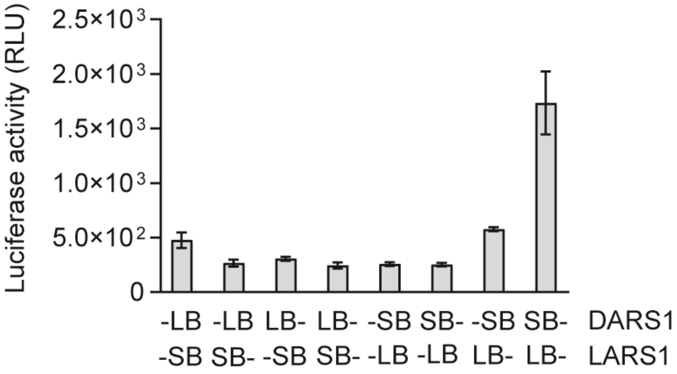
Luciferase activity (RLU)
2.5×10³
2.0×10³
1.5×10³
1.0×10³
5.0×10²
0
-LB -LB LB- LB- -SB SB- -SB SB- DARS1
-SB SB- -SB SB- -LB -LB LB- LB- LARS1

F

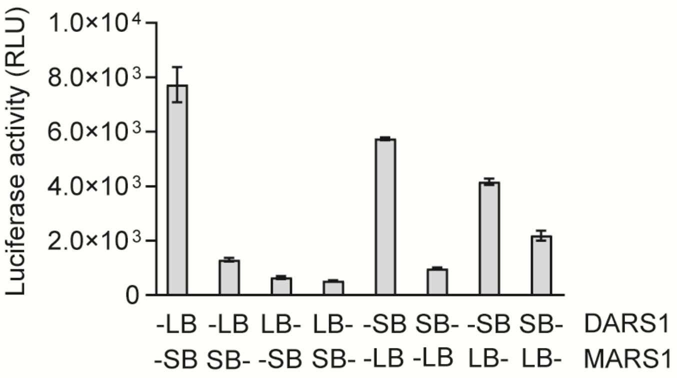
Luciferase activity (RLU)
1.0×10⁴
8.0×10³
6.0×10³
4.0×10³
2.0×10³
0
-LB -LB LB- LB- -SB SB- -SB SB- DARS1
-SB SB- -SB SB- -LB -LB LB- LB- MARS1

G

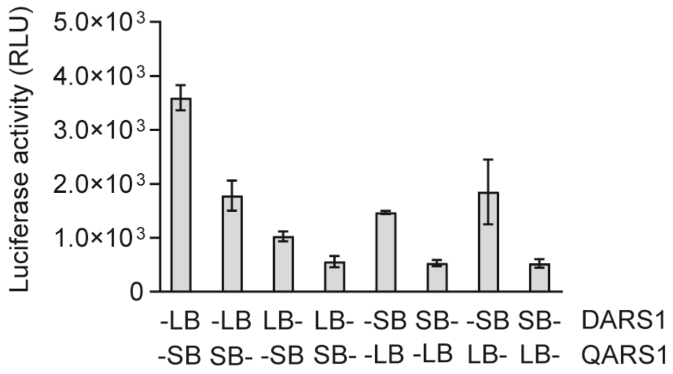

H

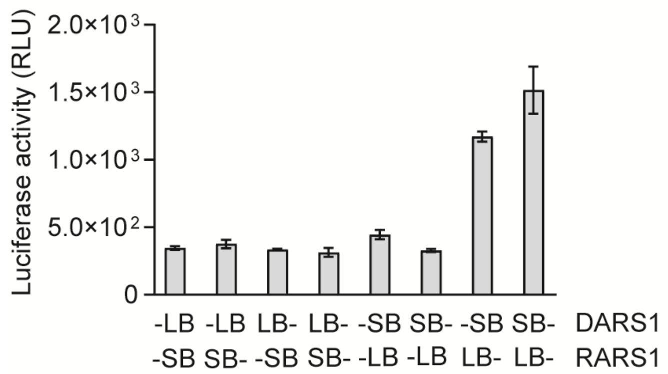

Figure 5 DARS1 binary interactions with the MSC components. (**A**) DARS1:DARS1 interaction. (**B**) DARS1:EPRS1 interaction. (**C**) DARS1:IARS1 interaction. (**D**) DARS1:KARS1 interaction. (**E**) DARS1:LARS1 interaction. (**F**) DARS1:MARS1 interaction. (**G**) DARS1:QARS1 interaction. (**H**) DARS1:RARS1 interaction. The experiments were repeated for three times.

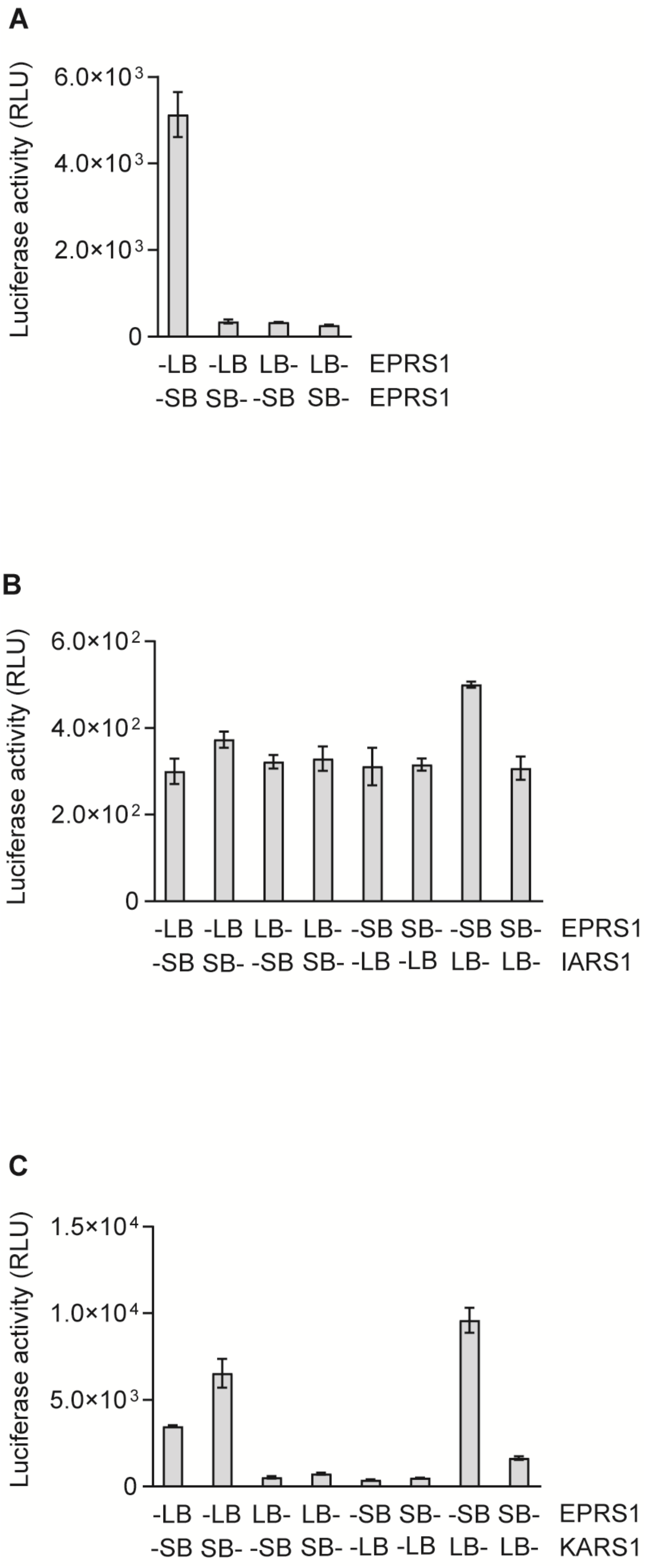
A
Luciferase activity (RLU)
6.0×10³
4.0×10³
2.0×10³
0
-LB -LB LB- LB- EPRS1
-SB SB- -SB SB- EPRS1
B
Luciferase activity (RLU)
6.0×10²
4.0×10²
2.0×10²
0
-LB -LB LB- LB- -SB SB- -SB SB- EPRS1
-SB SB- -SB SB- -LB -LB LB- LB- IARS1
C
Luciferase activity (RLU)
1.5×10⁴
1.0×10⁴
5.0×10³
0
-LB -LB LB- LB- -SB SB- -SB SB- EPRS1
-SB SB- -SB SB- -LB -LB LB- LB- KARS1

D

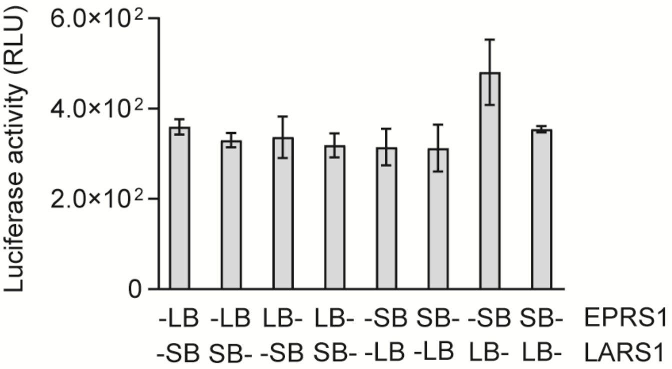
Luciferase activity (RLU)
6.0×10²
4.0×10²
2.0×10²
0
-LB -LB LB- LB- -SB SB- -SB SB- EPRS1
-SB SB- -SB SB- -LB -LB LB- LB- LARS1

E

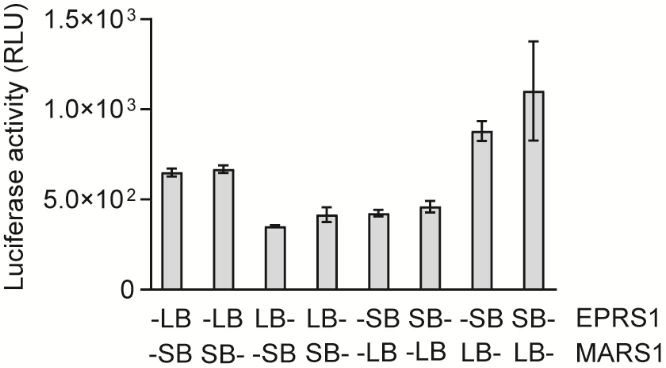
Luciferase activity (RLU)
1.5×10³
1.0×10³
5.0×10²
0
-LB -LB LB- LB- -SB SB- -SB SB- EPRS1
-SB SB- -SB SB- -LB -LB LB- LB- MARS1

F

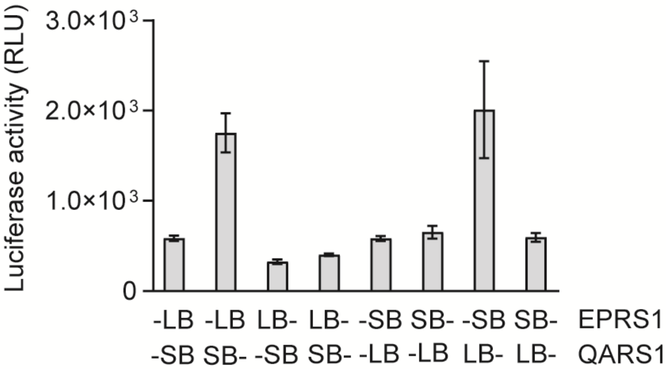
Luciferase activity (RLU)
3.0×10³
2.0×10³
1.0×10³
0
-LB -LB LB- LB- -SB SB- -SB SB- EPRS1
-SB SB- -SB SB- -LB -LB LB- LB- QARS1

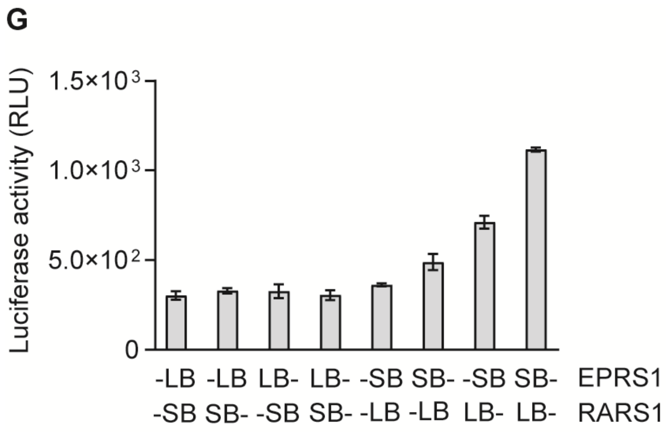

Figure 6 EPRS1 binary interactions with the MSC components. (**A**) EPRS1:EPRS1 interaction. (**B**) EPRS1:IARS1 interaction. (**C**) EPRS1:KARS1 interaction. (**D**) EPRS1:LARS1 interaction. (**E**) EPRS1:MARS1 interaction. (**F**) EPRS1:QARS1 interaction. (**G**) EPRS1:RARS1 interaction. The experiments were repeated for three times.

A

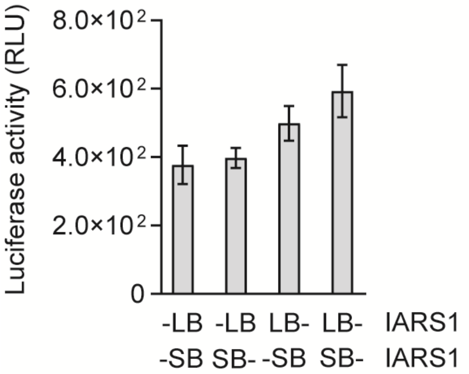

Luciferase activity (RLU)
8.0×10²
6.0×10²
4.0×10²
2.0×10²
0
-LB -LB LB- LB- IARS1
-SB SB- -SB SB- IARS1

B

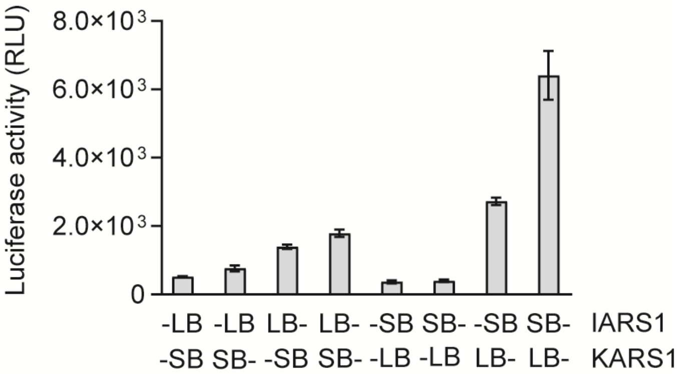

Luciferase activity (RLU)
8.0×10³
6.0×10³
4.0×10³
2.0×10³
0
-LB -LB LB- LB- -SB SB- -SB SB- IARS1
-SB SB- -SB SB- -LB -LB LB- LB- KARS1

C

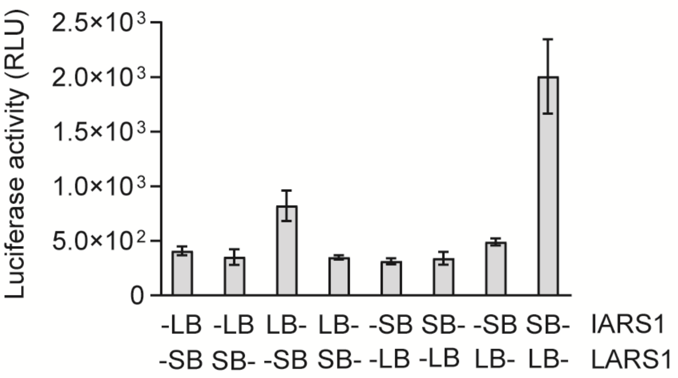

Luciferase activity (RLU)
2.5×10³
2.0×10³
1.5×10³
1.0×10³
5.0×10²
0
-LB -LB LB- LB- -SB SB- -SB SB- IARS1
-SB SB- -SB SB- -LB -LB LB- LB- LARS1

D

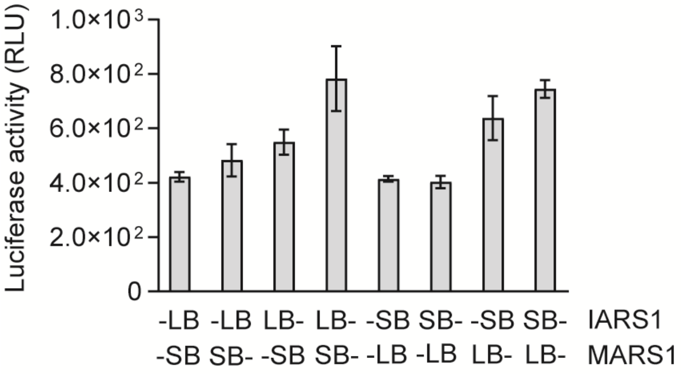
Luciferase activity (RLU)
1.0×10³
8.0×10²
6.0×10²
4.0×10²
2.0×10²
0
-LB -LB LB- LB- -SB SB- -SB SB- IARS1
-SB SB- -SB SB- -LB -LB LB- LB- MARS1

E

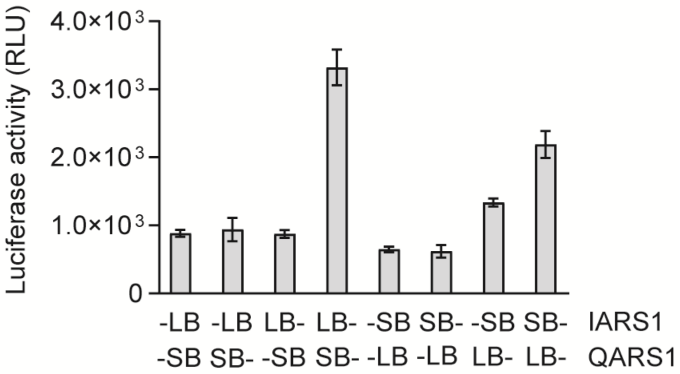
Luciferase activity (RLU)
4.0×10³
3.0×10³
2.0×10³
1.0×10³
0
-LB -LB LB- LB- -SB SB- -SB SB- IARS1
-SB SB- -SB SB- -LB -LB LB- LB- QARS1

F

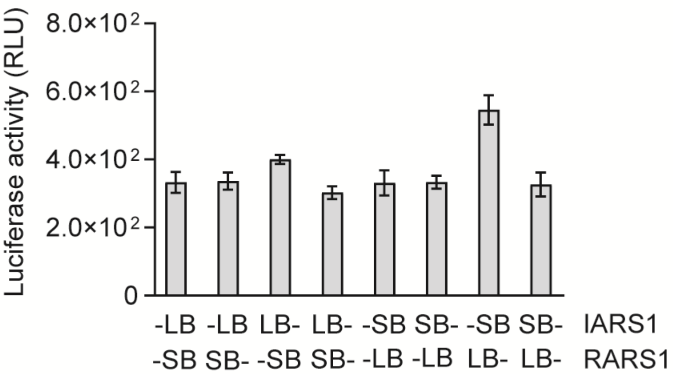
Luciferase activity (RLU)
8.0×10²
6.0×10²
4.0×10²
2.0×10²
0
-LB -LB LB- LB- -SB SB- -SB SB- IARS1
-SB SB- -SB SB- -LB -LB LB- LB- RARS1

Figure 7 IARS1 binary interactions with the MSC components. (**A**) IARS1:IARS1 interaction. (**B**) IARS1:KARS1 interaction. (**C**) IARS1:LARS1 interaction. (**D**) IARS1:MARS1 interaction. (**E**) IARS1:QARS1 interaction. (**F**) IARS1:RARS1 interaction. The experiments were repeated for three times.

A

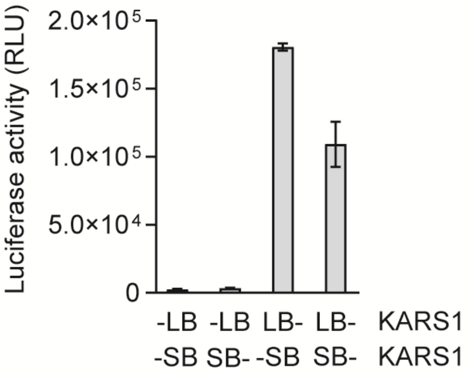
Luciferase activity (RLU)
2.0×10^5
1.5×10^5
1.0×10^5
5.0×10^4
0
-LB -LB LB- LB- KARS1
-SB SB- -SB SB- KARS1

B

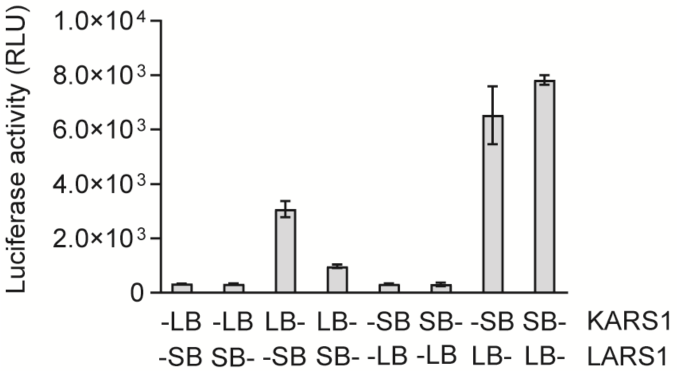
Luciferase activity (RLU)
1.0×10^4
8.0×10^3
6.0×10^3
4.0×10^3
2.0×10^3
0
-LB -LB LB- LB- -SB SB- -SB SB- KARS1
-SB SB- -SB SB- -LB -LB LB- LB- LARS1

C

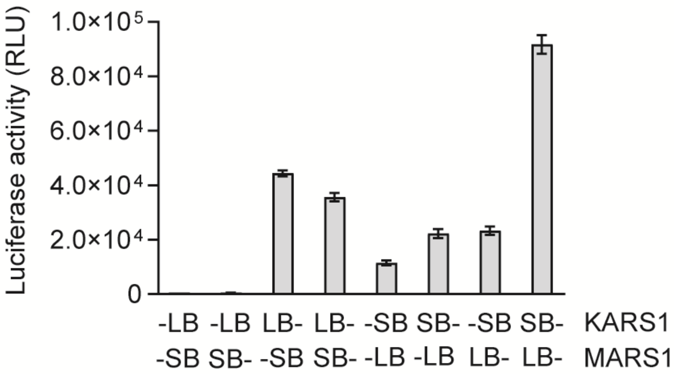
Luciferase activity (RLU)
1.0×10^5
8.0×10^4
6.0×10^4
4.0×10^4
2.0×10^4
0
-LB -LB LB- LB- -SB SB- -SB SB- KARS1
-SB SB- -SB SB- -LB -LB LB- LB- MARS1

D

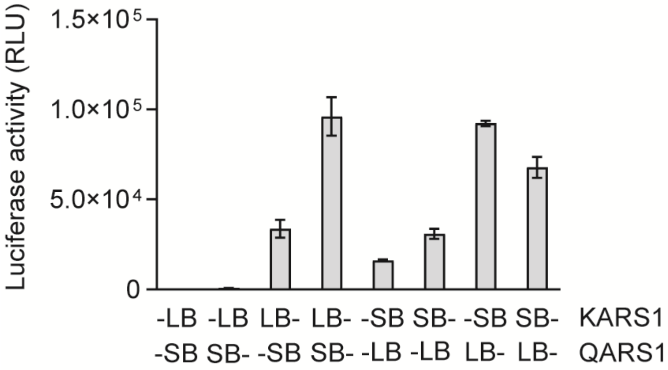

E

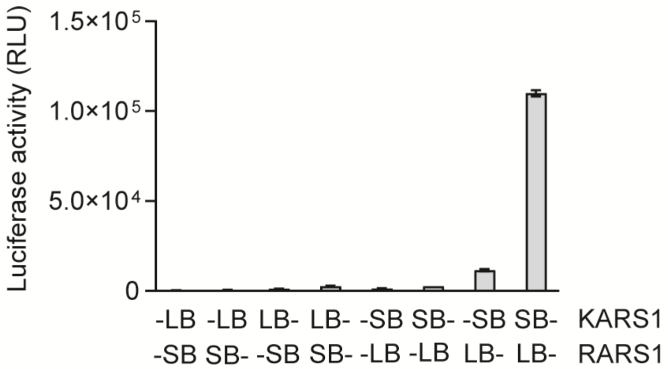

Figure 8 KARS1 binary interactions with the MSC components. (**A**) KARS1:KARS1 interaction. (**B**) KARS1:LARS1 interaction. (**C**) KARS1:MARS1 interaction. (**D**) KARS1:QARS1 interaction. (**E**) KARS1:RARS1 interaction. The experiments were repeated for three times.

A

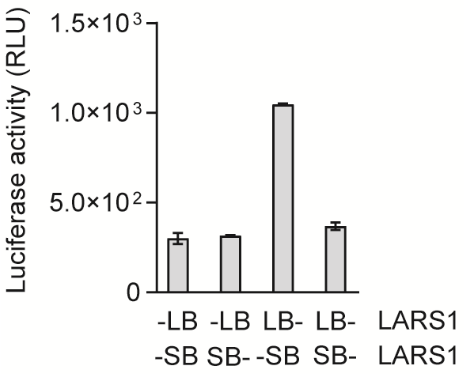

Luciferase activity (RLU)
1.5×10³
1.0×10³
5.0×10²
0
-LB -LB LB- LB- LARS1
-SB SB- -SB SB- LARS1

B

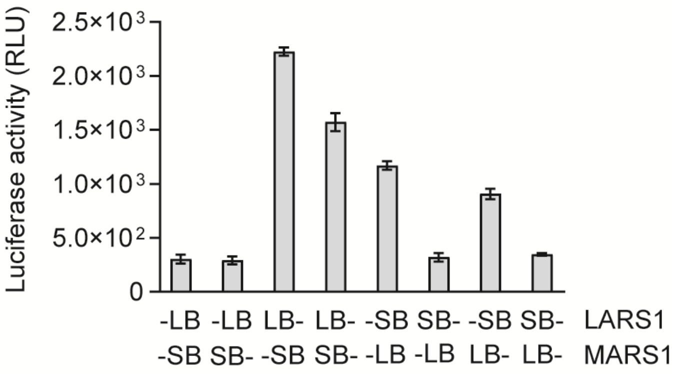

Luciferase activity (RLU)
2.5×10³
2.0×10³
1.5×10³
1.0×10³
5.0×10²
0
-LB -LB LB- LB- -SB SB- -SB SB- LARS1
-SB SB- -SB SB- -LB -LB LB- LB- MARS1

C

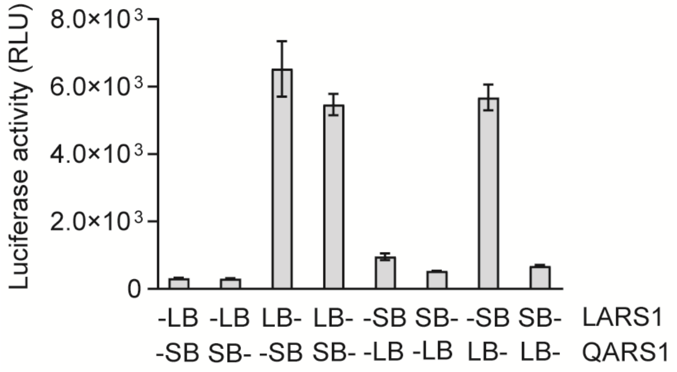

Luciferase activity (RLU)
8.0×10³
6.0×10³
4.0×10³
2.0×10³
0
-LB -LB LB- LB- -SB SB- -SB SB- LARS1
-SB SB- -SB SB- -LB -LB LB- LB- QARS1

D

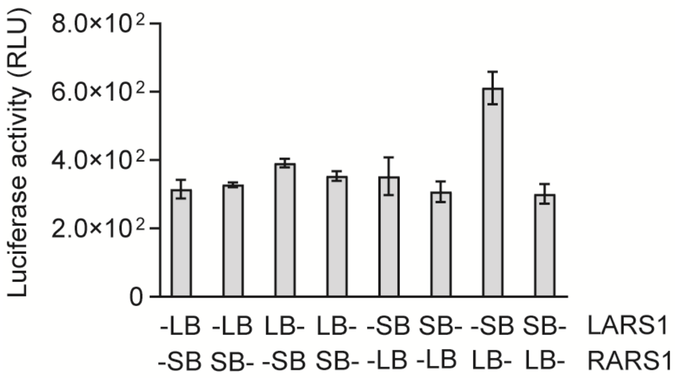

Figure 9 LARS1 binary interactions with the MSC components. (**A**) LARS1:LARS1 interaction. (**B**) LARS1:MARS1 interaction. (**C**) LARS1:QARS1 interaction. (**D**) LARS1:RARS1 interaction. The experiments were repeated for three times.

A

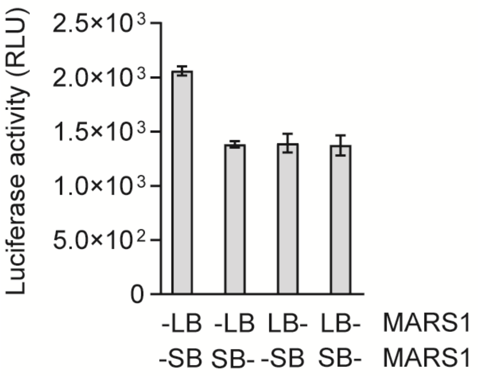
Luciferase activity (RLU)
2.5×10³
2.0×10³
1.5×10³
1.0×10³
5.0×10²
0
-LB -LB LB- LB- MARS1
-SB SB- -SB SB- MARS1

B

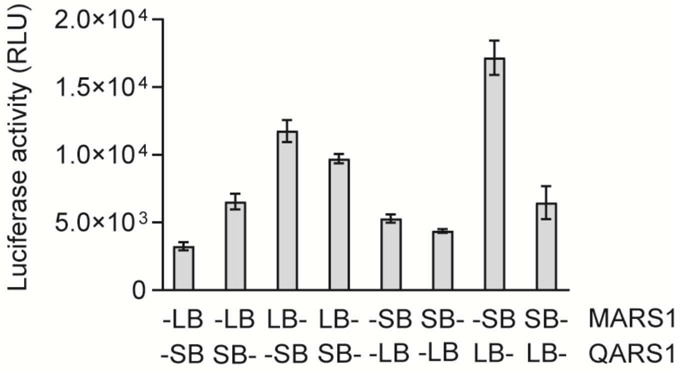
Luciferase activity (RLU)
2.0×10⁴
1.5×10⁴
1.0×10⁴
5.0×10³
0
-LB -LB LB- LB- -SB SB- -SB SB- MARS1
-SB SB- -SB SB- -LB -LB LB- LB- QARS1

C

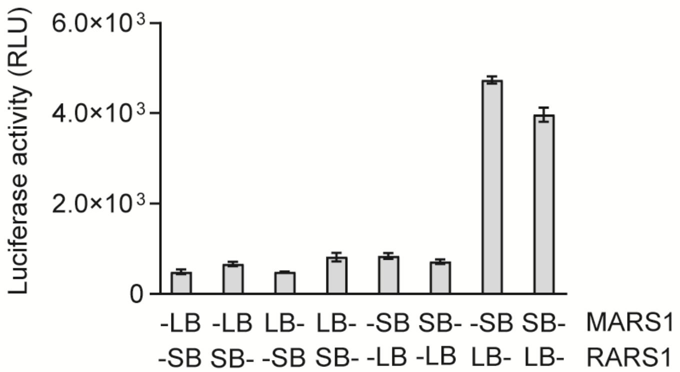
Luciferase activity (RLU)
6.0×10³
4.0×10³
2.0×10³
0
-LB -LB LB- LB- -SB SB- -SB SB- MARS1
-SB SB- -SB SB- -LB -LB LB- LB- RARS1

Figure 10 MARS1 binary interactions with the MSC components. (**A**) MARS1:MARS1 interaction. (**B**) MARS1:QARS1 interaction. (**C**) MARS1:RARS1 interaction. The experiments were repeated for three times.

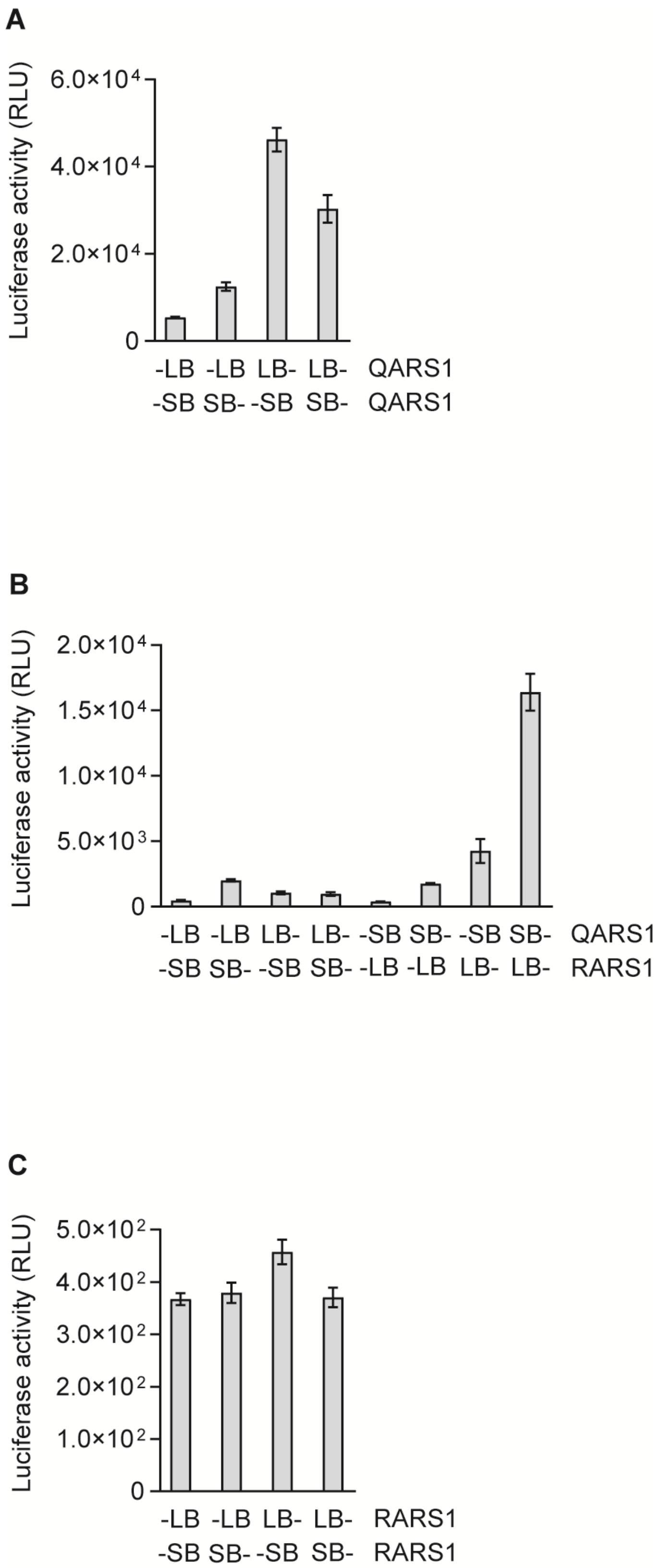

A
Luciferase activity (RLU)
6.0×10⁴
4.0×10⁴
2.0×10⁴
0
-LB -LB LB- LB- QARS1
-SB SB- -SB SB- QARS1
B
Luciferase activity (RLU)
2.0×10⁴
1.5×10⁴
1.0×10⁴
5.0×10³
0
-LB -LB LB- LB- -SB SB- -SB SB- QARS1
-SB SB- -SB SB- -LB -LB LB- LB- RARS1
C
Luciferase activity (RLU)
5.0×10²
4.0×10²
3.0×10²
2.0×10²
1.0×10²
0
-LB -LB LB- LB- RARS1
-SB SB- -SB SB- RARS1

Figure 11 QARS1 and RARS1 binary interactions with the MSC components. (**A**) QARS1:QARS1 interaction. (**B**) QARS1:RARS1 interaction. (**C**) RARS1:RARS1 interaction. The experiments were repeated for three times.

A

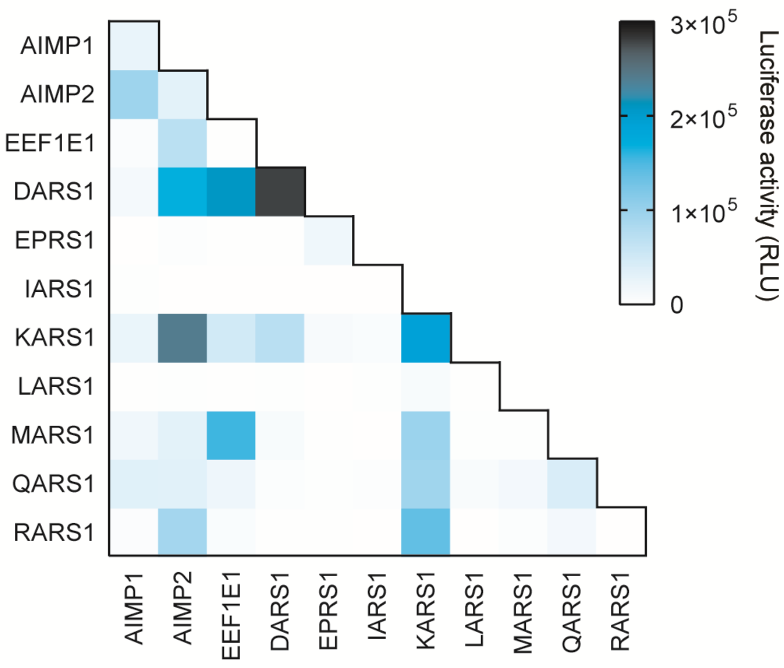
AIMP1
AIMP2
EEF1E1
DARS1
EPRS1
IARS1
KARS1
LARS1
MARS1
QARS1
RARS1
3×10^5
2×10^5
1×10^5
0
Luciferase activity (RLU)

B

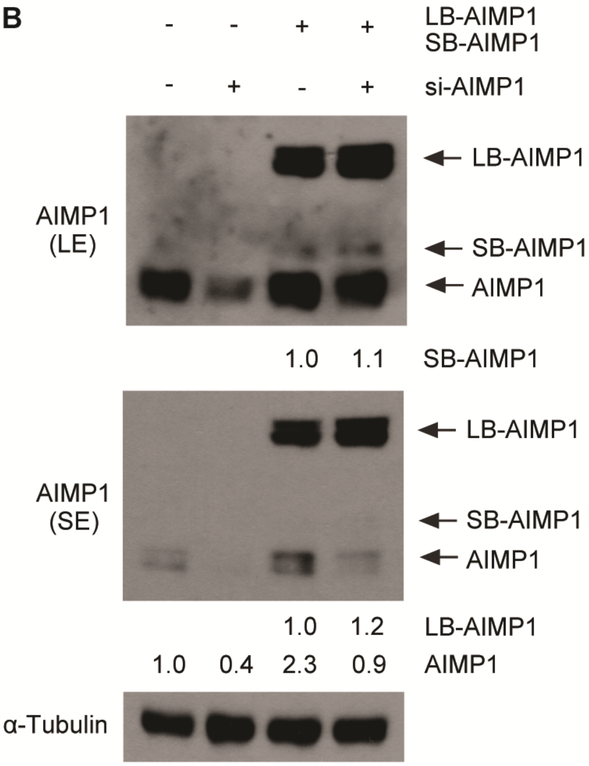
- - + + LB-AIMP1
SB-AIMP1
- + - + si-AIMP1
AIMP1 (LE)
LB-AIMP1
SB-AIMP1
AIMP1
1.0 1.1 SB-AIMP1
AIMP1 (SE)
LB-AIMP1
SB-AIMP1
AIMP1
1.0 1.2 LB-AIMP1
1.0 0.4 2.3 0.9 AIMP1
α-Tubulin

C

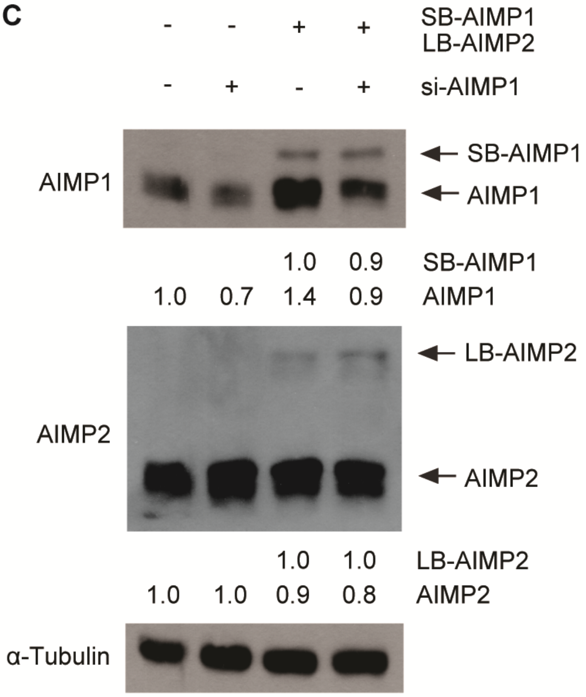
- - + + SB-AIMP1
LB-AIMP2
- + - + si-AIMP1
AIMP1
SB-AIMP1
AIMP1
1.0 0.9 SB-AIMP1
1.0 0.7 1.4 0.9 AIMP1
AIMP2
LB-AIMP2
AIMP2
1.0 1.0 LB-AIMP2
1.0 1.0 0.9 0.8 AIMP2
α-Tubulin

D

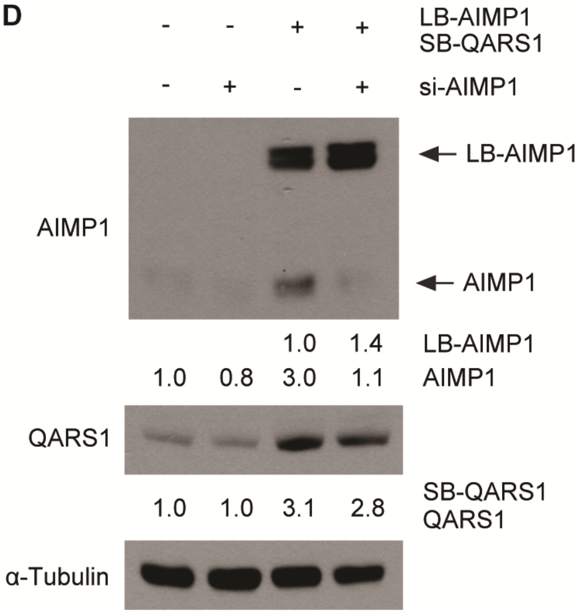
- - + + LB-AIMP1
SB-QARS1
- + - + si-AIMP1
AIMP1
LB-AIMP1
AIMP1
1.0 1.4 LB-AIMP1
1.0 0.8 3.0 1.1 AIMP1
QARS1
1.0 1.0 3.1 2.8 SB-QARS1
QARS1
α-Tubulin

E

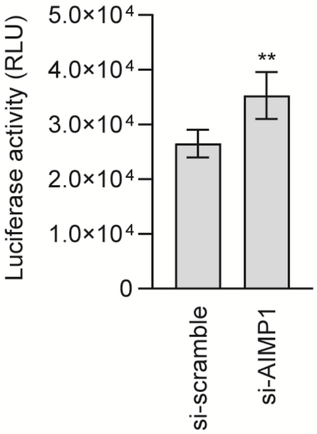

Luciferase activity (RLU)
5.0×10⁴
4.0×10⁴
3.0×10⁴
2.0×10⁴
1.0×10⁴
0
**
si-scramble
si-AIMP1

F

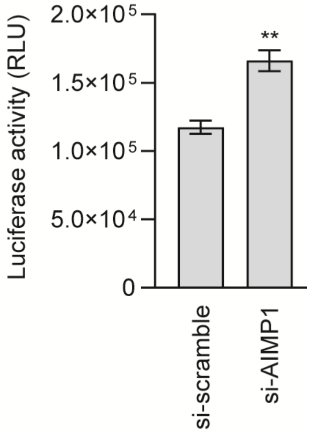

Luciferase activity (RLU)
2.0×10⁵
1.5×10⁵
1.0×10⁵
5.0×10⁴
0
**
si-scramble
si-AIMP1

G

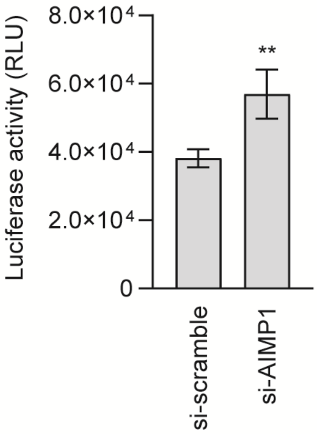

Luciferase activity (RLU)
8.0×10⁴
6.0×10⁴
4.0×10⁴
2.0×10⁴
0
**
si-scramble
si-AIMP1

H

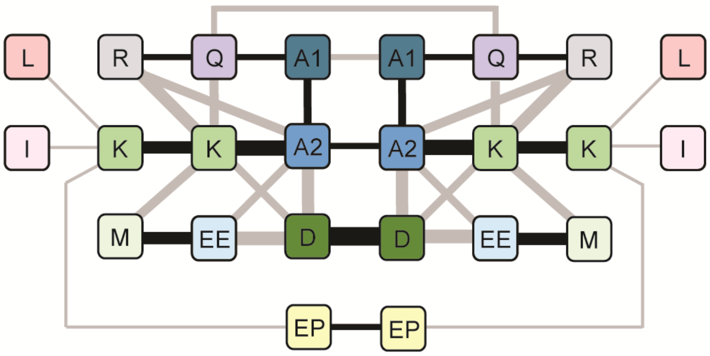

L R Q A1 A1 Q R L
I K K A2 A2 K K I
M EE D D EE M
EP EP

Figure 12 The steady-state configuration of the MSC was analyzed in pairwise interactions. (**A**) Representative pairs of each binary interaction were compared with each other at the same time. (**B-G**) Effect of siRNA-mediated knockdown of endogenous AIMP1 on the reporter signals. Protein levels were quantified compared to α-Tubulin. (**B**) Protein expression levels of the reporters (LB-AIMP1 and SB-AIMP1) and endogenous AIMP1. (**C**) Protein expression levels of the reporters (SB-AIMP1 and LB-AIMP2) and endogenous AIMP1 and AIMP2. (**D**) Protein expression levels of the reporters (LB-AIMP1 and SB-QARS1) and endogenous AIMP1 and QARS1. (**E**) The luminescent signals of LB-AIMP1:SB-AIMP1 with endogenous-AIMP1 knockdown (n = 9 per group; unpaired t test; **P < 0.0001; mean ± SEM). (**F**) The luminescent signals of SB-AIMP1:LB-AIMP2 with endogenous-AIMP1 knockdown (n = 9 per group; unpaired t test; **P < 0.0001; mean ± SEM). (**G**) The luminescent signals of LB-AIMP1:SB-QARS1 with endogenous-AIMP1 knockdown (n = 9 per group; unpaired t test; **P < 0.0001; mean ± SEM). (**H**) The steady-state configuration of the MSC; the thickness of connecting lines was weighted based on the luminescence intensities of (**A**). A1, AIMP1; A2, AIMP2; EE, EEF1E1; D, DARS1; EP, EPRS1; I, IARS1; K,

KARS1; L, LARS1; M, MARS1; Q, QARS1; R, RARS1.

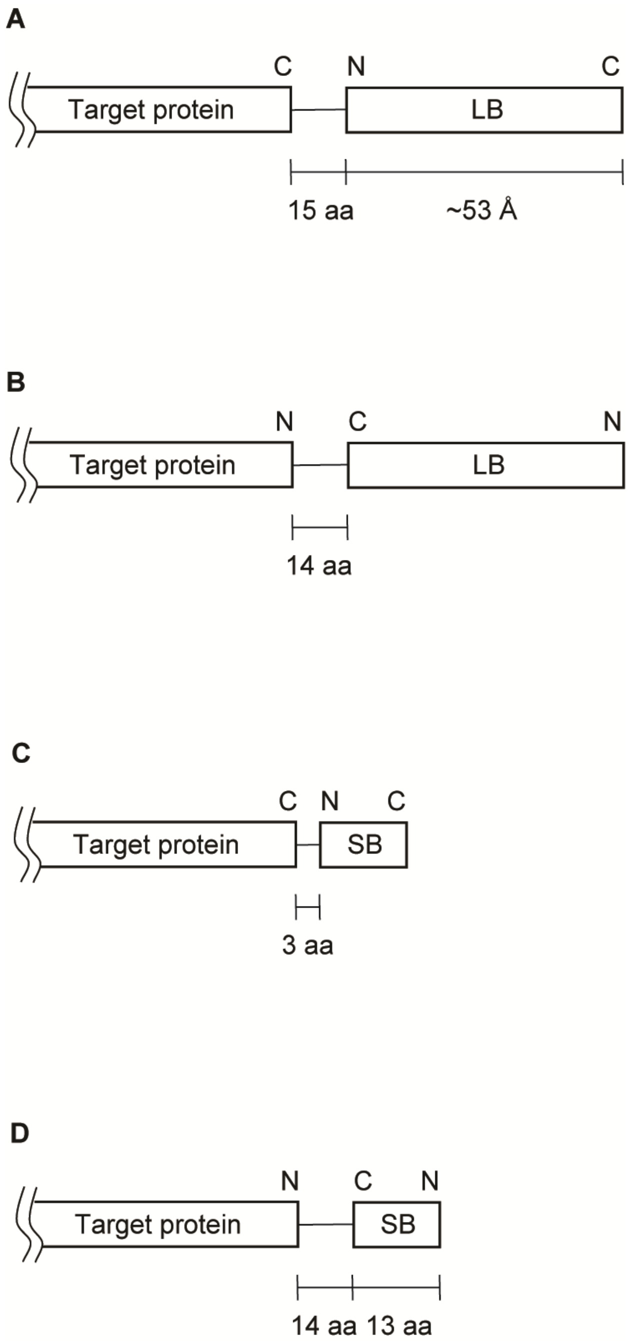
A
C
N
C
Target protein
LB
15 aa
~53 Å
B
N
C
N
Target protein
LB
14 aa
C
C
N
C
Target protein
SB
3 aa
D
N
C
N
Target protein
SB
14 aa
13 aa

Figure 13 The lengths of linker peptides and LB, SB tags of the reporter constructs. (**A**) The reporter construct with C-terminal LB tag (pBiT1.1-C [TK_LgBiT]). (**B**) The reporter construct with N-terminal LB tag (pBiT1.1-N [TK_LgBiT]). (**C**) The reporter construct with C-terminal SB tag (pBiT2.1-C [TK_SmBiT]). (**D**) The reporter construct with N-terminal SB tag (pBiT2.1-N [TK_SmBiT]).

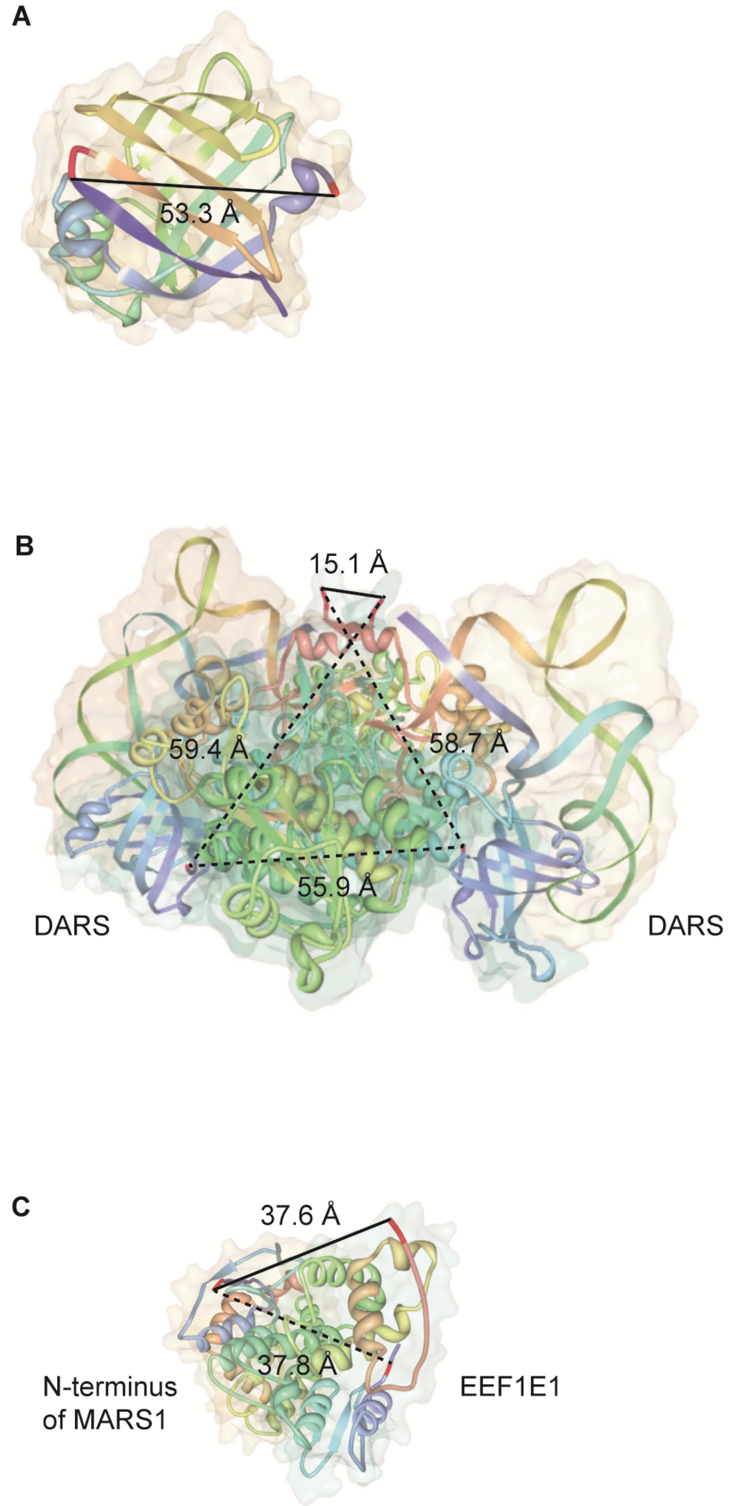
A
53.3 Å
B
15.1 Å
59.4 Å
58.7 Å
55.9 Å
DARS
DARS
C
37.6 Å
37.8 Å
N-terminus
of MARS1
EEF1E1

D

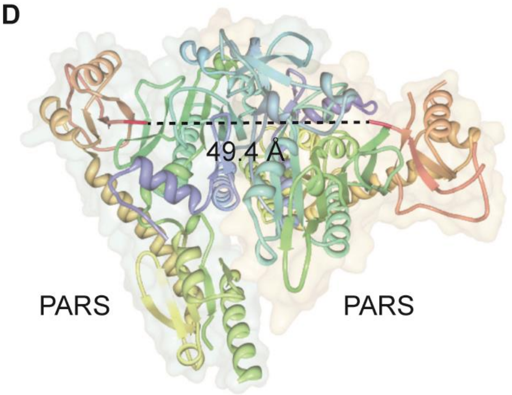
49.4 Å
PARS
PARS

E

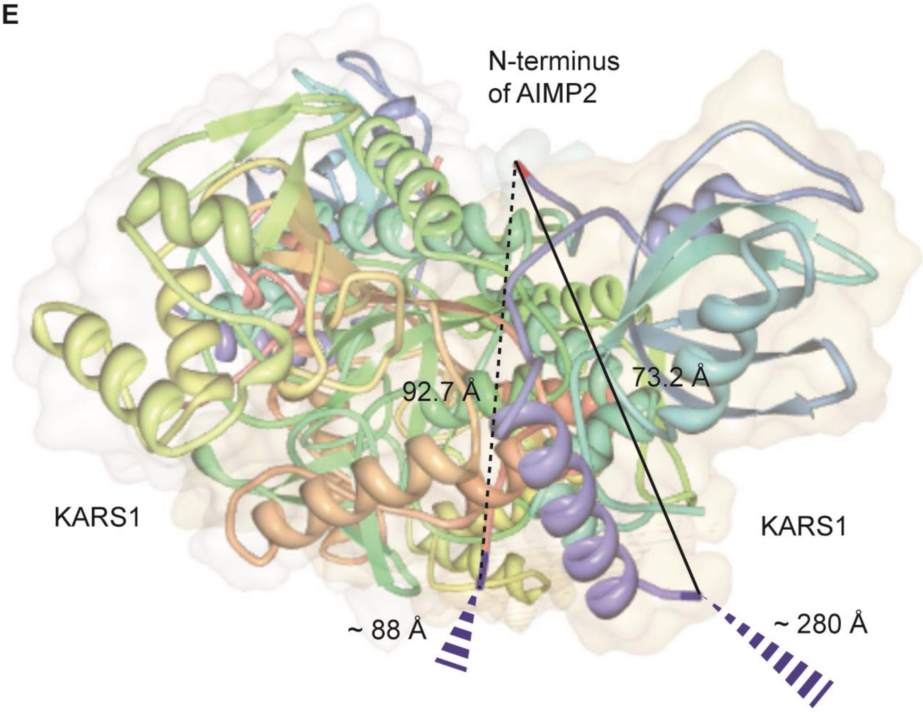
N-terminus
of AIMP2
92.7 Å
73.2 Å
KARS1
KARS1
~ 88 Å
~ 280 Å

F

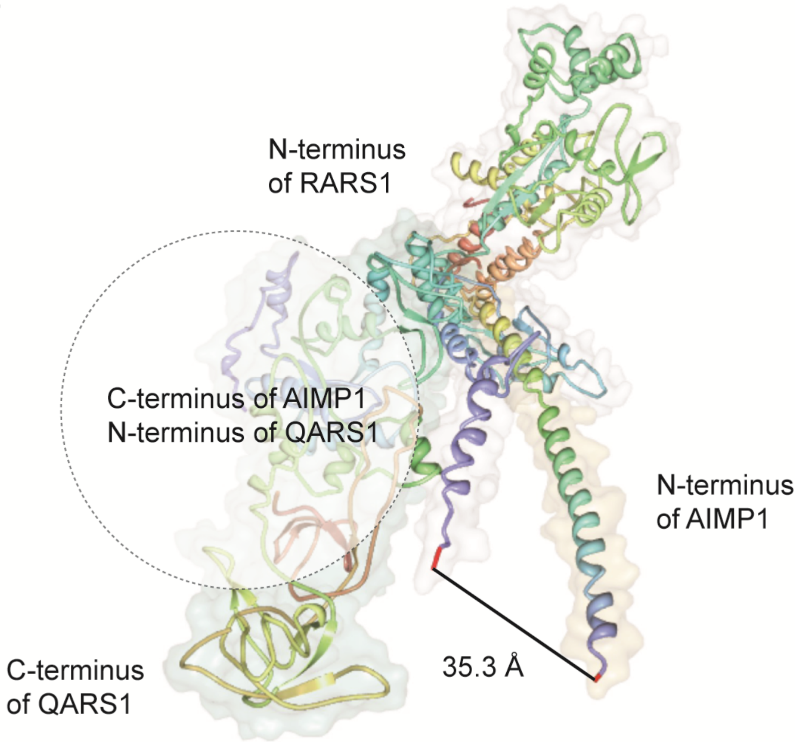

Figure 14 Validation of the reporter system by the sub-MSC structures. (**A**) The distance between the N- and C-termini of LB was measured for a crystal structure of the NanoLuc (PDB ID: 5IBO). (**B**) The distances between the N- and C-termini of the DARS homodimer were measured for a crystal structure of Escherichia coli DARS:yeast $tRNA^{Asp}$:aspartyl-adenylate complex (PDB ID: 1IL2). (**C**) The distances between the N-terminus of MARS1 and the N- and C-termini of EEF1E1 were measured for a crystal structure of human MARS1 N-terminal domain:EEF1E1:I3C complex (PDB ID: 4BVX). (**D**) The distance between the C-termini of the PARS homodimer was

measured for a crystal structure of human PARS:halofuginone:ATP analog complex (PDB ID: 4HVC). (**E**) The distances between the N-terminus of AIMP2 and the proximal regions of the N- and C-termini of KARS1 were measured for a crystal structure of human AIMP2 N-terminal domain:KARS1 complex (PDB ID: 4DPG). (**F**) The distance between the N-termini of AIMP1 and RARS1 was measured for a crystal structure of human AIMP1 N-terminal domain:RARS1 N-terminal domain:QARS1 C-terminal domain complex (PDB ID: 4R3Z). The expected localization of the AIMP1 C-terminal and QARS1 N-terminal regions was indicated as a dotted circle. The distances with steric bulk between the measured points were shown by dotted lines. Others without steric hindrance were indicated by solid lines.

A

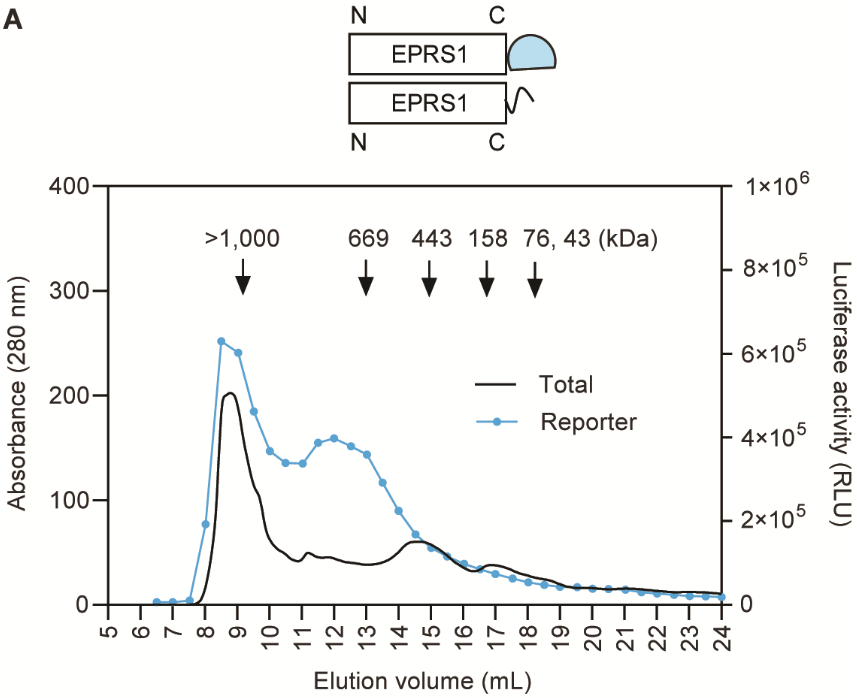
N
C
EPRS1
EPRS1
N
C
400
300
200
100
0
Absorbance (280 nm)
1×10^6
8×10^5
6×10^5
4×10^5
2×10^5
0
Luciferase activity (RLU)
>1,000
669
443
158
76, 43 (kDa)
Total
Reporter
5 6 7 8 9 10 11 12 13 14 15 16 17 18 19 20 21 22 23 24
Elution volume (mL)

B

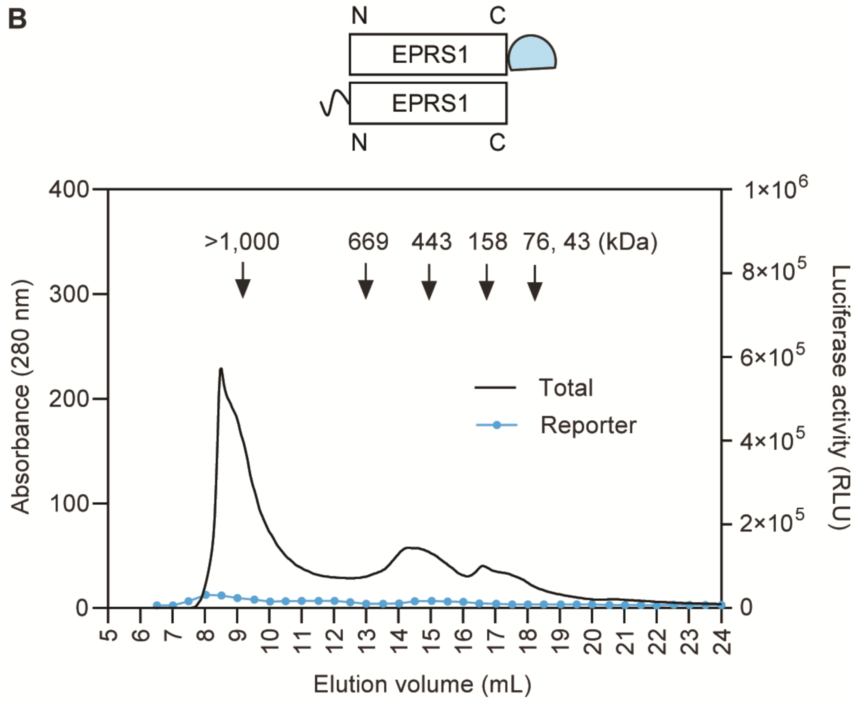
N
C
EPRS1
EPRS1
N
C
400
300
200
100
0
Absorbance (280 nm)
1×10^6
8×10^5
6×10^5
4×10^5
2×10^5
0
Luciferase activity (RLU)
>1,000
669
443
158
76, 43 (kDa)
Total
Reporter
5 6 7 8 9 10 11 12 13 14 15 16 17 18 19 20 21 22 23 24
Elution volume (mL)

C

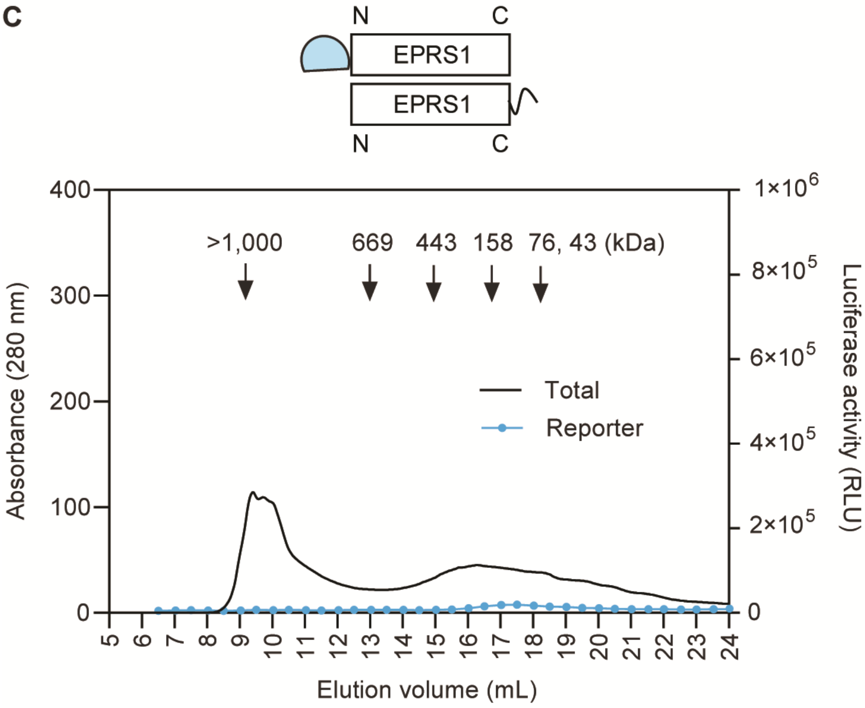
N
C
EPRS1
EPRS1
N
C
400
300
200
100
0
Absorbance (280 nm)
>1,000
669
443
158
76, 43 (kDa)
Total
Reporter
1×10^6
8×10^5
6×10^5
4×10^5
2×10^5
0
Luciferase activity (RLU)
5 6 7 8 9 10 11 12 13 14 15 16 17 18 19 20 21 22 23 24
Elution volume (mL)

D

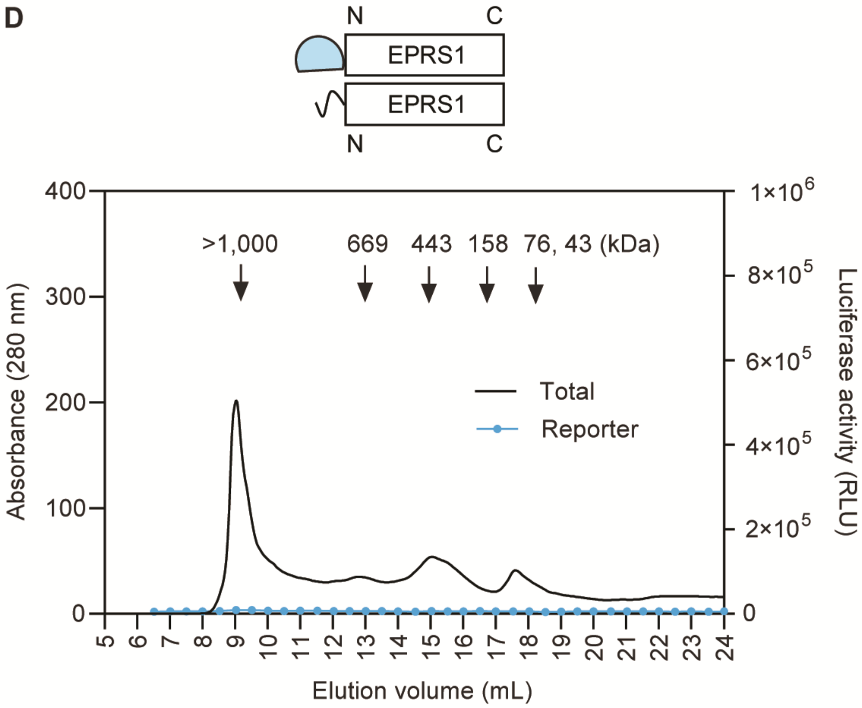
N
C
EPRS1
EPRS1
N
C
400
300
200
100
0
Absorbance (280 nm)
>1,000
669
443
158
76, 43 (kDa)
Total
Reporter
1×10^6
8×10^5
6×10^5
4×10^5
2×10^5
0
Luciferase activity (RLU)
5 6 7 8 9 10 11 12 13 14 15 16 17 18 19 20 21 22 23 24
Elution volume (mL)

E

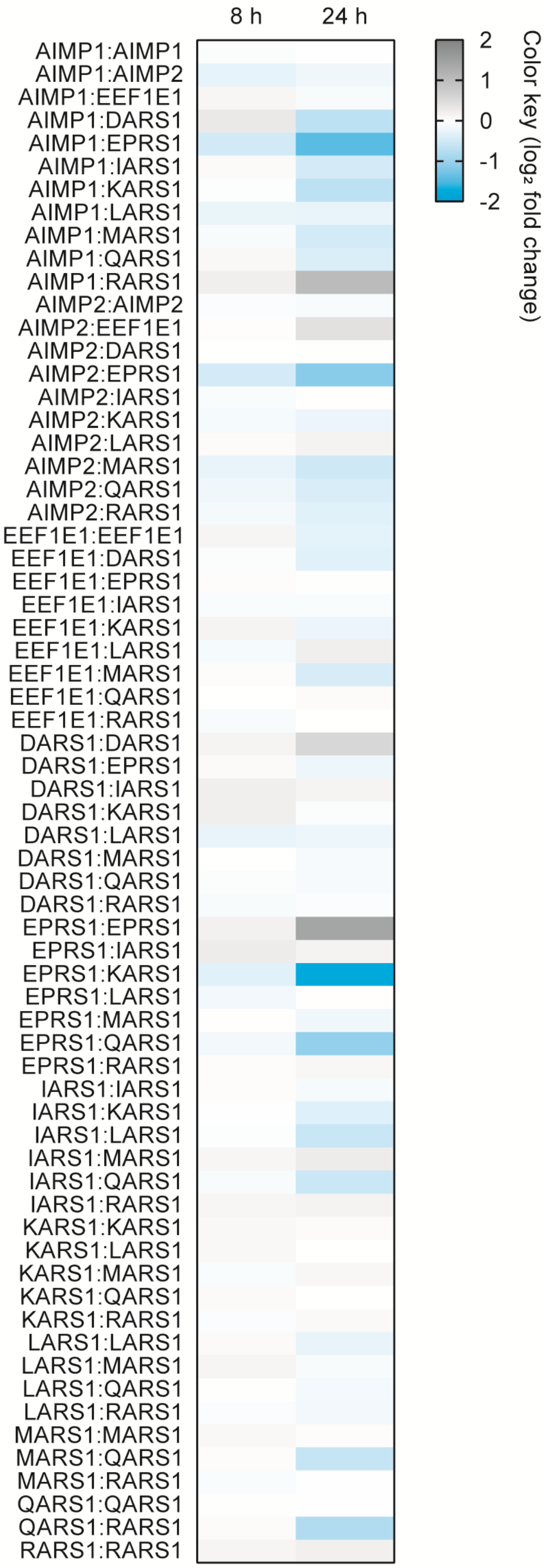
8 h
24 h
AIMP1:AIMP1
AIMP1:AIMP2
AIMP1:EEF1E1
AIMP1:DARS1
AIMP1:EPRS1
AIMP1:IARS1
AIMP1:KARS1
AIMP1:LARS1
AIMP1:MARS1
AIMP1:QARS1
AIMP1:RARS1
AIMP2:AIMP2
AIMP2:EEF1E1
AIMP2:DARS1
AIMP2:EPRS1
AIMP2:IARS1
AIMP2:KARS1
AIMP2:LARS1
AIMP2:MARS1
AIMP2:QARS1
AIMP2:RARS1
EEF1E1:EEF1E1
EEF1E1:DARS1
EEF1E1:EPRS1
EEF1E1:IARS1
EEF1E1:KARS1
EEF1E1:LARS1
EEF1E1:MARS1
EEF1E1:QARS1
EEF1E1:RARS1
DARS1:DARS1
DARS1:EPRS1
DARS1:IARS1
DARS1:KARS1
DARS1:LARS1
DARS1:MARS1
DARS1:QARS1
DARS1:RARS1
EPRS1:EPRS1
EPRS1:IARS1
EPRS1:KARS1
EPRS1:LARS1
EPRS1:MARS1
EPRS1:QARS1
EPRS1:RARS1
IARS1:IARS1
IARS1:KARS1
IARS1:LARS1
IARS1:MARS1
IARS1:QARS1
IARS1:RARS1
KARS1:KARS1
KARS1:LARS1
KARS1:MARS1
KARS1:QARS1
KARS1:RARS1
LARS1:LARS1
LARS1:MARS1
LARS1:QARS1
LARS1:RARS1
MARS1:MARS1
MARS1:QARS1
MARS1:RARS1
QARS1:QARS1
QARS1:RARS1
RARS1:RARS1
2
1
0
-1
-2
Color key (log_2 fold change)

Figure 15 Incorporation of the EPRS1 reporters into the endogenous MSC. (**A**) EPRS1-LB and EPRS1-SB, (**B**) EPRS1-LB and SB-EPRS1, (**C**) LB-EPRS1 and EPRS1-SB, and (**D**) LB-EPRS1 and SB-EPRS1 were overexpressed and subjected to size-exclusion chromatography. (**E**) The reporter system treated with interferon gamma (IFNγ) was used to detect the release of EPRS1 and accompanying changes of other binary interactions of the MSC.

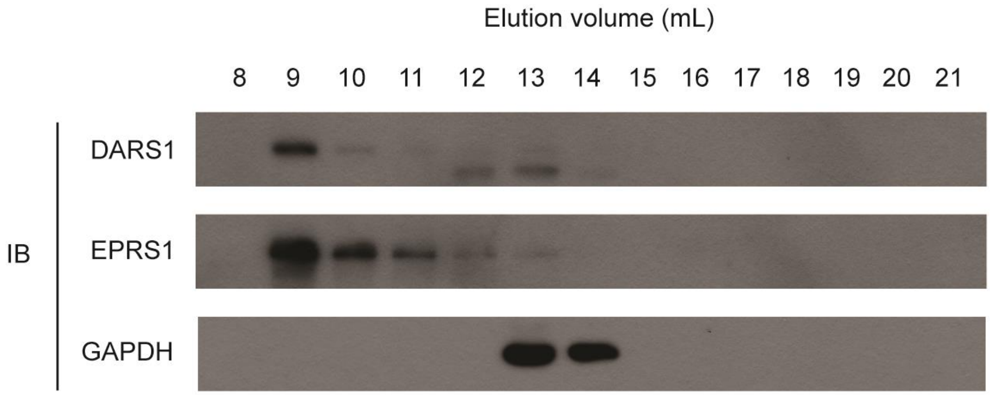

Figure 16 The endogenous DARS1 and GAPDH, and both endogenous and exogenous EPRS1 proteins of the chromatographic fractions were detected by immunoblotting. The signals from the exogenous EPRS1 reporters were detected as luminescence in **Figure 14*A***.

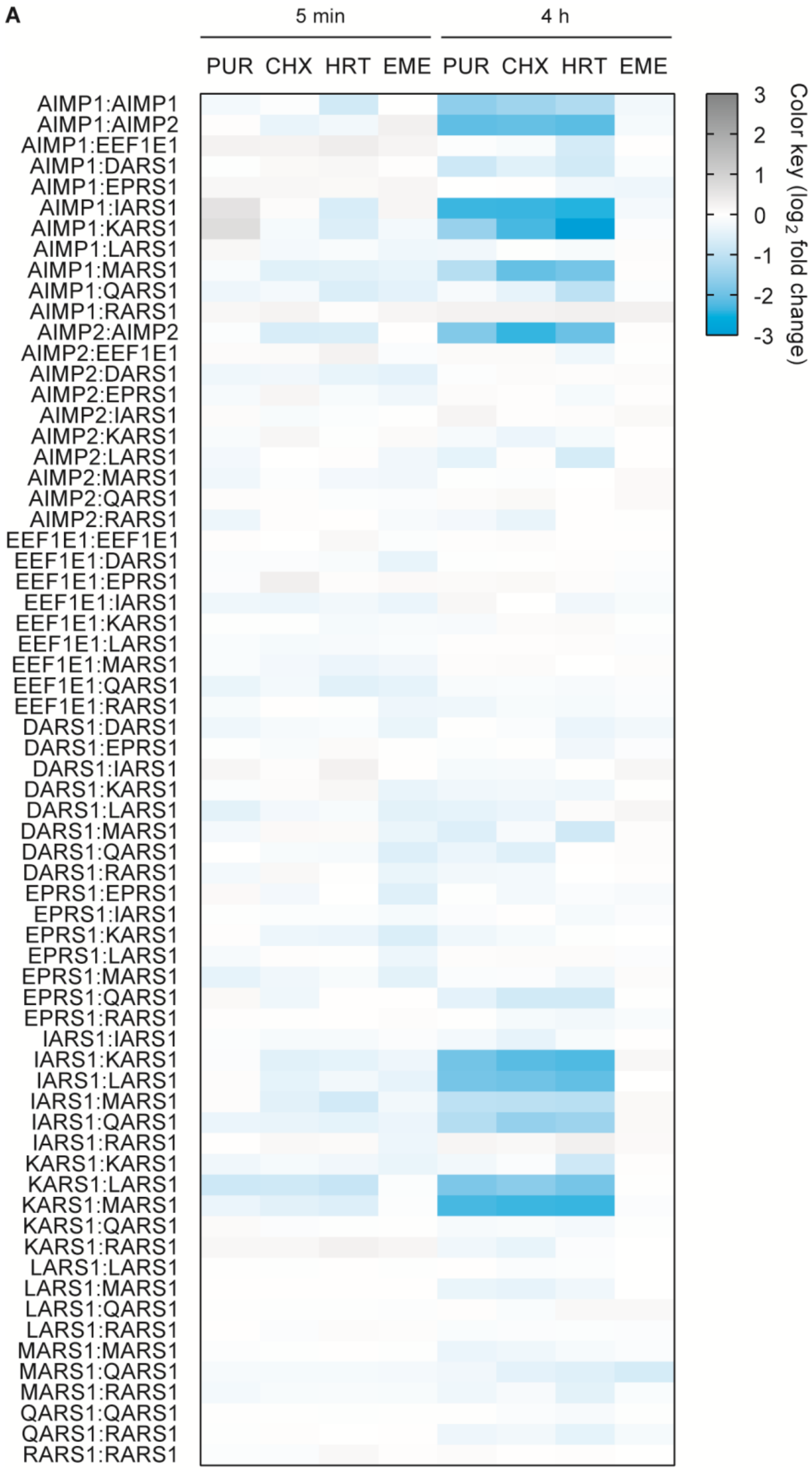
A
5 min
4 h
PUR CHX HRT EME PUR CHX HRT EME
AIMP1:AIMP1
AIMP1:AIMP2
AIMP1:EEF1E1
AIMP1:DARS1
AIMP1:EPRS1
AIMP1:IARS1
AIMP1:KARS1
AIMP1:LARS1
AIMP1:MARS1
AIMP1:QARS1
AIMP1:RARS1
AIMP2:AIMP2
AIMP2:EEF1E1
AIMP2:DARS1
AIMP2:EPRS1
AIMP2:IARS1
AIMP2:KARS1
AIMP2:LARS1
AIMP2:MARS1
AIMP2:QARS1
AIMP2:RARS1
EEF1E1:EEF1E1
EEF1E1:DARS1
EEF1E1:EPRS1
EEF1E1:IARS1
EEF1E1:KARS1
EEF1E1:LARS1
EEF1E1:MARS1
EEF1E1:QARS1
EEF1E1:RARS1
DARS1:DARS1
DARS1:EPRS1
DARS1:IARS1
DARS1:KARS1
DARS1:LARS1
DARS1:MARS1
DARS1:QARS1
DARS1:RARS1
EPRS1:EPRS1
EPRS1:IARS1
EPRS1:KARS1
EPRS1:LARS1
EPRS1:MARS1
EPRS1:QARS1
EPRS1:RARS1
IARS1:IARS1
IARS1:KARS1
IARS1:LARS1
IARS1:MARS1
IARS1:QARS1
IARS1:RARS1
KARS1:KARS1
KARS1:LARS1
KARS1:MARS1
KARS1:QARS1
KARS1:RARS1
LARS1:LARS1
LARS1:MARS1
LARS1:QARS1
LARS1:RARS1
MARS1:MARS1
MARS1:QARS1
MARS1:RARS1
QARS1:QARS1
QARS1:RARS1
RARS1:RARS1
3
2
1
0
-1
-2
-3
Color key (log2 fold change)

B

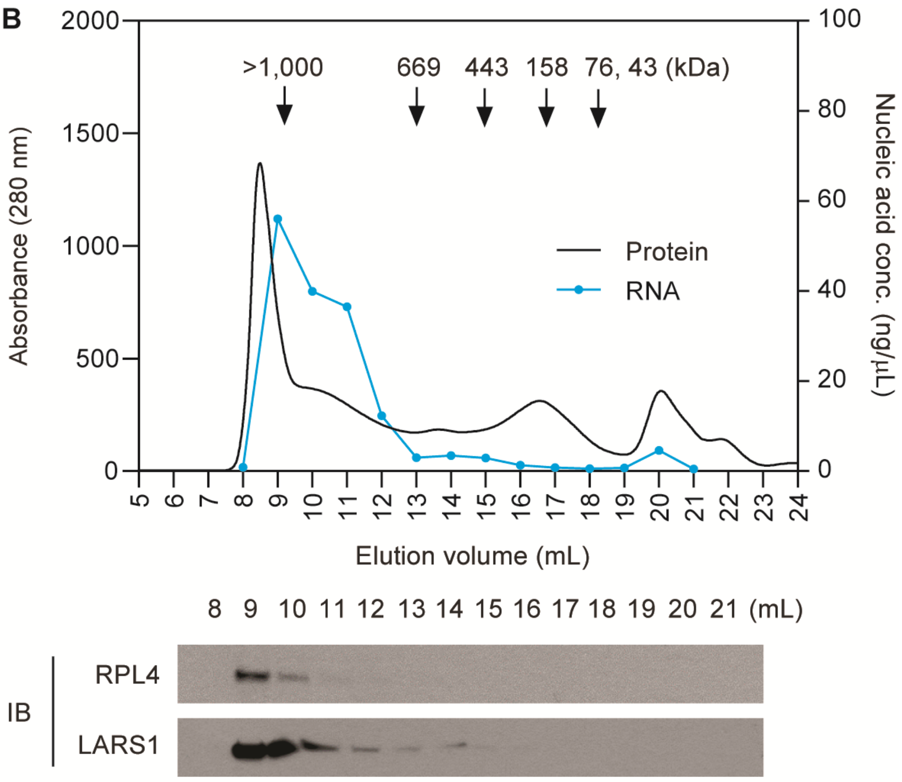

>1,000
669
443
158
76, 43 (kDa)
Absorbance (280 nm)
Nucleic acid conc. (ng/μL)
Protein
RNA
Elution volume (mL)
8 9 10 11 12 13 14 15 16 17 18 19 20 21 (mL)
IB
RPL4
LARS1

C

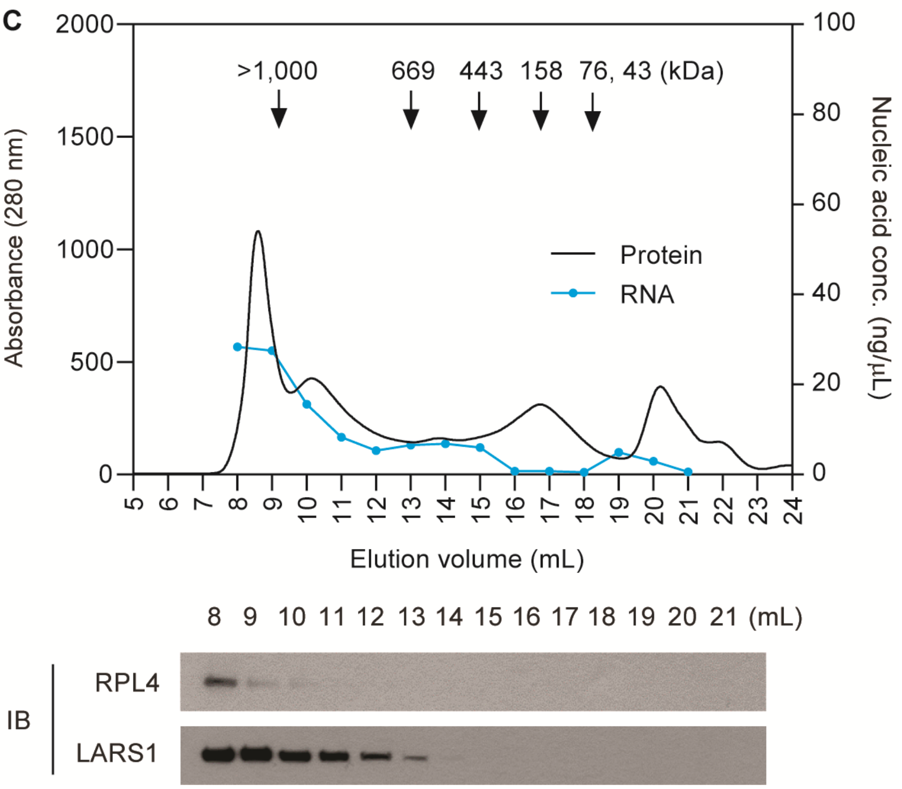

>1,000
669
443
158
76, 43 (kDa)
Absorbance (280 nm)
Nucleic acid conc. (ng/μL)
Protein
RNA
Elution volume (mL)
8 9 10 11 12 13 14 15 16 17 18 19 20 21 (mL)
IB
RPL4
LARS1

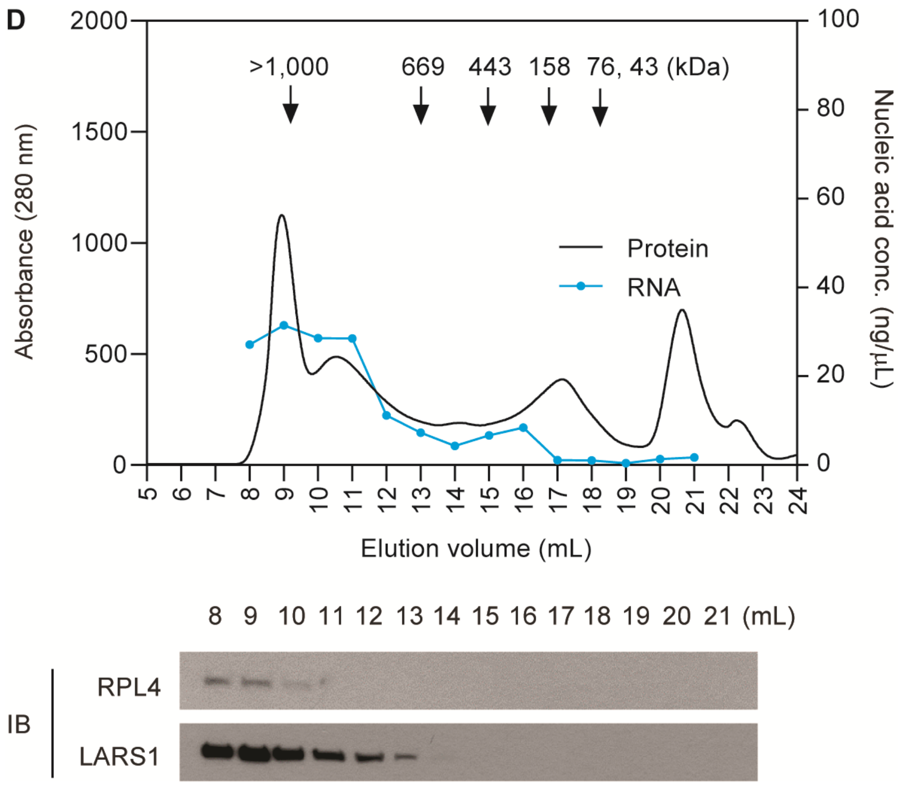

Figure 17 The sub-interactions of the MSC were weakened by ribosome inhibition. (**A**) The reporter system was treated with various ribosome inhibitors for 5 min and 4 h. PUR, puromycin; CHX, cycloheximide; HRT, harringtonine; EME, emetine. (**B-D**) Size-exclusion chromatography with puromycin. (**B**) Untreated control, (**C**) puromycin for 5 min, and (**D**) puromycin for 4 h.

Table 1 List of representative reporter pairs.

No.	Binary interaction	Reporter construct 1	Reporter construct 2
1	AIMP1:AIMP1	LB-AIMP1	SB-AIMP1
2	AIMP1:AIMP2	SB-AIMP1	LB-AIMP2
3	AIMP1:EEF1E1	AIMP1-LB	SB-EEF1E1
4	AIMP1:DARS1	AIMP1-LB	DARS1-SB
5	AIMP1:EPRS1	AIMP1-LB	EPRS1-SB
6	AIMP1:IARS1	LB-AIMP1	SB-IARS1
7	AIMP1:KARS1	LB-AIMP1	SB-KARS1
8	AIMP1:LARS1	LB-AIMP1	LARS1-SB
9	AIMP1:MARS1	LB-AIMP1	SB-MARS1
10	AIMP1:QARS1	LB-AIMP1	SB-QARS1
11	AIMP1:RARS1	AIMP1-SB	LB-RARS1
12	AIMP2:AIMP2	LB-AIMP2	SB-AIMP2
13	AIMP2:EEF1E1	AIMP2-SB	EEF1E1-LB
14	AIMP2:DARS1	LB-AIMP2	DARS1-SB
15	AIMP2:EPRS1	AIMP2-SB	EPRS1-LB
16	AIMP2:IARS1	LB-AIMP2	IARS1-SB
17	AIMP2:KARS1	LB-AIMP2	SB-KARS1
18	AIMP2:LARS1	SB-AIMP2	LB-LARS1
19	AIMP2:MARS1	SB-AIMP2	LB-MARS1
20	AIMP2:QARS1	SB-AIMP2	QARS1-LB
21	AIMP2:RARS1	SB-AIMP2	LB-RARS1
22	EEF1E1:EEF1E1	LB-EEF1E1	EEF1E1-SB
23	EEF1E1:DARS1	EEF1E1-LB	DARS1-SB
24	EEF1E1:EPRS1	LB-EEF1E1	EPRS1-SB
25	EEF1E1:IARS1	EEF1E1-SB	LB-IARS1
26	EEF1E1:KARS1	LB-EEF1E1	SB-KARS1
27	EEF1E1:LARS1	SB-EEF1E1	LB-LARS1
28	EEF1E1:MARS1	EEF1E1-LB	SB-MARS1
29	EEF1E1:QARS1	LB-EEF1E1	SB-QARS1
30	EEF1E1:RARS1	SB-EEF1E1	LB-RARS1
31	DARS1:DARS1	DARS1-LB	DARS1-SB

32	DARS1:EPRS1	DARS1-SB	EPRS1-LB
33	DARS1:IARS1	DARS1-LB	IARS1-SB
34	DARS1:KARS1	DARS1-SB	LB-KARS1
35	DARS1:LARS1	SB-DARS1	LB-LARS1
36	DARS1:MARS1	DARS1-LB	MARS1-SB
37	DARS1:QARS1	DARS1-LB	QARS1-SB
38	DARS1:RARS1	SB-DARS1	LB-RARS1
39	EPRS1:EPRS1	EPRS1-LB	EPRS1-SB
40	EPRS1:IARS1	EPRS1-SB	LB-IARS1
41	EPRS1:KARS1	EPRS1-SB	LB-KARS1
42	EPRS1:LARS1	EPRS1-SB	LB-LARS1
43	EPRS1:MARS1	SB-EPRS1	LB-MARS1
44	EPRS1:QARS1	EPRS1-SB	LB-QARS1
45	EPRS1:RARS1	SB-EPRS1	LB-RARS1
46	IARS1:IARS1	LB-IARS1	SB-IARS1
47	IARS1:KARS1	SB-IARS1	LB-KARS1
48	IARS1:LARS1	SB-IARS1	LB-LARS1
49	IARS1:MARS1	LB-IARS1	SB-MARS1
50	IARS1:QARS1	LB-IARS1	SB-QARS1
51	IARS1:RARS1	IARS1-SB	LB-RARS1
52	KARS1:KARS1	LB-KARS1	KARS1-SB
53	KARS1:LARS1	SB-KARS1	LB-LARS1
54	KARS1:MARS1	SB-KARS1	LB-MARS1
55	KARS1:QARS1	LB-KARS1	SB-QARS1
56	KARS1:RARS1	SB-KARS1	LB-RARS1
57	LARS1:LARS1	LB-LARS1	LARS1-SB
58	LARS1:MARS1	LB-LARS1	MARS1-SB
59	LARS1:QARS1	LB-LARS1	QARS1-SB
60	LARS1:RARS1	LARS1-SB	LB-RARS1
61	MARS1:MARS1	MARS1-LB	MARS1-SB
62	MARS1:QARS1	MARS1-SB	LB-QARS1
63	MARS1:RARS1	MARS1-SB	LB-RARS1
64	QARS1:QARS1	LB-QARS1	QARS1-SB
65	QARS1:RARS1	SB-QARS1	LB-RARS1
66	RARS1:RARS1	LB-RARS1	RARS1-SB

Part II

High-throughput screening for protein synthesis inhibitors targeting aminoacyl-tRNA synthetases

Graphical abstract

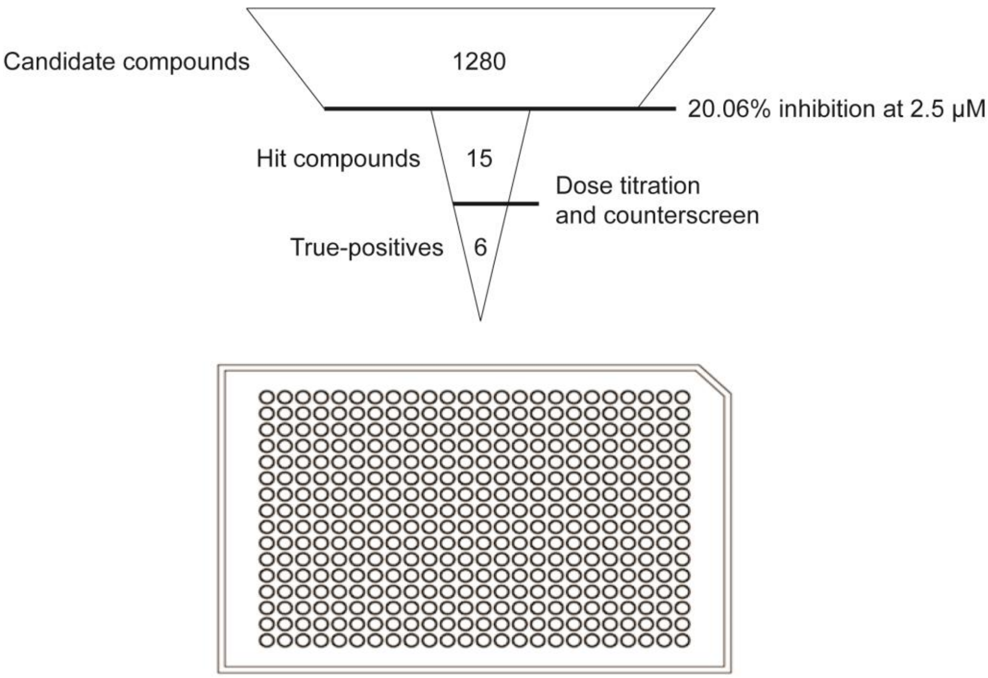

Highlights

- Conventional radioactive aminoacylation assay could be harmful for researcher's health.
- For high-throughput screening (HTS), therefore, a non-radioactive aminoacylation assay should be optimized.
- Aminoacyl-tRNA synthetases (ARSs) of rabbit reticulocyte closely resemble both the individual and complexed structures of human ARSs.
- A luminescence-based aminoacylation assay can give a high signal window and resolve the health and safety issue.
- The HTS-optimized *in vitro* translation system using the rabbit-reticulocyte lysate and the luminescence reporter showed great potential for larger screening campaigns.

Introduction

Dysregulation of translation is one of the most prominent characteristics of oncogenic transformation and tumor maintenance. Moreover, a large portion of signal transduction pathways altered in the cancer cells are ultimately integrated into the protein synthesis (Ruggero 2013). Therefore, therapeutic interventions targeting the translational machinery have been expected to overcome drug resistance from genomic heterogeneity which derived from the therapies for the upstream signaling pathways (Bhat, Robichaud et al. 2015). At times, a group of translation apparatuses become overabundant in cells, and the excess is hijacked by the cancer metabolism. For example, a surplus of eukaryotic translation initiation factor 4E (eIF4E), one of the cap-binding factors, is coupled with the translation of stress-response transcripts that are critical for survival of the cancer cells. Meanwhile, to accomplish its physiological role, only a half level of eIF4E expression is sufficient in the normal cells compared to the cancer cells (Truitt, Conn et al. 2015). Similarly, another elongation factor, eukaryotic translation initiation factor 5A (eIF5A), has a specific isotype which is highly expressed in various cancers, and drives tumorigenesis, malignant growth of the cancer cells, and epithelial-mesenchymal transition for increased cancer cell motility and metastasis (Wang, Guan et al. 2013).

The aminoacylation is another nonlimiting element of the translation. Firstly, tRNA, one of the substrates of the aminoacylation, outnumbers the binding capacity of the ribosomes (Chu and von der Haar 2012). And the aminoacylation of tRNAs occurs faster than depletion of the aminoacyl-tRNAs (Chu, Barnes et al. 2011). Meanwhile, other processes such as the transportation of tRNAs are under a tight control, through the tRNA supply network. Furthermore, most ARSs are upregulated in cancers, and their aminoacylation activity promotes the cancer progression: alanyl-tRNA synthetase 1 (AARS1), phenylalanyl-tRNA synthetase 1 (FARS1), glycyl-tRNA synthetase 1 (GARS1), threonyl-tRNA synthetase 1 (TARS1), histidyl-tRNA synthetase 1 (HARS1), tryptophanyl-tRNA synthetase 1 (WARS1), aspartyl-tRNA synthetase 1 (DARS1), and lysyl-tRNA synthetase 1 (KARS1) are dysregulated in prostate cancer, and methionyl-tRNA synthetase 1 (MARS1) in colon and non-small cell lung cancers (Kushner, Boll et al. 1976, Vellaichamy, Sreekumar et al. 2009, Lee, Kim et al. 2019).

The cancer cells also can take an advantage of mis-aminoacylation. For instance, MARS1 acylates noncognate tRNAs to scavenge reactive oxygen species (ROS) (Lee, Kim et al. 2014). However, under prolonged oxidative stress which is a common feature of the cancer cells, preferentially incorporated l-methionine may promote multiple random mutations on the protein level, that can lead to tumorigenesis (Burton and Jauniaux 2011).

Inhibitors for the ARSs have been used mainly as the antibacterial, antifungal, and antimalarial drugs (Tao, Wendler et al. 2000, Rock, Mao et al. 2007, Lv and Zhu 2012, Dewan, Reader et al. 2014, Novoa, Camacho et al. 2014). Since the first-generation natural ARS inhibitors had broad effects for the different species, most developments of them were based on chemical derivation to achieve the selectivity for the bacterial, fungal, malarial species and not for humans (Vondenhoff, Pugach et al. 2013, Zhao, Meng et al. 2014). Only recently, several studies have revisited borrelidin and halofuginone as the anticancer drug to target human ARSs (Reifsnider, Kaur et al. 2005, Habibi, Ogloff et al. 2012, Keller, Zocco et al. 2012, Sidhu, Miller et al. 2015, Kim, Sundrud et al. 2020). Hence, using the large-scale screening campaigns testing the ARSs against a wide variety of chemical entities will be beneficial and may broaden the availability of the anticancer drugs with novel candidates of the mammalian ARS inhibitors.

Previously, an *in vitro* translation system monitoring the selective inhibition of TARS1 was developed (Fang, Yu et al. 2015). In this study, the assay was optimized for the high-throughput screening (HTS) and demonstrated its potential applications to other ARSs. A library of pharmaceutically active compounds (LOPAC; n = 1280) was successfully screened with suitable Z and Z' values (0.79 ± 0.06 and 0.93 ± 0.02, respectively), thus proving the suitability of the assay for further screenings to find the novel mammalian ARS inhibitors. A counterscreen was also implemented, which discriminated between specific and nonspecific chemicals for the protein synthesis; it helped to select a set of inhibitors for follow-up target-identification studies.

Materials and methods

Primary *in vitro* translation assay

In the previous study, rabbit reticulocyte lysate (L416A (L4960), Promega) was diluted in buffer A (10 mg L^{-1} yeast total tRNA (10109509001, Roche, Basel, Switzerland), 80 mM potassium chloride (KCl; P9541, Sigma-Aldrich), 0.25 mM magnesium chloride ($MgCl_2$; M2670, Sigma-Aldrich), 0.1 mM spermidine (AC132740010, Thermo Fisher Scientific), and 50 μM amino-acid mixture (L4461, Promega) or buffer T (80 mM KCl, 0.25 mM $MgCl_2$, and 0.1 mM spermidine) by 10-fold. Firefly luciferase mRNA (L-6107, TriLink BioTechnologies, San Diego, CA, USA) was added at 20 mg L^{-1} as a template. The mixture was incubated at 30°C for 20 hours. Bright-glo luciferase assay system (E2620, Promega) was used for luminescence detection and all the procedures followed the manufacturer's manual (Promega).

HTS-optimized *in vitro* translation assay

The *in vitro* translation assay described above was modified to be compatible with HTS format. The buffer A was chosen as the diluent, and the final concentrations of yeast total tRNA and KCl were reduced to 3.53 mg L^{-1} and 25.20 mM, respectively. The amount of spermidine was adjusted to 63 µM, and the amino-acid mixture was excluded. 1.25 mg L^{-1} firefly luciferase mRNA was used as the template. The mixture of all the components, including the 10-fold diluted rabbit reticulocyte and test compounds, was incubated at 26.5°C for 25 hours in a gray 384-well microplate (6005310, PerkinElmer, Waltham, MA, USA). The luminescence signal was read by the Enhanced2 luminescence option (US Luminescence) of EnVision (EnVision, PerkinElmer).

Counterscreen

For the counterscreen, the mixture of 3.53 mg L^{-1} yeast total tRNA, 25.20 mM KCl, 0.25 mM $MgCl_2$, 63 µM spermidine, 1.25 mg L^{-1} firefly luciferase mRNA, and 10-fold diluted rabbit reticulocyte lysate was incubated at 26.5°C for 25 hours. At that time (i.e., when the reaction was already completed), the compounds were added right before the step of luciferase substrate addition and subsequently read. All other procedures were kept the same as in the HTS-optimized *in vitro* translation assay.

Data processing

All parameters were calculated with the GraphPad Prism 6.02 suite of programs (GraphPad Software) or Scripps internal database software (Symyx, Santa Clara, CA, USA).

Results

Assay principle

To maximize the system's efficiency, each step in the primary *in vitro* translation assay was optimized individually. When titrating the firefly luciferase mRNA from 0.04 to 20 mg L^{-1}, the luciferase activity increased fourfold when the concentration was diluted 16-fold (**Figure 18*A***). The data points adjacent to the final concentration, 1.25 mg L^{-1}, yielded steep slopes, suggesting that the efficiency of *in vitro* translation was highly dependent on the optimal number of target molecules (e.g. ~1010 molecules of the firefly luciferase mRNA).

KCl, $MgCl_2$, and spermidine were the components with electric charges in the dilution buffer A. They were tested in wide ranges of concentration (at 1.6–100 mM, 0.02–1.3 mM, and 8–500 µM, respectively), and all three factors were affirmed as indispensable for the assay system (**Figure 18*B-D***). The initial concentrations were (or were near) optimal condition; slight changes were made for KCl (from 80 mM to 32 mM) and spermidine (from 0.1 mM to 33 µM), but not for $MgCl_2$. Furthermore, to examine whether other cation concentrations had potential for signal improvement, several monovalent (Na^+, Li^+, and Cs^+) and divalent (Ca^{2+}, Mn^{2+}, Ni^{2+}, and Cd^{2+}) cations were supplemented in forms of chloride salt in addition to KCl and $MgCl_2$. These factors showed signal disruption instead of enhancement, however, and the patterns were correlated with their charges (**Figure 18*E***); the ionic pool of KCl and $MgCl_2$ already may be sufficient to the system. Surprisingly, in further test at which K^+ and Mg^{2+} were excluded, none of the combinations of monovalent and divalent cations produced a signal (data not shown).

The previous concentration of yeast total tRNA tested was found to generate a downhill slope of a concentration-signal curve and was adjusted by threefold to fall into a plateau (**Figure 18*F***).

The temperature was another determinant for the efficient protein synthesis, and a range between 20 and 30°C produced the highest signal–background ratio (S/B) (**Figure 18*G***).

When the incubation time was lengthened, the luciferase activity kept increasing linearly throughout 3 days of measurement (**Figure 18*H***), followed by a sharp drop in signal to the level of null at day 4. This may be due to the longtime exposure of bare cellular components *in vitro*. Therefore, the Z’ factor, coefficient of variation (%CV), and S/B value were considered to determine an appropriate time length for incubation. In principle, the incubation time can be scaled to preference because all the *Z'* values calculated were greater than the threshold of a robust HTS, > 0.5. The %CV value was, however, the lowest at 9.5 hours and stayed stable between 24.5 and 40 hours. Thus, 25 hours was chosen for the convenience of operation (**Table 2**).

The additional supplement of amino-acid mixture of the buffer A was withheld to allow for high sensitivity toward amino-acid analogs.

Selection of compound for positive control

Prior to the compound addition, dimethyl sulfoxide (DMSO) tolerance was examined; DMSO is the most common solvent of drug libraries (**Figure 19*A***). Since there was a small affect seen in the range between 1 and 3% along with the highest signal intensity, 2% was chosen to allow room for minor mechanical errors that may arise from dispensing or pinning.

5'-O-[(L-methionyl)-sulfamoyl]adenosine (MetSA) has an unmodified amino terminus that can compete with l-methionine for the catalytic pocket of MARS1 (**Figure 19*B***). From this structure-based hypothesis, MetSA was expected to perturb the translational activity of MARS1. And the optimized assay system was inhibited by

MetSA dose-dependently at nanomolar scale (**Figure 19*C***).

To further verify sensitization of the system, IC_{50} values of MetSA from different compositions of the four individual factors were compared to each other. Separate adjustments of yeast total tRNA (**Figure 18*F*** and **19*C***) and KCl (**Figure 18*B*** and **19*C***) to their most favored concentrations for the signal intensity made the assay less sensitive to MetSA than the primary setup. When both yeast total tRNA and KCl were altered at the same time, the basal level of signal increased even with the high doses of MetSA. In contrast, those of spermidine (**Figure 18*D*** and **19*C***) and firefly luciferase mRNA (**Figure 18*A*** and **19*C***) improved the responsiveness of the assay. Furthermore, the combination of spermidine and firefly luciferase mRNA refinements gave better responsiveness than the two components individually did. In this case, however, the luciferase activity at the low concentrations of MetSA became unstable; this may be due to the lack of balance between the buffered ions. Surprisingly, the simultaneous optimization of all four factors enhanced not only the signal window but also the sensitivity of the system, while maintaining the signal stability at the low MetSA concentrations (**Figure 19*C***).

The blockage of the translation induced by MetSA was restored by exogenous addition of l-methionine, but not by 19 other amino acids, supporting the presumption that the inhibition is due to the specific interference of MARS1 (**Figure 19*D***). Additionally, l-methionine recovered the protein synthesis in the dose-dependent manner (**Figure 19*E***).

Furthermore, I hypothesized that an anti-MARS1 antibody directly depriving MARS1 protein could further validate the specificity of the system. However, currently available mouse and rabbit immunoglobulins (IgGs) themselves showed nonspecific inhibitory effects on the assay (data not shown). Thus, the amino-acid analog was chosen as the direct positive control for the further screening process.

Pilot screen of the LOPAC collection

The HTS readiness of the assay was confirmed by pilot screening of the LOPAC library (n = 1280) in the 384-well format. Before the pilot screen, it was made sure that concentration-response curves and the IC_{50} values generated from benchtop and automated formats were overlapping (**Figure 20*A***). The concentration of MetSA for the high-inhibition control was set as 3.16 μM to achieve complete (> 97%) inhibition. The low-inhibition control wells received DMSO only. The

LOPAC compounds were dispensed nominally as 2.5 μM final, done with 10 nL pinned from the 2.5 mM compound stock. To match up the final concentration of DMSO at 2%, additional DMSO was supplemented in the dilution buffer. Statistics from the LOPAC pilot screen remained steady, indicating an excellent assay with Z values = 0.79 ± 0.06, Z' values = 0.93 ± 0.02, and S/B = 132.0 ± 2.2 among all plates (**Figure 20*B***). Reproducibility of individual compounds was also high enough, as the coefficient of determination (R squared; R^2) from the scatterplots of replicated measurements was > 0.9 (R^2 = 0.9887; **Figure 20*C***). Preliminary hit-identification cutoff was set as the sum of the mean and three times the standard of all samples tested (cutoff = 20.06% inhibition), which identified 1.17% of compounds from the LOPAC collection (*n* = 15) showing greater response than the cutoff (**Figure 20*D***).

Counterscreen and hit classification

The preliminary hits were subjected to both serial dilution and retesting with the primary assay and the counterscreen in parallel. The primary assay again showed consistent Z' and S/B values (Z' = 0.84 ± 0.01 and S/B = 23.8 ± 0.9, and Z' = 0.91 ± 0.02 and S/B = 26.8 ± 0.4, respectively) in the same HTS format. In the serial dilution with starting concentration of 8.5 μM, 13% of the compounds failed to show dose-dependent inhibition and were excluded from further analysis (*n* = 2) (**Figure 21*A***, group A). And the counterscreen effectively eliminated false-positive compounds from the rest, which, as tested, identified compounds that interrupted the activity of luciferase itself or quenched luminescence. As a result, 47% of the preliminary hits were identified as false-positive compounds (*n* = 7) (**Figure 21*A***, group B). The remaining 40% (*n* = 6) showed great selectivity over the counterscreen (**Figure 21*B***).

All six true-positive compounds are known to be directly or remotely related to part of protein translation. Emetine dihydrochloride hydrate ((2S,3R,11bS)-2-[[(1R)-6,7-dimethoxy-1,2,3,4-tetrahydroisoquinolin-1-yl]methyl]-3ethyl-9,10-dimethoxy-2,3,4,6,7,11b-hexahydro-1H-benzo[a]quinolizine;hydrate;hydrochloride), the most potent one, is the well-known protein-synthesis inhibitor targeting the ribosomal 40S subunit (Jimenez, Carrasco et al. 1977, Meijerman, Blom et al. 1999). IC_{50} of emetine from the system was at the nanomolar concentration, proving that the assay is a promising platform for further screening campaigns for the potential protein-synthesis inhibitors. NSC 95397 (2,3-bis(2-hydroxyethylsulfanyl)naphthalene-1,4-dione) and DMNQ (2,3-dimethoxynaphthalene-1,4-dione) share a 1,4-naphthoquinone moiety which causes oxidative stress and leads to global suppression of protein-synthesis initiation (Shenton, Smirnova et al. 2006, Liu, Wise et al. 2008, Kumar, Aithal et al. 2009, Klotz, Hou et al. 2014). β-Lapachone (2,2-dimethyl-3,4-dihydrobenzo[h]chromene-5,6-dione) resembles a part of 1,4-naphthoquinone structure. Interestingly, these three compounds with the 1,4-naphthoquinone scaffold showed similar IC_{50} values in the system. Other two compounds, Ruthenium red (azane;ruthenium(2+); hexachloride;dehydrate) and propylpyrazole triol (4-[2,3-bis(4-hydroxyphenyl)-4-propyl1H-pyrazol-5-ylidene]cyclohexa-2,5-dien-1-one), regulates cytoplasmic polyadenylation element binding protein (CPEB)-dependent mRNA translation and controls the protein translation through microRNAs (miRNAs), respectively (Wells, Richter et al. 2000, Atkins, Nozaki et al. 2004, Adams, Furneaux et al. 2007, Goljanek-Whysall, Pais et al. 2012). The structure, IC_{50}, hill slope values, and general activity information of the true-positive compounds are listed in **Table 3**.

Discussion

The HTS-optimized *in vitro* translation system successfully identified the familiar protein-synthesis inhibitors as the true-positive compounds. Among them, several compounds shared similar structural properties, suggesting that the assay was ready to pick up a structure–activity relationship (SAR) from the chemical entities. The system can be readily transfer to larger screening campaigns, based on the stable QC parameters throughout the primary screen, the serial dilutions, and the counterscreen, all performed in the same format. With a proper target-validation approach, this assay would provide a powerful screening platform for finding the novel ARS inhibitors.

Figures and tables

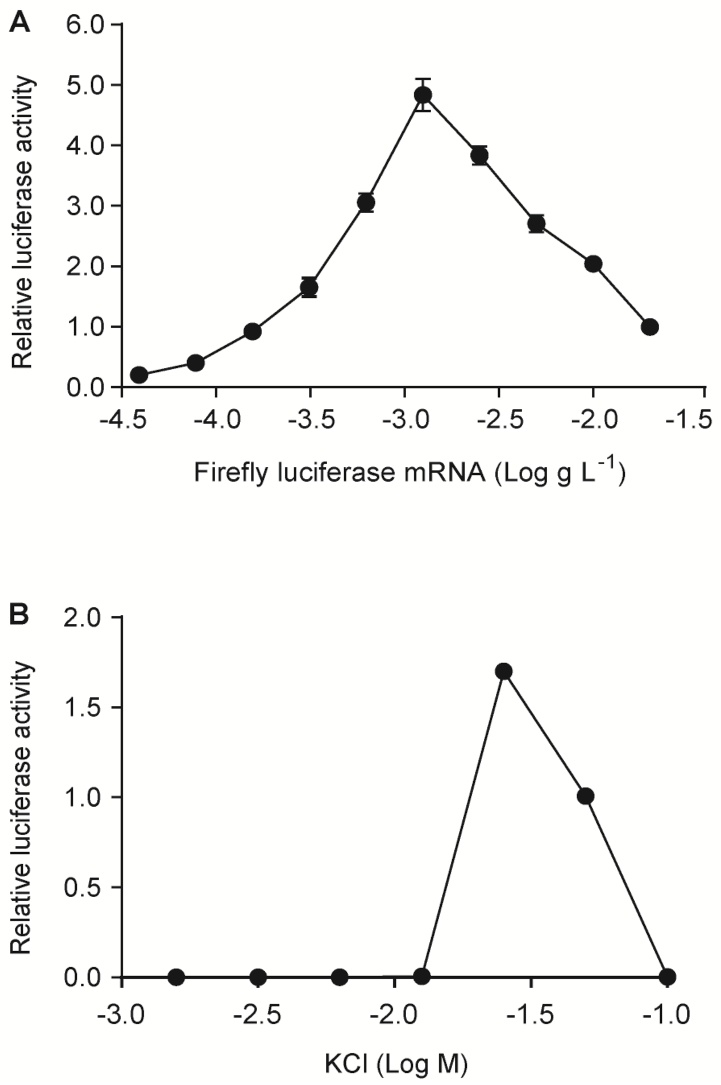

C

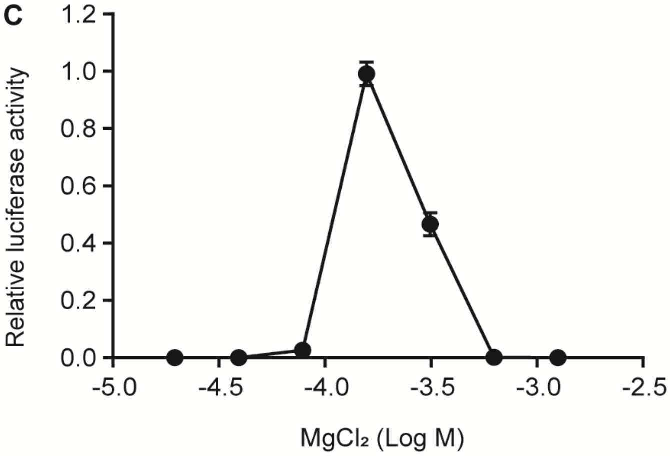

Relative luciferase activity
1.2
1.0
0.8
0.6
0.4
0.2
0.0
-5.0
-4.5
-4.0
-3.5
-3.0
-2.5
MgCl₂ (Log M)

D

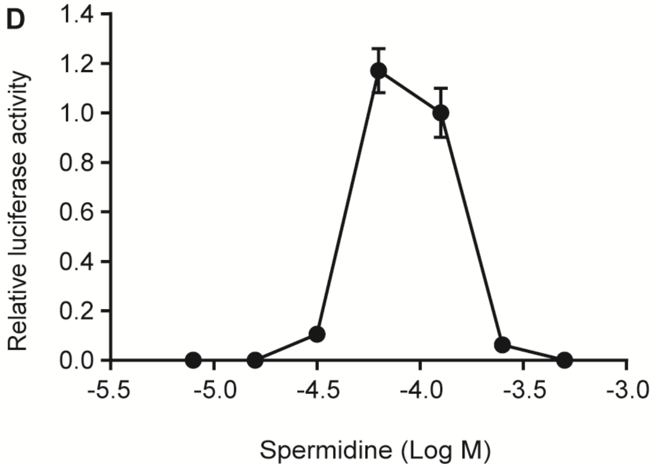

Relative luciferase activity
1.4
1.2
1.0
0.8
0.6
0.4
0.2
0.0
-5.5
-5.0
-4.5
-4.0
-3.5
-3.0
Spermidine (Log M)

E

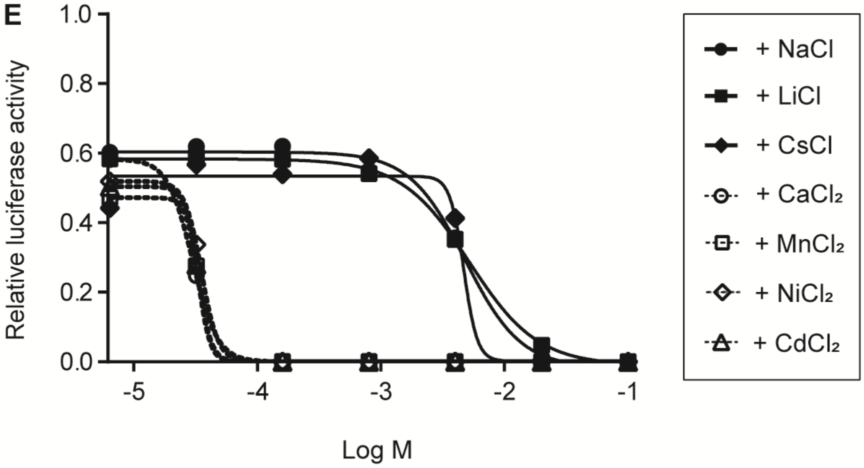

Relative luciferase activity
1.0
0.8
0.6
0.4
0.2
0.0
-5
-4
-3
-2
-1
Log M
+ NaCl
+ LiCl
+ CsCl
+ CaCl₂
+ MnCl₂
+ NiCl₂
+ CdCl₂

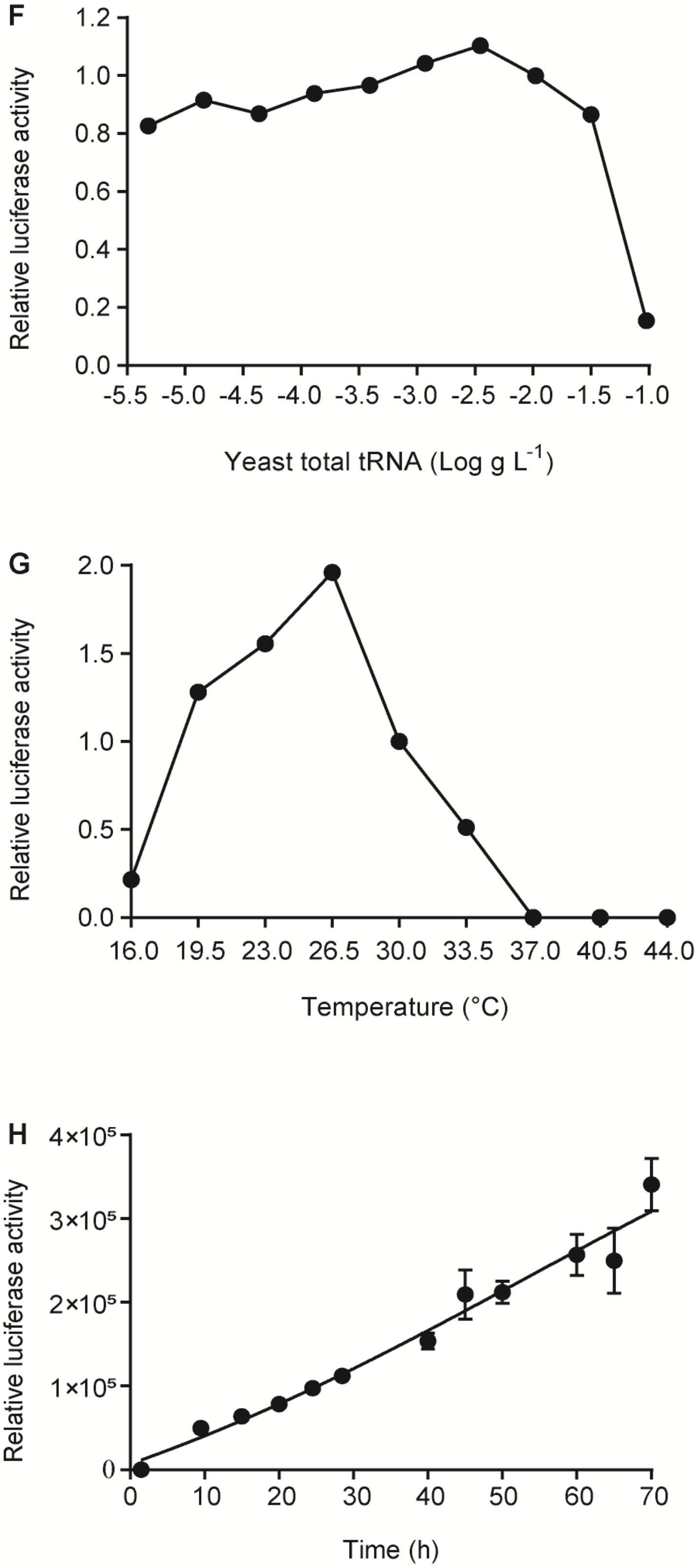
F
Relative luciferase activity
1.2
1.0
0.8
0.6
0.4
0.2
0.0
-5.5 -5.0 -4.5 -4.0 -3.5 -3.0 -2.5 -2.0 -1.5 -1.0
Yeast total tRNA (Log g L^{-1})
G
Relative luciferase activity
2.0
1.5
1.0
0.5
0.0
16.0 19.5 23.0 26.5 30.0 33.5 37.0 40.5 44.0
Temperature (°C)
H
Relative luciferase activity
4×10⁵
3×10⁵
2×10⁵
1×10⁵
0
0 10 20 30 40 50 60 70
Time (h)

Figure 18 Optimization of the *in vitro* translation system for an automated high-throughput screening (HTS) format. The optimal concentrations of (**A**) firefly luciferase mRNA, (**B**) KCl, (**C**) $MgCl_2$, (**D**) spermidine, and (**F**) yeast total tRNA were determined. All the original concentrations of each component fell into the range of serial dilution. When the exact concentration was not included in the experiment, the approximate point (50 mM KCl and 0.2 mM $MgCl_2$) was considered as the reference value for the relative-difference calculation. (**E**) NaCl, LiCl, CsCl, $CaCl_2$, $MnCl_2$, $NiCl_2$, and $CdCl_2$ were added for various concentrations in the presence of 32 mM KCl and 33 μM $MgCl_2$. The assay conditions were also tested for (**G**) temperature and (**H**) length of time. The experiments were repeated for three times.

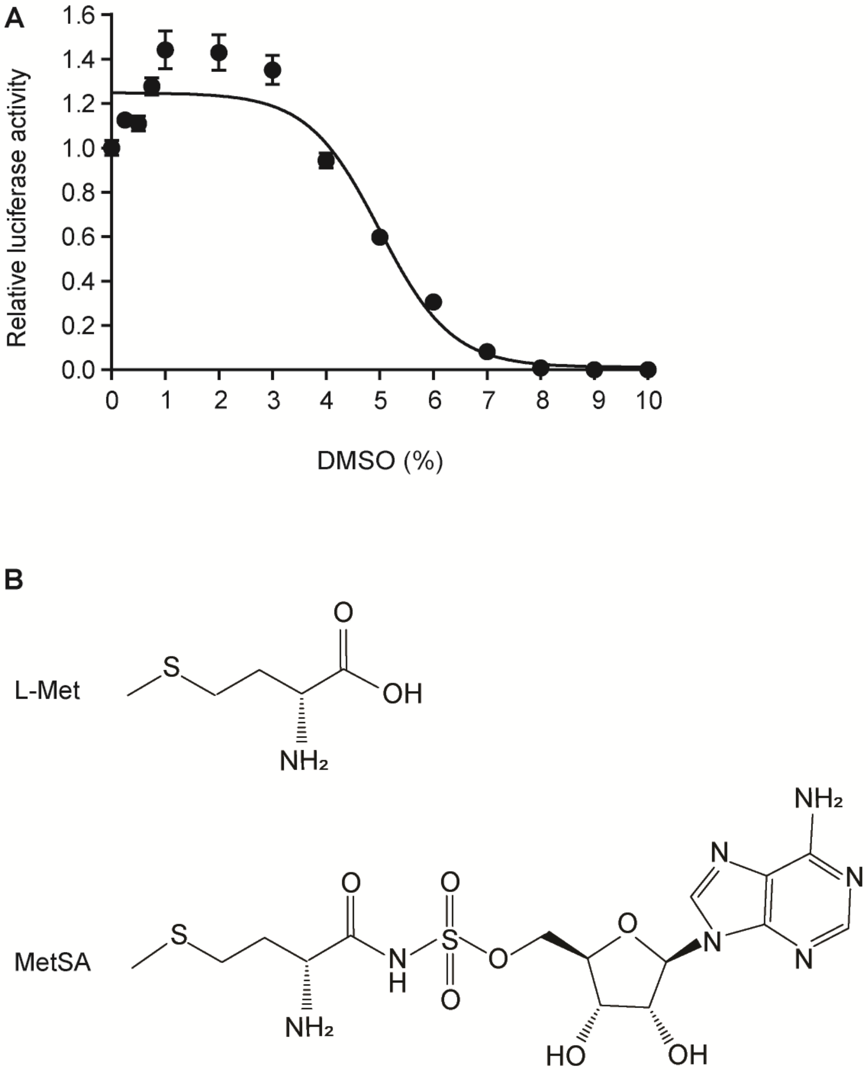
A
B
Relative luciferase activity
DMSO (%)
0.0
0.2
0.4
0.6
0.8
1.0
1.2
1.4
1.6
0
1
2
3
4
5
6
7
8
9
10
L-Met
MetSA

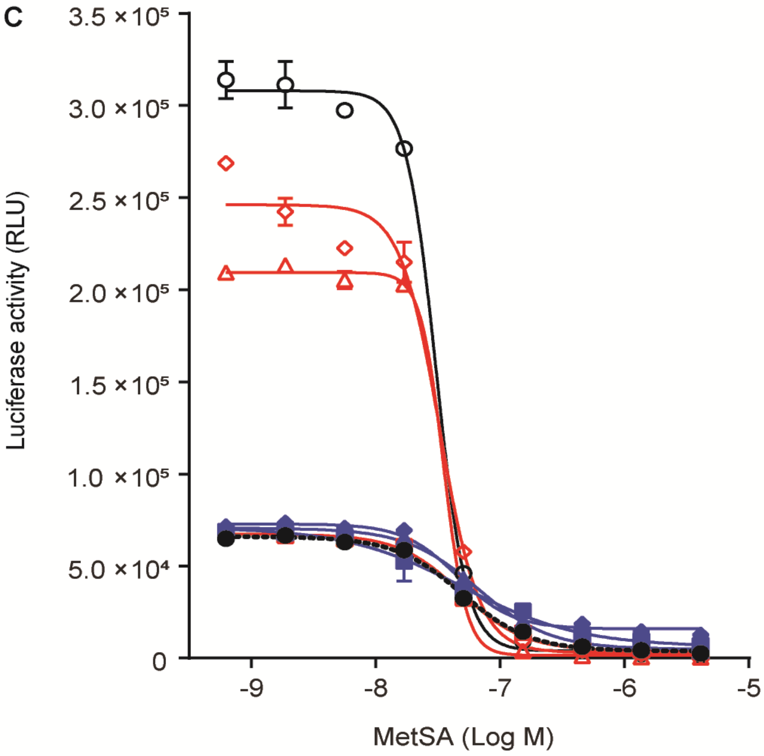

	Yeast total tRNA	KCl	Spermidine	Firefly luciferase mRNA	IC_{50} (M)
●(black, dotted)	P	P	P	P	4.974e-008
■(blue)	H	P	P	P	5.000e-008
▲(blue)	P	H	P	P	6.627e-008
□(red)	P	P	H	P	4.868e-008
△(red)	P	P	P	H	3.507e-008
◆(blue)	H	H	P	P	4.571e-008
◇(red)	P	P	H	H	3.273e-008
○(black)	H	H	H	H	3.069e-008

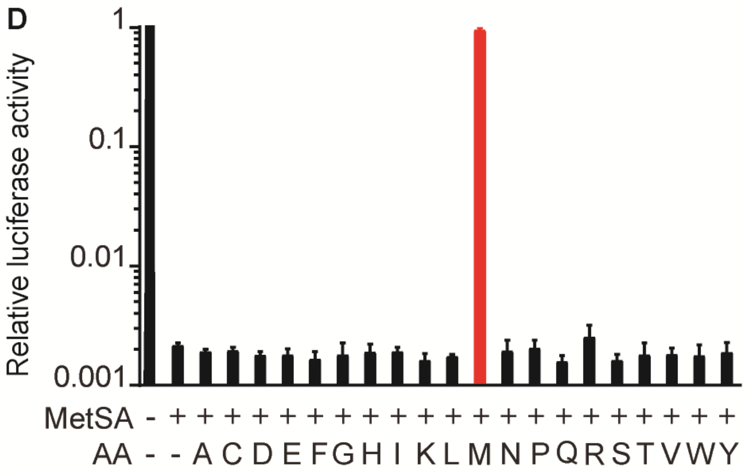
D
Relative luciferase activity
1
0.1
0.01
0.001
MetSA - +
AA - - A C D E F G H I K L M N P Q R S T V W Y

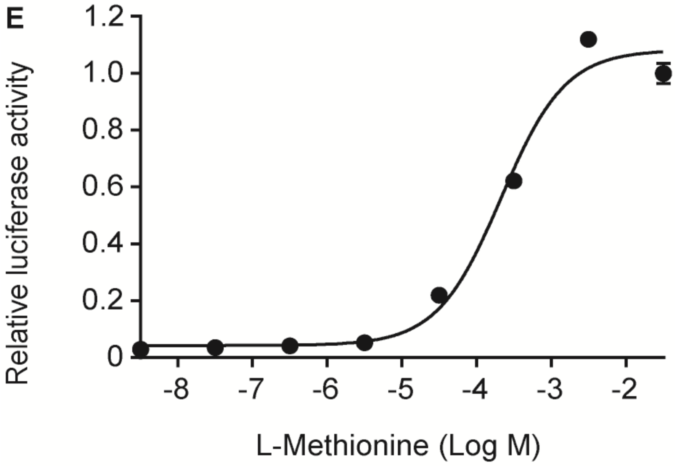
E
Relative luciferase activity
1.2
1.0
0.8
0.6
0.4
0.2
0
-8 -7 -6 -5 -4 -3 -2
L-Methionine (Log M)

Figure 19 Sensitivity and specificity of the HTS-compatible system. (**A**) Dimethyl sulfoxide (DMSO) tolerance of the setup was measured. (**B**) Comparison of the structures between l-methionine and and 5'-O-[(l-methionyl)-sulfamoyl]adenosine (MetSA). (**C**) Quantification of sensitization by the optimization of the individual components. MetSA was serially diluted from 4 μM by threefold. P, primary condition; H, HTS-optimized condition. (**D**) L-amino acids were added to rescue translational activity inhibited by MetSA. 10 mM l-amino acids and 200 nM MetSA were used. A, alanine; C, cysteine; D, aspartic acid; E, glutamic acid; F, phenylalanine; G, glycine; H, histidine; I, isoleucine; K, lysine; L, leucine; M, methionine; N, asparagine; P, proline; Q, glutamine; R, arginine; S, serine; T, tyrosine; V, valine; W, tryptophan; Y, tyrosine. (**E**) L-methionine restored the translational activity dose-dependently. EC_{50} = 224.0 ± 66.2 μM. The experiments were repeated for three times.

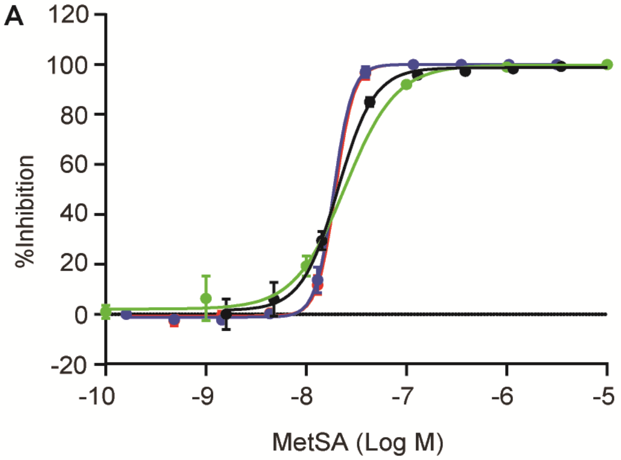

	IC_{50} (M)
In-house CRC 1	2.441e-008
In-house CRC 2	2.069e-008
HTS CRC 1	1.955e-008
HTS CRC 2	1.881e-008

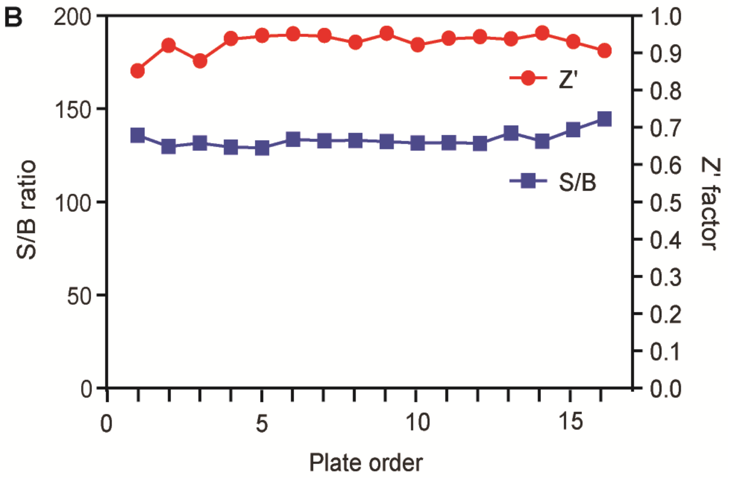

C

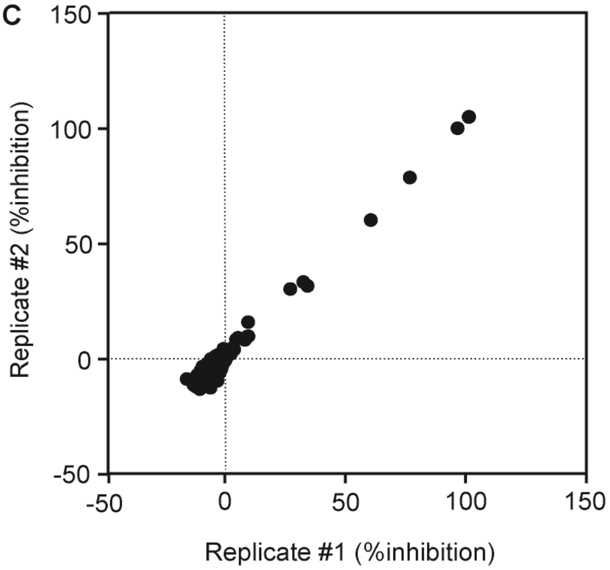

P value summary	***
Is the correlation significant? (alpha = 0.05)	Yes
R squared	0.9887

D

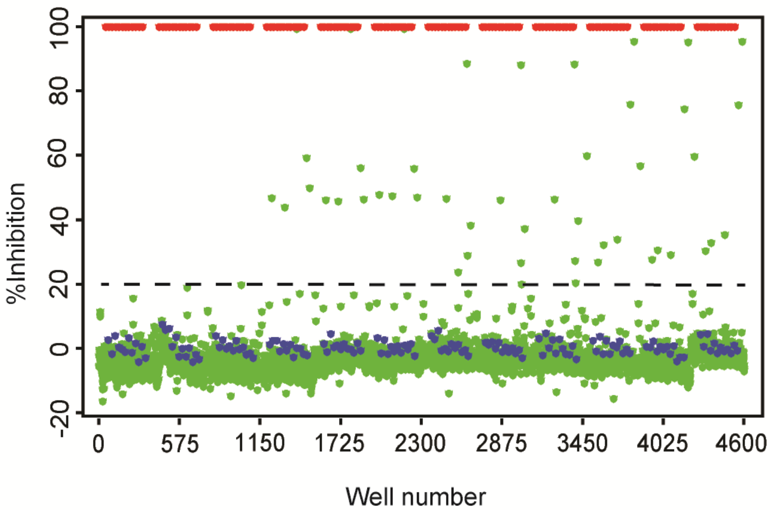

Figure 20 Pilot screen result from the library of pharmaceutically active compounds (LOPAC). (**A**) Overlap of concentration-response curves (CRCs) of MetSA from benchtop and automated procedures. Each independent experiment was in triplicate. (**B**) Z' and S/B values from whole plates were stable. (**C**) Reproducibility of inhibition profiles from the LOPAC compounds. (**D**) A scatter plot from the LOPAC library (green dot), high-control (red dot) and low-control (blue dot). Black-dotted line indicates a hit cutoff.

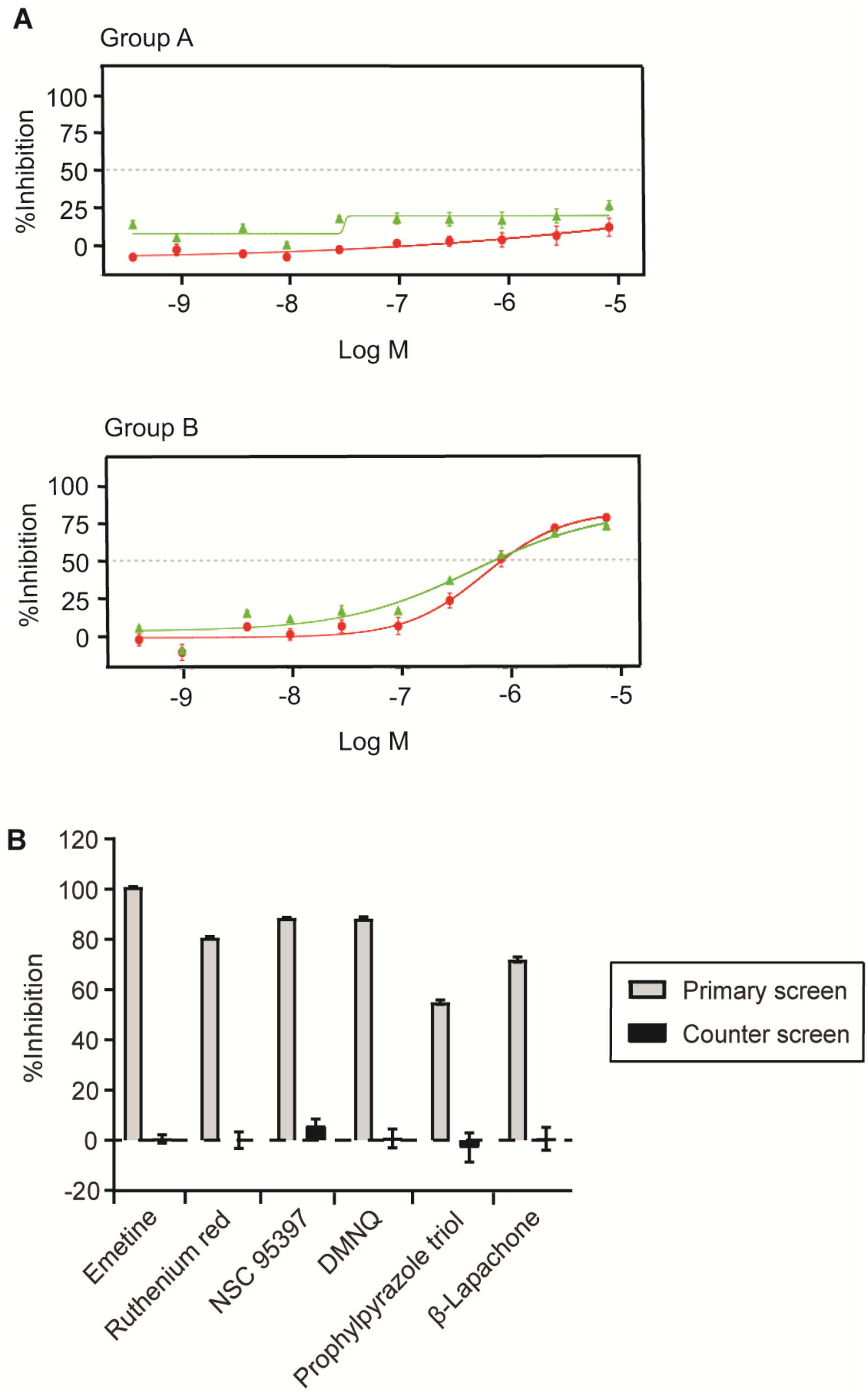
A
Group A
%Inhibition
100
75
50
25
0
-9
-8
-7
-6
-5
Log M
Group B
%Inhibition
100
75
50
25
0
-9
-8
-7
-6
-5
Log M
B
%Inhibition
120
100
80
60
40
20
0
-20
Emetine
Ruthenium red
NSC 95397
DMNQ
Prophylpyrazole triol
β-Lapachone
Primary screen
Counter screen

Figure 21 Dose-dependent titration and counter screen of preliminary hits. (**A**) Representative dose-response curves of false-positive and -negative compounds. Green line is the CRC from the primary screen. Red line is from the counterscreen. (**B**) Percentage inhibition of 6 true-positive compounds at 8.5 μM. The experiments were repeated for three times.

Table 2 Statistics from various incubation times.

Time (h)	Avg. ± Std.	Z’	%CV	S/B
1.5	53 ± 23	-	43	-
9.5	49,893 ± 2,785	0.83	6	936
15.0	63,840 ± 5,373	0.75	8	1,197
20.0	78,400 ± 6,626	0.75	8	1,470
24.5	97,587 ± 5,993	0.81	6	1,830
28.5	112,173 ± 7,165	0.81	6	2,103
40.0	153,973 ± 9,603	0.81	6	2,887
45.0	209,507 ± 29,263	0.58	14	3,928
50.0	212,267 ± 13,477	0.81	6	3,980
60.0	256,853 ± 24,812	0.71	10	4,816
65.0	249,907 ± 38,893	0.53	16	4,686
70.0	340,720 ± 31,311	0.72	9	6,389

Z’, %CV, and S/B values are calculated in comparison with 1.5 h which is assumed to be the basal level. All points were measured in triplicate. Avg., average; Std., standard deviation; %CV, coefficient of variation; S/B, signal-to-background ratio.

Table 3 List of true-positive hit compounds.

Structure	Name	IC_{50} (M), primary assay	IC_{50} (M), counter screen	Fold-selective#	General-activity information
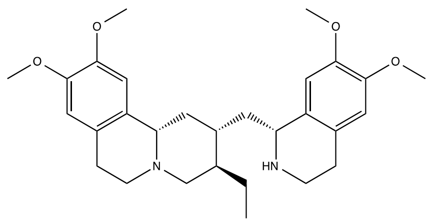	Emetine dihydrochloride hydrate	176.1E-09	> 8.5E-6	> 48.1-fold	RNA-protein translation inhibitor
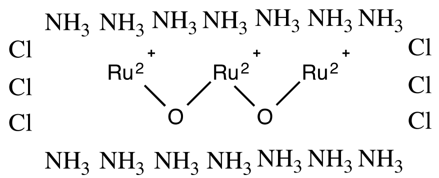	Ruthenium red	3.0E-06	> 8.5E-6	> 2.8-fold	Broad-target Ca^{2+} signaling inhibitor
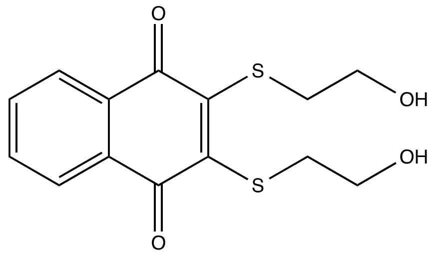	NSC 95397	3.2E-06	> 8.5E-6	> 2.6-fold	MAPK/Cdc25 phosphatase inhibitor; HDAC inhibitor

Table 3 (continued)

Structure	**Name**	**IC_{50} (M), primary assay**	**IC_{50} (M), counter screen**	**Fold-selective[#]**	**General-activity information**
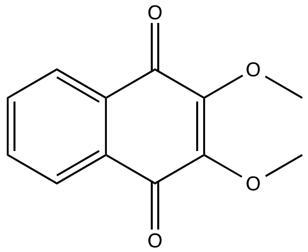	DMNQ	3.6E-06	> 8.5E-6	> 2.4-fold	Redox cycling agent
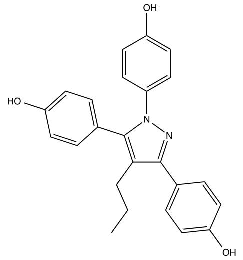	Propylpyrazole triol	3.8E-06	> 8.5E-6	> 2.2-fold	Estrogen receptor alpha agonist
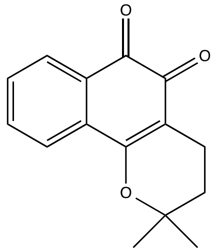	β-Lapachone	4.2E-06	> 8.5E-6	> 2.0-fold	Apoptosis inducer; anticancer agent

Fold-selective was calculated as [IC_{50} for the primary assay] / [IC_{50} for the counter screen].

Glossary

%CV a measure of dispersion of a probability or frequency distribution

equation:

$$\%CV = \frac{[standard\ deviation\ of\ the\ sample]}{[mean\ of\ the\ sample]} \times 100\%$$

R^2 coefficient of determination

equation:

$$R^2 = \frac{[explained\ variation]}{[total\ variation]}$$

Z value standard score

equation:

$$Z = \frac{[observed\ value] - [mean\ of\ the\ sample]}{[standard\ deviation\ of\ the\ sample]}$$

Z' value a measure of statistical effect size

equation:

$$Z' = 1 - \frac{3\{[standard\ deviation\ of\ positive\ control] + [standard\ deviation\ of\ negative\ control]\}}{|[mean\ of\ positive\ control] - [mean\ of\ negative\ control]|}$$

Abbreviations

aa-AMP	aminoacyl-adenylate
AARS1	alanyl-tRNA synthetase 1
ADP	adenosine diphosphate
AIMP1	aminoacyl-tRNA synthetase complex-interacting multifunctional protein 1
AIMP2	aminoacyl-tRNA synthetase complex-interacting multifunctional protein 2
Aminoacyl-tRNA	aminoacylated tRNA
ARC1	aminoacyl-tRNA synthetase cofactor 1
ARS	aminoacyl-tRNA synthetase
ASK1	apoptosis signal-regulating kinase 1
ATM	ataxia telangiectasia mutated
ATP	adenosine triphosphate
ATR	ATM and Rad3-related
cDNA	complementary DNA
CPEB	cytoplasmic polyadenylation element binding protein
CRC	concentration-response curve
C-terminus	carboxyl-terminus

CV	coefficient of variation
DARS(1)	aspartyl-tRNA synthetase (1)
DMSO	dimethyl sulfoxide
EARS	glutamyl-tRNA synthetase
EC_{50}	half maximal effective concentration
(e)EF1A	**(**eukaryotic) translation elongation factor 1A
EEF1E1	eukaryotic translation elongation factor 1 epsilon 1
EF-1H	heavy form of elongation factor 1
eIF2	eukaryotic translation initiation factor 2
eIF4E	eukaryotic translation initiation factor 4E
eIF5A	eukaryotic translation initiation factor 5A
EPRS1	glutamyl-prolyl-tRNA synthetase 1
E site	exit site
FARS1	phenylalanyl-tRNA synthetase 1
FBP	FUSE-binding protein
FBS	fetal bovine serum
GAIT	interferon gamma activated inhibitor of translation
GAPDH	glyceraldehyde-3-phosphate dehydrogenase
GARS1	glycyl-tRNA synthetase 1

GST	glutathione S-transferase
HARS(1)	histidyl-tRNA synthetase (1)
HTS	high-throughput screening
IARS1	isoleucyl-tRNA synthetase 1
IC_{50}	half maximal inhibitory concentration
IgG	immunoglobulin
KARS(1)	lysyl-tRNA synthetase (1)
LOPAC	library of pharmaceutically active compounds
LARS(1)	leucyl-tRNA synthetase (1)
MARS(1)	methionyl-tRNA synthetase (1)
MetSA	5’-O-[(L-methionyl)-sulfamoyl]adenosine
miRNA	micro RNA
mRNA	messenger RNA
MSC	multi-tRNA synthetase complex
mTORC1	mammalian target of rapamycin complex 1
N-terminus	amino-terminus
PARP1	poly(ADP-ribose) polymerase 1
PARS	prolyl-tRNA synthetase
PEX21	peroxin 21
PPI	protein-protein interaction
P site	peptidyl site

QARS1	glutaminyl-tRNA synthetase 1
QC	quality control
RARS(1)	arginyl-tRNA synthetase (1)
ROS	reactive oxygen species
SAR	structure–activity relationship
SARS	seryl-tRNA synthetase
S/B	signal–to-background ratio
SDS-PAGE	sodium dodecyl sulfate-polyacrylamide gel electrophoresis
siRNA	small interfering RNA
TARS(1)	threonyl-tRNA synthetase (1)
tRNA	transfer RNA
VARS1	valyl-tRNA synthetase 1
WARS1	tryptophanyl-tRNA synthetase 1
WHEP domain	a domain found in tryptophanyl-tRNA synthetase 1 (WARS1), histidyl-tRNA synthetase 1 (HARS1), and glutamyl-prolyl-tRNA synthetase 1 (EPRS1)
YARS1	tyrosyl-tRNA synthetase 1

References

Adams, B. D., H. Furneaux and B. A. White (2007). "The micro-ribonucleic acid (miRNA) miR-206 targets the human estrogen receptor-alpha (ERalpha) and represses ERalpha messenger RNA and protein expression in breast cancer cell lines." Mol Endocrinol **21**(5): 1132-1147.

Andersson, S. G., A. Zomorodipour, J. O. Andersson, T. Sicheritz-Ponten, U. C. Alsmark, R. M. Podowski, A. K. Naslund, A. S. Eriksson, H. H. Winkler and C. G. Kurland (1998). "The genome sequence of Rickettsia prowazekii and the origin of mitochondria." Nature **396**(6707): 133-140.

Atkins, C. M., N. Nozaki, Y. Shigeri and T. R. Soderling (2004). "Cytoplasmic polyadenylation element binding protein-dependent protein synthesis is regulated by calcium/calmodulin-dependent protein kinase II." J Neurosci **24**(22): 5193-5201.

Azad, T., A. Tashakor and S. Hosseinkhani (2014). "Split-luciferase complementary assay: applications, recent developments, and future perspectives." Anal Bioanal Chem **406**(23): 5541-5560.

Azzam, M. E. and I. D. Algranati (1973). "Mechanism of puromycin action: fate of ribosomes after release of nascent protein chains from polysomes." Proc Natl Acad Sci U S A **70**(12): 3866-3869.

Baur, J. A., K. J. Pearson, N. L. Price, H. A. Jamieson, C. Lerin, A. Kalra, V. V. Prabhu, J. S. Allard, G. Lopez-Lluch, K. Lewis, P. J.

Pistell, S. Poosala, K. G. Becker, O. Boss, D. Gwinn, M. Wang, S. Ramaswamy, K. W. Fishbein, R. G. Spencer, E. G. Lakatta, D. Le Couteur, R. J. Shaw, P. Navas, P. Puigserver, D. K. Ingram, R. de Cabo and D. A. Sinclair (2006). "Resveratrol improves health and survival of mice on a high-calorie diet." Nature **444**(7117): 337-342.

Beuning, P. J. and K. Musier-Forsyth (2001). "Species-specific differences in amino acid editing by class II prolyl-tRNA synthetase." Journal of Biological Chemistry **276**(33): 30779-30785.

Bhat, M., N. Robichaud, L. Hulea, N. Sonenberg, J. Pelletier and I. Topisirovic (2015). "Targeting the translation machinery in cancer." Nat Rev Drug Discov **14**(4): 261-278.

Burton, G. J. and E. Jauniaux (2011). "Oxidative stress." Best Pract Res Clin Obstet Gynaecol **25**(3): 287-299.

Buryanovskyy, L., Y. Fu, M. Boyd, Y. Ma, T. C. Hsieh, J. M. Wu and Z. Zhang (2004). "Crystal structure of quinone reductase 2 in complex with resveratrol." Biochemistry **43**(36): 11417-11426.

Calleri, E., G. Pochetti, K. S. S. Dossou, A. Laghezza, R. Montanari, D. Capelli, E. Prada, F. Loiodice, G. Massolini, M. Bernier and R. Moaddel (2014). "Resveratrol and its metabolites bind to PPARs." Chembiochem **15**(8): 1154-1160.

Carrion-Vazquez, M., P. E. Marszalek, A. F. Oberhauser and J. M. Fernandez (1999). "Atomic force microscopy captures length phenotypes in single proteins." Proc Natl Acad Sci U S A **96**(20): 11288-11292.

Cestari, I., S. Kalidas, S. Monnerat, A. Anupama, M. A. Phillips and K. Stuart (2013). "A multiple aminoacyl-tRNA synthetase complex that enhances tRNA-aminoacylation in African trypanosomes." Mol Cell Biol **33**(24): 4872-4888.

Chen, G. Q., R. H. Gong, D. J. Yang, G. Zhang, A. P. Lu, S. C. Yan, S. H. Lin and Z. X. Bian (2017). "Halofuginone dually regulates autophagic flux through nutrient-sensing pathways in colorectal cancer." Cell Death Dis **8**(5): e2789.

Cho, H. Y., S. J. Maeng, H. J. Cho, Y. S. Choi, J. M. Chung, S. Lee, H. K. Kim, J. H. Kim, C. Y. Eom, Y. G. Kim, M. Guo, H. S. Jung, B. S. Kang and S. Kim (2015). "Assembly of Multi-tRNA Synthetase Complex via Heterotetrameric Glutathione Transferase-homology Domains." J Biol Chem **290**(49): 29313-29328.

Choi, J. W., D. G. Kim, A. E. Lee, H. R. Kim, J. Y. Lee, N. H. Kwon, Y. K. Shin, S. K. Hwang, S. H. Chang, M. H. Cho, Y. L. Choi, J. Kim, S. H. Oh, B. Kim, S. Y. Kim, H. S. Jeon, J. Y. Park, H. P. Kang, B. J. Park, J. M. Han and S. Kim (2011). "Cancer-associated splicing variant of tumor suppressor AIMP2/p38: pathological implication in tumorigenesis." PLoS Genet **7**(3): e1001351.

Chu, D., D. J. Barnes and T. von der Haar (2011). "The role of tRNA and ribosome competition in coupling the expression of different mRNAs in Saccharomyces cerevisiae." Nucleic Acids Res **39**(15): 6705-6714.

Chu, D. and T. von der Haar (2012). "The architecture of eukaryotic translation." Nucleic Acids Res **40**(20): 10098-10106.

David, A., N. Netzer, M. B. Strader, S. R. Das, C. Y. Chen, J. Gibbs, P. Pierre, J. R. Bennink and J. W. Yewdell (2011). "RNA binding targets aminoacyl-tRNA synthetases to translating ribosomes." J Biol Chem **286**(23): 20688-20700.

Davies, D. R., B. Mamat, O. T. Magnusson, J. Christensen, M. H. Haraldsson, R. Mishra, B. Pease, E. Hansen, J. Singh, D. Zembower, H. Kim, A. S. Kiselyov, A. B. Burgin, M. E. Gurney and L. J. Stewart (2009). "Discovery of leukotriene A4 hydrolase inhibitors using metabolomics biased fragment crystallography." J Med Chem **52**(15): 4694-4715.

Dewan, V., J. Reader and K. M. Forsyth (2014). "Role of aminoacyl-tRNA synthetases in infectious diseases and targets for therapeutic development." Top Curr Chem **344**: 293-329.

Dias, J., L. Renault, J. Perez and M. Mirande (2013). "Small-angle X-ray solution scattering study of the multi-aminoacyl-tRNA synthetase complex reveals an elongated and multi-armed particle." J Biol Chem **288**(33): 23979-23989.

Dixon, A. S., M. K. Schwinn, M. P. Hall, K. Zimmerman, P. Otto, T. H. Lubben, B. L. Butler, B. F. Binkowski, T. Machleidt, T. A. Kirkland, M. G. Wood, C. T. Eggers, L. P. Encell and K. V. Wood (2016). "NanoLuc Complementation Reporter Optimized for Accurate Measurement of Protein Interactions in Cells." ACS Chem Biol **11**(2): 400-408.

Eswarappa, S. M. and P. L. Fox (2013). "Citric acid cycle and the origin of MARS." Trends Biochem Sci **38**(5): 222-228.

Fang, P., H. Han, J. Wang, K. Chen, X. Chen and M. Guo (2015). "Structural Basis for Specific Inhibition of tRNA Synthetase by an ATP Competitive Inhibitor." Chem Biol **22**(6): 734-744.

Fang, P., X. Yu, S. J. Jeong, A. Mirando, K. Chen, X. Chen, S. Kim, C. S. Francklyn and M. Guo (2015). "Structural basis for full-spectrum inhibition of translational functions on a tRNA synthetase." Nat Commun **6**: 6402.

Fang, P., H. M. Zhang, R. Shapiro, A. G. Marshall, P. Schimmel, X. L. Yang and M. Guo (2011). "Structural context for mobilization of a human tRNA synthetase from its cytoplasmic complex." Proc Natl Acad Sci U S A **108**(20): 8239-8244.

Flydal, M. I. and A. Martinez (2013). "Phenylalanine hydroxylase: function, structure, and regulation." IUBMB Life **65**(4): 341-349.

Fu, Y., Y. Kim, K. S. Jin, H. S. Kim, J. H. Kim, D. Wang, M. Park, C. H. Jo, N. H. Kwon, D. Kim, M. H. Kim, Y. H. Jeon, K. Y. Hwang, S. Kim and Y. Cho (2014). "Structure of the ArgRS-GlnRS-AIMP1 complex and its implications for mammalian translation." Proc Natl Acad Sci U S A **111**(42): 15084-15089.

Gao, X., Y. Jiang, L. Han, X. Chen, C. Hu, H. Su, Y. Mu, P. Guan and X. Huang (2017). "Effect of borrelidin on hepatocellular carcinoma cells in vitro and in vivo." RSC Advances **7**(70): 44401-44409.

Gaskell, E. A., J. E. Smith, J. W. Pinney, D. R. Westhead and G. A. McConkey (2009). "A unique dual activity amino acid hydroxylase in Toxoplasma gondii." PLoS One **4**(3): e4801.

Gertz, M., G. T. Nguyen, F. Fischer, B. Suenkel, C. Schlicker, B. Franzel, J. Tomaschewski, F. Aladini, C. Becker, D. Wolters and C. Steegborn (2012). "A molecular mechanism for direct sirtuin activation by resveratrol." PLoS One **7**(11): e49761.

Godinic-Mikulcic, V., J. Jaric, C. D. Hausmann, M. Ibba and I. Weygand-Durasevic (2011). "An archaeal tRNA-synthetase complex that enhances aminoacylation under extreme conditions." J Biol Chem **286**(5): 3396-3404.

Godinic, V., M. Mocibob, S. Rocak, M. Ibba and I. Weygand-Durasevic (2007). "Peroxin Pex21p interacts with the C-terminal noncatalytic domain of yeast seryl-tRNA synthetase and forms a specific ternary complex with tRNA(Ser)." FEBS J **274**(11): 2788-2799.

Goljanek-Whysall, K., H. Pais, T. Rathjen, D. Sweetman, T. Dalmay and A. Münsterberg (2012). "Regulation of multiple target genes by miR-1 and miR-206 is pivotal for C2C12 myoblast differentiation." J Cell Sci **125**(Pt 15): 3590-3600.

Guo, M., M. Ignatov, K. Musier-Forsyth, P. Schimmel and X. L. Yang (2008). "Crystal structure of tetrameric form of human lysyl-tRNA synthetase: Implications for multisynthetase complex formation." Proc Natl Acad Sci U S A **105**(7): 2331-2336.

Guo, M. and P. Schimmel (2013). "Essential nontranslational functions of tRNA synthetases." Nat Chem Biol **9**(3): 145-153.

Gupta, R. S. and L. Siminovitch (1977). "The molecular basis of emetine resistance in Chinese hamster ovary cells: alteration in the 40S ribosomal subunit." Cell **10**(1): 61-66.

Habibi, D., N. Ogloff, R. B. Jalili, A. Yost, A. P. Weng, A. Ghahary and C. J. Ong (2012). "Borrelidin, a small molecule nitrile-containing macrolide inhibitor of threonyl-tRNA synthetase, is a potent inducer of apoptosis in acute lymphoblastic leukemia." Invest New Drugs **30**(4): 1361-1370.

Hahn, H., S. H. Park, H. J. Kim, S. Kim and B. W. Han (2019). "The DRS-AIMP2-EPRS subcomplex acts as a pivot in the multi-tRNA synthetase complex." IUCrJ **6**(Pt 5): 958-967.

Hall, M. P., J. Unch, B. F. Binkowski, M. P. Valley, B. L. Butler, M. G. Wood, P. Otto, K. Zimmerman, G. Vidugiris, T. Machleidt, M. B. Robers, H. A. Benink, C. T. Eggers, M. R. Slater, P. L. Meisenheimer, D. H. Klaubert, F. Fan, L. P. Encell and K. V. Wood (2012). "Engineered luciferase reporter from a deep sea shrimp utilizing a novel imidazopyrazinone substrate." ACS Chem Biol **7**(11): 1848-1857.

Han, J. M., S. J. Jeong, M. C. Park, G. Kim, N. H. Kwon, H. K. Kim, S. H. Ha, S. H. Ryu and S. Kim (2012). "Leucyl-tRNA synthetase is an intracellular leucine sensor for the mTORC1-signaling pathway." Cell **149**(2): 410-424.

Hausmann, C. D., M. Praetorius-Ibba and M. Ibba (2007). "An aminoacyl-tRNA synthetase:elongation factor complex for substrate channeling in archaeal translation." Nucleic Acids Res **35**(18): 6094-6102.

Havrylenko, S., R. Legouis, B. Negrutskii and M. Mirande (2011). "Caenorhabditis elegans evolves a new architecture for the multi-aminoacyl-tRNA synthetase complex." J Biol Chem **286**(32): 28476-28487.

Hei, Z., S. Wu, Z. Liu, J. Wang and P. Fang (2019). "Retractile lysyl-tRNA synthetase-AIMP2 assembly in the human multi-aminoacyl-tRNA synthetase complex." J Biol Chem **294**(13): 4775-4783.

Howitz, K. T., K. J. Bitterman, H. Y. Cohen, D. W. Lamming, S. Lavu, J. G. Wood, R. E. Zipkin, P. Chung, A. Kisielewski, L. L. Zhang, B. Scherer and D. A. Sinclair (2003). "Small molecule activators of sirtuins extend Saccharomyces cerevisiae lifespan." Nature **425**(6954): 191-196.

Ingolia, N. T., L. F. Lareau and J. S. Weissman (2011). "Ribosome profiling of mouse embryonic stem cells reveals the complexity and dynamics of mammalian proteomes." Cell **147**(4): 789-802.

Jeong, S. J., J. H. Kim, B. J. Lim, I. Yoon, J. A. Song, H. S. Moon, D. Kim, D. K. Lee and S. Kim (2018). "Inhibition of MUC1 biosynthesis via threonyl-tRNA synthetase suppresses pancreatic cancer cell migration." Exp Mol Med **50**(1): e424.[1]

Jeong, M., H. Kim, S. Kim and J. H. Park (2018). "Liposomal borrelidin for treatment of metastatic breast cancer." Drug Deliv Transl Res **8**(5): 1380-1388.[2]

Jimenez, A., L. Carrasco and D. Vazquez (1977). "Enzymic and nonenzymic translocation by yeast polysomes. Site of action of a number of inhibitors." Biochemistry **16**(21): 4727-4730.

Juarez, P., K. S. Mohammad, J. J. Yin, P. G. Fournier, R. C. McKenna, H. W. Davis, X. H. Peng, M. Niewolna, D. Javelaud, J. M. Chirgwin, A. Mauviel and T. A. Guise (2012). "Halofuginone inhibits the establishment and progression of melanoma bone metastases." Cancer Res **72**(23): 6247-6256.

Kaminska, M., S. Havrylenko, P. Decottignies, P. Le Marechal, B. Negrutskii and M. Mirande (2009). "Dynamic Organization of Aminoacyl-tRNA Synthetase Complexes in the Cytoplasm of Human Cells." J Biol Chem **284**(20): 13746-13754.

Kang, T., N. H. Kwon, J. Y. Lee, M. C. Park, E. Kang, H. H. Kim, T. J. Kang and S. Kim (2012). "AIMP3/p18 controls translational initiation by mediating the delivery of charged initiator tRNA to initiation complex." J Mol Biol **423**(4): 475-481.

Keller, T. L., D. Zocco, M. S. Sundrud, M. Hendrick, M. Edenius, J. Yum, Y. J. Kim, H. K. Lee, J. F. Cortese, D. F. Wirth, J. D. Dignam, A. Rao, C. Y. Yeo, R. Mazitschek and M. Whitman (2012). "Halofuginone and other febrifugine derivatives inhibit prolyl-tRNA synthetase." Nat Chem Biol **8**(3): 311-317.

Kerjan, P., C. Cerini, M. Sémériva and M. Mirande (1994). "The multienzyme complex containing nine aminoacyl-tRNA synthetases is ubiquitous from Drosophila to mammals." Biochim Biophys Acta **1199**(3): 293-297.

Kikuchi, H., H. Tasaka, S. Hirai, Y. Takaya, Y. Iwabuchi, H. Ooi, S.

Hatakeyama, H. S. Kim, Y. Wataya and Y. Oshima (2002). "Potent antimalarial febrifugine analogues against the plasmodium malaria parasite." J Med Chem **45**(12): 2563-2570.

Kim, D. G., J. Y. Lee, N. H. Kwon, P. Fang, Q. Zhang, J. Wang, N. L. Young, M. Guo, H. Y. Cho, A. U. Mushtaq, Y. H. Jeon, J. W. Choi, J. M. Han, H. W. Kang, J. E. Joo, Y. Hur, W. Kang, H. Yang, D. H. Nam, M. S. Lee, J. W. Lee, E. S. Kim, A. Moon, K. Kim, D. Kim, E. J. Kang, Y. Moon, K. H. Rhee, B. W. Han, J. S. Yang, G. Han, W. S. Yang, C. Lee, M. W. Wang and S. Kim (2014). "Chemical inhibition of prometastatic lysyl-tRNA synthetase-laminin receptor interaction." Nat Chem Biol **10**(1): 29-34.

Kim, E. Y., J. Y. Jung, A. Kim, K. Kim and Y. S. Chang (2017). "Methionyl-tRNA synthetase overexpression is associated with poor clinical outcomes in non-small cell lung cancer." BMC Cancer **17**(1): 467.

Kim, M. J., B. J. Park, Y. S. Kang, H. J. Kim, J. H. Park, J. W. Kang, S. W. Lee, J. M. Han, H. W. Lee and S. Kim (2003). "Downregulation of FUSE-binding protein and c-myc by tRNA synthetase cofactor p38 is required for lung cell differentiation." Nat Genet **34**(3): 330-336.

Kim, S. B., H. R. Kim, M. C. Park, S. Cho, P. C. Goughnour, D. Han, I. Yoon, Y. Kim, T. Kang, E. Song, P. Kim, H. Choi, J. Y. Mun, C. Song, S. Lee, H. S. Jung and S. Kim (2017). "Caspase-8 controls the secretion of inflammatory lysyl-tRNA synthetase in exosomes from cancer cells." J Cell Biol **216**(7): 2201-2216.

Kim, Y., M. S. Sundrud, C. Zhou, M. Edenius, D. Zocco, K. Powers,M.

Zhang, R. Mazitschek, A. Rao, C.-Y. Yeo, E. H. Noss, M. B. Brenner, M. Whitman and T. L. Keller (2020). "Aminoacyl-tRNA synthetase inhibition activates a pathway that branches from the canonical amino acid response in mammalian cells." Proceedings of the National Academy of Sciences **117**(16): 8900-8911.

Klabunde, T., H. M. Petrassi, V. B. Oza, P. Raman, J. W. Kelly and J. C. Sacchettini (2000). "Rational design of potent human transthyretin amyloid disease inhibitors." Nat Struct Biol **7**(4): 312-321.

Klotz, L. O., X. Hou and C. Jacob (2014). "1,4-naphthoquinones: from oxidative damage to cellular and inter-cellular signaling." Molecules **19**(9): 14902-14918.

Ko, Y. G., E. Y. Kim, T. Kim, H. Park, H. S. Park, E. J. Choi and S. Kim (2001). "Glutamine-dependent antiapoptotic interaction of human glutaminyl-tRNA synthetase with apoptosis signal-regulating kinase 1." J Biol Chem **276**(8): 6030-6036.

Koh, C. Y., L. K. Siddaramaiah, R. M. Ranade, J. Nguyen, T. Jian, Z. Zhang, J. R. Gillespie, F. S. Buckner, C. L. Verlinde, E. Fan and W. G. Hol (2015). "A binding hotspot in Trypanosoma cruzi histidyl-tRNA synthetase revealed by fragment-based crystallographic cocktail screens." Acta Crystallogr D Biol Crystallogr **71**(Pt 8): 1684-1698.

Kumar, M. R., K. Aithal, B. N. Rao, N. Udupa and B. S. Rao (2009). "Cytotoxic, genotoxic and oxidative stress induced by 1,4-naphthoquinone in B16F1 melanoma tumor cells." Toxicol In Vitro **23**(2): 242-250.

Kushner, J. P., D. Boll, J. Quagliana and S. Dickman (1976). "Elevated methionine-tRNA synthetase activity in human colon cancer." Proc Soc Exp Biol Med **153**(2): 273-276.

Kwon, N. H., P. L. Fox and S. Kim (2019). "Aminoacyl-tRNA synthetases as therapeutic targets." Nat Rev Drug Discov **18**(8): 629-650.

Kwon, N. H., T. Kang, J. Y. Lee, H. H. Kim, H. R. Kim, J. Hong, Y. S. Oh, J. M. Han, M. J. Ku, S. Y. Lee and S. Kim (2011). "Dual role of methionyl-tRNA synthetase in the regulation of translation and tumor suppressor activity of aminoacyl-tRNA synthetase-interacting multifunctional protein-3." Proc Natl Acad Sci U S A **108**(49): 19635-19640.

Kyriacou, S. V. and M. P. Deutscher (2008). "An important role for the multienzyme aminoacyl-tRNA synthetase complex in mammalian translation and cell growth." Mol Cell **29**(4): 419-427.

Laschet, C., N. Dupuis and J. Hanson (2019). "A dynamic and screening-compatible nanoluciferase-based complementation assay enables profiling of individual GPCR-G protein interactions." J Biol Chem **294**(11): 4079-4090.

Lee, J. M., T. Kim, E. Y. Kim, A. Kim, D. K. Lee, N. H. Kwon, S. Kim and Y. S. Chang (2019). "Methionyl-tRNA Synthetase is a Useful Diagnostic Marker for Lymph Node Metastasis in Non-Small Cell Lung Cancer." Yonsei Med J **60**(11): 1005-1012.

Lee, J. Y., D. G. Kim, B. G. Kim, W. S. Yang, J. Hong, T. Kang, Y. S.

Oh, K. R. Kim, B. W. Han, B. J. Hwang, B. S. Kang, M. S. Kang, M. H. Kim, N. H. Kwon and S. Kim (2014). "Promiscuous methionyl-tRNA synthetase mediates adaptive mistranslation to protect cells against oxidative stress." J Cell Sci **127**(Pt 19): 4234-4245.

Litt, M. and K. Weiser (1978). "Histidine transfer RNA levels in Friend leukemia cells: stimulation by histidine deprivation." Science **201**(4355): 527-529.

Liu, L., D. R. Wise, J. A. Diehl and M. C. Simon (2008). "Hypoxic reactive oxygen species regulate the integrated stress response and cell survival." J Biol Chem **283**(45): 31153-31162.

Lv, P. C. and H. L. Zhu (2012). "Aminoacyl-tRNA synthetase inhibitors as potent antibacterials." Curr Med Chem **19**(21): 3550-3563.

Margulis, L. (1970). Origin of Eukaryotic Cells: Evidence and Research Implications for a Theory of the Origin and Evolution of Microbial, Plant, and Animal Cells on the Precambrian Earth, Yale University Press.

Martijn, J., J. Vosseberg, L. Guy, P. Offre and T. J. G. Ettema (2018). "Deep mitochondrial origin outside the sampled alphaproteobacteria." Nature **557**(7703): 101-105.

Martin-Nieto, J. and D. J. Roufa (1997). "Functional analysis of human RPS14 null alleles." J Cell Sci **110 (Pt 8)**: 955-963.

Meijerman, I., W. M. Blom, H. J. de Bont, G. J. Mulder and J. F. Nagelkerke (1999). "Induction of apoptosis and changes in nuclear Gactin are mediated by different pathways: the effect of inhibitors of protein and RNA synthesis in isolated rat hepatocytes." Toxicol Appl Pharmacol **156**(1): 46-55.

Milne, J. C., P. D. Lambert, S. Schenk, D. P. Carney, J. J. Smith, D. J. Gagne, L. Jin, O. Boss, R. B. Perni, C. B. Vu, J. E. Bemis, R. Xie, J. S. Disch, P. Y. Ng, J. J. Nunes, A. V. Lynch, H. Yang, H. Galonek, K. Israelian, W. Choy, A. Iffland, S. Lavu, O. Medvedik, D. A. Sinclair, J. M. Olefsky, M. R. Jirousek, P. J. Elliott and C. H. Westphal (2007). "Small molecule activators of SIRT1 as therapeutics for the treatment of type 2 diabetes." Nature **450**(7170): 712-716.

Moreland, J. L., A. Gramada, O. V. Buzko, Q. Zhang and P. E. Bourne (2005). "The Molecular Biology Toolkit (MBT): a modular platform for developing molecular visualization applications." BMC Bioinformatics **6**: 21.

Moulinier, L., S. Eiler, G. Eriani, J. Gangloff, J. C. Thierry, K. Gabriel, W. H. McClain and D. Moras (2001). "The structure of an AspRS-tRNA(Asp) complex reveals a tRNA-dependent control mechanism." EMBO J **20**(18): 5290-5301.

Murray, J. C., Y. M. Heng, P. Symonds, K. Rice, W. Ward, M. Huggins, I. Todd and R. A. Robins (2004). "Endothelial monocyte-activating polypeptide-II (EMAP-II): a novel inducer of lymphocyte apoptosis." Journal of Leukocyte Biology **75**(5): 772-776.

Negrutskii, B. S., V. F. Shalak, P. Kerjan, A. V. El'skaya and M. Mirande (1999). "Functional interaction of mammalian valyl-tRNA synthetase with elongation factor EF-1alpha in the complex with EF-

1H." J Biol Chem **274**(8): 4545-4550.

Nguyen, G. T., M. Gertz and C. Steegborn (2013). "Crystal structures of Sirt3 complexes with 4'-bromo-resveratrol reveal binding sites and inhibition mechanism." Chem Biol **20**(11): 1375-1385.

Novoa, E. M., N. Camacho, A. Tor, B. Wilkinson, S. Moss, P. Marin-Garcia, I. G. Azcarate, J. M. Bautista, A. C. Mirando, C. S. Francklyn, S. Varon, M. Royo, A. Cortes and L. Ribas de Pouplana (2014). "Analogs of natural aminoacyl-tRNA synthetase inhibitors clear malaria in vivo." Proc Natl Acad Sci U S A **111**(51): E5508-5517.

Nwachukwu, J. C., S. Srinivasan, N. E. Bruno, A. A. Parent, T. S. Hughes, J. A. Pollock, O. Gjyshi, V. Cavett, J. Nowak, R. D. Garcia-Ordonez, R. Houtman, P. R. Griffin, D. J. Kojetin, J. A. Katzenellenbogen, M. D. Conkright and K. W. Nettles (2014). "Resveratrol modulates the inflammatory response via an estrogen receptor-signal integration network." Elife **3**: e02057.

Ofir-Birin, Y., P. Fang, S. P. Bennett, H. M. Zhang, J. Wang, I. Rachmin, R. Shapiro, J. Song, A. Dagan, J. Pozo, S. Kim, A. G. Marshall, P. Schimmel, X. L. Yang, H. Nechushtan, E. Razin and M. Guo (2013). "Structural switch of lysyl-tRNA synthetase between translation and transcription." Mol Cell **49**(1): 30-42.

Park, B. J., J. W. Kang, S. W. Lee, S. J. Choi, Y. K. Shin, Y. H. Ahn, Y. H. Choi, D. Choi, K. S. Lee and S. Kim (2005). "The haploinsufficient tumor suppressor p18 upregulates p53 via interactions with ATM/ATR." Cell **120**(2): 209-221.

Park, H., S. G. Park, J. Kim, Y. G. Ko and S. Kim (2002). "Signaling pathways for TNF production induced by human aminoacyl-tRNA synthetase-associating factor, p43." Cytokine **20**(4): 148-153.

Park, S. G., H. J. Kim, Y. H. Min, E. C. Choi, Y. K. Shin, B. J. Park, S. W. Lee and S. Kim (2005). "Human lysyl-tRNA synthetase is secreted to trigger proinflammatory response." Proc Natl Acad Sci U S A **102**(18): 6356-6361.

Pineda-Sanabria, S. E., I. M. Robertson and B. D. Sykes (2011). "Structure of trans-resveratrol in complex with the cardiac regulatory protein troponin C." Biochemistry **50**(8): 1309-1320.

Praetorius-Ibba, M., C. D. Hausmann, M. Paras, T. E. Rogers and M. Ibba (2007). "Functional association between three archaeal aminoacyl-tRNA synthetases." J Biol Chem **282**(6): 3680-3687.

Raina, M., S. Elgamal, T. J. Santangelo and M. Ibba (2012). "Association of a multi-synthetase complex with translating ribosomes in the archaeon Thermococcus kodakarensis." FEBS Lett **586**(16): 2232-2238.

Ray, P. S. and P. L. Fox (2014). "Origin and evolution of glutamyl-prolyl tRNA synthetase WHEP domains reveal evolutionary relationships within Holozoa." PLoS One **9**(6): e98493.

Reader, J. S., P. T. Ordoukhanian, J. G. Kim, V. de Crecy-Lagard, I. Hwang, S. Farrand and P. Schimmel (2005). "Major biocontrol of plant tumors targets tRNA synthetase." Science **309**(5740): 1533.

Reifsnider, N., G. Kaur, D. Scudiero and A. Monks (2005).

"Halofuginone treatment in vitro elevates VEGF gene expression and secretion in certain human tumor cell lines." Cancer Research **65**(9 Supplement): 1379-1380.

Rho, S. B., M. J. Kim, J. S. Lee, W. Seol, H. Motegi, S. Kim and K. Shiba (1999). "Genetic dissection of protein-protein interactions in multi-tRNA synthetase complex." Proc Natl Acad Sci U S A **96**(8): 4488-4493.

Ribas de Pouplana, L. and P. Schimmel (2001). "Aminoacyl-tRNA synthetases: potential markers of genetic code development." Trends Biochem Sci **26**(10): 591-596.

Rock, F. L., W. Mao, A. Yaremchuk, M. Tukalo, T. Crepin, H. Zhou, Y. K. Zhang, V. Hernandez, T. Akama, S. J. Baker, J. J. Plattner, L. Shapiro, S. A. Martinis, S. J. Benkovic, S. Cusack and M. R. Alley (2007). "An antifungal agent inhibits an aminoacyl-tRNA synthetase by trapping tRNA in the editing site." Science **316**(5832): 1759-1761.

Rodova, M., V. Ankilova and M. G. Safro (1999). "Human phenylalanyl-tRNA synthetase: cloning, characterization of the deduced amino acid sequences in terms of the structural domains and coordinately regulated expression of the alpha and beta subunits in chronic myeloid leukemia cells." Biochem Biophys Res Commun **255**(3): 765-773.

Ruggero, D. (2013). "Translational control in cancer etiology." Cold Spring Harb Perspect Biol **5**(2).

Sajish, M. and P. Schimmel (2015). "A human tRNA synthetase is a potent PARP1-activating effector target for resveratrol." Nature **519**(7543): 370-373.

Sampath, P., B. Mazumder, V. Seshadri, C. A. Gerber, L. Chavatte, M. Kinter, S. M. Ting, J. D. Dignam, S. Kim, D. M. Driscoll and P. L. Fox (2004). "Noncanonical function of glutamyl-prolyl-tRNA synthetase: gene-specific silencing of translation." Cell **119**(2): 195-208.

Scandurro, A. B., C. W. Weldon, Y. G. Figueroa, J. Alam and B. S. Beckman (2001). "Gene microarray analysis reveals a novel hypoxia signal transduction pathway in human hepatocellular carcinoma cells." Int J Oncol **19**(1): 129-135.

Schneider-Poetsch, T., J. Ju, D. E. Eyler, Y. Dang, S. Bhat, W. C. Merrick, R. Green, B. Shen and J. O. Liu (2010). "Inhibition of eukaryotic translation elongation by cycloheximide and lactimidomycin." Nat Chem Biol **6**(3): 209-217.

Schneider, C. A., W. S. Rasband and K. W. Eliceiri (2012). "NIH Image to ImageJ: 25 years of image analysis." Nature Methods **9**(7): 671-675.

Schwarz, M. A., J. Kandel, J. Brett, J. Li, J. Hayward, R. E. Schwarz, O. Chappey, J. L. Wautier, J. Chabot, P. Lo Gerfo and D. Stern (1999). "Endothelial-monocyte activating polypeptide II, a novel antitumor cytokine that suppresses primary and metastatic tumor growth and induces apoptosis in growing endothelial cells." J Exp Med **190**(3): 341-354.

Shafqat, N., J. R. Muniz, E. S. Pilka, E. Papagrigoriou, F. von Delft, U.

Oppermann and W. W. Yue (2013). "Insight into S-adenosylmethionine biosynthesis from the crystal structures of the human methionine adenosyltransferase catalytic and regulatory subunits." Biochem J **452**(1): 27-36.

Shenton, D., J. B. Smirnova, J. N. Selley, K. Carroll, S. J. Hubbard, G. D. Pavitt, M. P. Ashe and C. M. Grant (2006). "Global translational responses to oxidative stress impact upon multiple levels of protein synthesis." J Biol Chem **281**(39): 29011-29021.

Sidhu, A., J. R. Miller, A. Tripathi, D. M. Garshott, A. L. Brownell, D. J. Chiego, C. Arevang, Q. Zeng, L. C. Jackson, S. A. Bechler, M. U. Callaghan, G. H. Yoo, S. Sethi, H. S. Lin, J. H. Callaghan, G. Tamayo-Castillo, D. H. Sherman, R. J. Kaufman and A. M. Fribley (2015). "Borrelidin Induces the Unfolded Protein Response in Oral Cancer Cells and Chop-Dependent Apoptosis." ACS Med Chem Lett **6**(11): 1122-1127.

Silvian, L. F., J. Wang and T. A. Steitz (1999). "Insights into editing from an ile-tRNA synthetase structure with tRNAile and mupirocin." Science **285**(5430): 1074-1077.

Simos, G., A. Sauer, F. Fasiolo and E. C. Hurt (1998). "A conserved domain within Arc1p delivers tRNA to aminoacyl-tRNA synthetases." Mol Cell **1**(2): 235-242.

Simos, G., A. Segref, F. Fasiolo, K. Hellmuth, A. Shevchenko, M. Mann and E. C. Hurt (1996). "The yeast protein Arc1p binds to tRNA and functions as a cofactor for the methionyl- and glutamyl-tRNA synthetases." Embo j **15**(19): 5437-5448.

Sivaram, P. and M. P. Deutscher (1990). "Existence of two forms of rat liver arginyl-tRNA synthetase suggests channeling of aminoacyl-tRNA for protein synthesis." Proc Natl Acad Sci U S A **87**(10): 3665-3669.

Stapulionis, R. and M. P. Deutscher (1995). "A channeled tRNA cycle during mammalian protein synthesis." Proc Natl Acad Sci U S A **92**(16): 7158-7161.

Sundrud, M. S., S. B. Koralov, M. Feuerer, D. P. Calado, A. E. Kozhaya, A. Rhule-Smith, R. E. Lefebvre, D. Unutmaz, R. Mazitschek, H. Waldner, M. Whitman, T. Keller and A. Rao (2009). "Halofuginone inhibits TH17 cell differentiation by activating the amino acid starvation response." Science **324**(5932): 1334-1338.

Tao, J., P. Wendler, G. Connelly, A. Lim, J. Zhang, M. King, T. Li, J. A. Silverman, P. R. Schimmel and F. P. Tally (2000). "Drug target validation: lethal infection blocked by inducible peptide." Proc Natl Acad Sci U S A **97**(2): 783-786.

Teng, M., M. T. Hilgers, M. L. Cunningham, A. Borchardt, J. B. Locke, S. Abraham, G. Haley, B. P. Kwan, C. Hall, G. W. Hough, K. J. Shaw and J. Finn (2013). "Identification of bacteria-selective threonyl-tRNA synthetase substrate inhibitors by structure-based design." J Med Chem **56**(4): 1748-1760.

Truitt, M. L., C. S. Conn, Z. Shi, X. Pang, T. Tokuyasu, A. M. Coady, Y. Seo, M. Barna and D. Ruggero (2015). "Differential Requirements for eIF4E Dose in Normal Development and Cancer." Cell **162**(1): 59-71.

Uhlen, M., C. Zhang, S. Lee, E. Sjostedt, L. Fagerberg, G. Bidkhori, R. Benfeitas, M. Arif, Z. Liu, F. Edfors, K. Sanli, K. von Feilitzen, P. Oksvold, E. Lundberg, S. Hober, P. Nilsson, J. Mattsson, J. M. Schwenk, H. Brunnstrom, B. Glimelius, T. Sjoblom, P. H. Edqvist, D. Djureinovic, P. Micke, C. Lindskog, A. Mardinoglu and F. Ponten (2017). "A pathology atlas of the human cancer transcriptome." Science **357**(6352).

van Rooyen, J. M., J. B. Murat, P. M. Hammoudi, S. Kieffer-Jaquinod, Y. Coute, A. Sharma, H. Pelloux, H. Belrhali and M. A. Hakimi (2014). "Assembly of the novel five-component apicomplexan multi-aminoacyl-tRNA synthetase complex is driven by the hybrid scaffold protein Tg-p43." PLoS One **9**(2): e89487.

Vaughan, M. H. and B. S. Hansen (1973). "Control of initiation of protein synthesis in human cells. Evidence for a role of uncharged transfer ribonucleic acid." J Biol Chem **248**(20): 7087-7096.

Vellaichamy, A., A. Sreekumar, J. R. Strahler, T. Rajendiran, J. Yu, S. Varambally, Y. Li, G. S. Omenn, A. M. Chinnaiyan and A. I. Nesvizhskii (2009). "Proteomic interrogation of androgen action in prostate cancer cells reveals roles of aminoacyl tRNA synthetases." PLoS One **4**(9): e7075.

Vondenhoff, G. H., S. Dubiley, K. Severinov, E. Lescrinier, J. Rozenski and A. Van Aerschot (2011). "Extended targeting potential and improved synthesis of Microcin C analogs as antibacterials." Bioorg Med Chem **19**(18): 5462-5467.

Vondenhoff, G. H., K. Pugach, B. Gadakh, L. Carlier, J. Rozenski, M.

Froeyen, K. Severinov and A. Van Aerschot (2013). "N-alkylated aminoacyl sulfamoyladenosines as potential inhibitors of aminoacylation reactions and microcin C analogues containing D-amino acids." PLoS One **8**(11): e79234.

Wang, F. W., X. Y. Guan and D. Xie (2013). "Roles of eukaryotic initiation factor 5A2 in human cancer." Int J Biol Sci **9**(10): 1013-1020.

Warrington, R. C., W. D. Fang and L. U. Zhang (1996). "L-histidinol reverses resistance to cisplatinum and other antineoplastics in a tumorigenic epithelial cell line." Anticancer Res **16**(6B): 3641-3646.

Wells, D. G., J. D. Richter and J. R. Fallon (2000). "Molecular mechanisms for activity-regulated protein synthesis in the synapto-dendritic compartment." Curr Opin Neurobiol **10**(1): 132-137.

Yaremchuk, A., I. Kriklivyi, S. Cusack and M. Tukalo (2000). "Improved crystals of Thermus thermophilus prolyl-tRNA synthetase complexed with cognate tRNA obtained by crystallization from precipitate." Acta Crystallogr D Biol Crystallogr **56**(Pt 2): 197-199.

Zhao, Y., Q. Meng, L. Bai and H. Zhou (2014). "In silico discovery of aminoacyl-tRNA synthetase inhibitors." Int J Mol Sci **15**(1): 1358-1373.

Zhou, H., L. Sun, X. L. Yang and P. Schimmel (2013). "ATP-directed capture of bioactive herbal-based medicine on human tRNA synthetase." Nature **494**(7435): 121-124.

국문초록

단백질 합성 (번역)은 모든 형태의 생명이 가지고 있는 공통적인 특성이다. 아미노산-운반RNA 연결효소 (aminoacyl-tRNA synthetase; ARS)는 단백질 합성 과정에서 가장 첫 번째 단계를 담당하고 있다. 아미노산-운반RNA 연결효소는 운반RNA (transfer RNA; tRNA)와 상보적인 아미노산 (amino acid) 사이의 에스터화 반응 (esterification/aminoacylation)을 촉매하여 아미노산-운반RNA 중합체 (aminoacyl-tRNA)로 연결한다. 생성된 아미노산-운반RNA 중합체는 리보솜 (ribosome)으로 전달되어 전령RNA (messenger RNA; mRNA)를 펩타이트 중합체 (polypeptide)로 번역하는 과정의 재료로 사용된다.

세포질 아미노산-운반RNA 연결효소 (cytoplasmic ARS)는 종에 따라 세포내에서 제어되는 방식이 다르다. 이 효소들은 진화과정 동안 추가적인 단백질 도메인 (protein domain)과 새로운 기능들을 획득해왔다. 또한 고등 진핵생물 (higher eukaryote)에는 진핵생물 (eukaryote) 중에서 가장 큰 아미노산-운반RNA 연결효소 복합체 (multi-tRNA synthetase complex; MSC)가 존재하며, 이 복합체는 8 종류의 아미노산-운반RNA 연결효소가 8 내지는 9종류의 아미노산을 담당한다. 이 중에서 포유동물의 아미노산-운반RNA 연결효소

복합체가 가장 복잡한 형태인데, 8종류의 세포질 아미노산-운반 RNA 연결효소가 9종류의 아미노산을 담당하며, 추가적으로 3종류의 뼈대 단백질 (scaffold protein)이 존재한다. 이처럼 포유동물의 세포 내에서는 아미노산-운반RNA 중합체 이동의 절반 정도가 아미노산-운반RNA 연결효소 복합체에서 시작되고 있다. 따라서 아미노산-운반RNA 중합체를 리보솜으로 안정적으로 공급하는 것이 포유동물 아미노산-운반RNA 연결효소 복합체의 가장 중요한 역할 중의 하나일 것이라 예상된다. 한편으로, 몇몇의 세포질 아미노산-운반RNA 연결효소들과 뼈대 단백질들은 복합체에서 벗어나 새로운 기능을 수행하기 때문에, 아미노산-운반RNA 연결효소 복합체는 이들을 위한 저장고 (reservoir)가 되기도 한다. 본 논문의 첫 번째 부분에서는 분할 루시퍼레이즈 상보 시스템 (split-luciferase complementation system)을 사용하여 포유동물 세포 내에서 아미노산-운반RNA 연결효소 복합체의 구성을 탐색하였다. 구성요소들 간의 복합적인 상호연결은 두 단백질 간의 상호작용 (binary protein-protein interaction; binary PPI)의 합으로 단순화시켰고, 그들 간의 쌍별 비교 (pairwise comparison; 구성 요소들의 서로 다른 모든 조합을 비교하는 방식)를 통하여 기존의 생체 외 연구 (*in vitro* studies)에 상응하는 복합체의 골조 (framework)를 유추해낼 수 있었다. 그리고 분할 루시퍼레이즈 리포터 (split-luciferase reporter)

간의 결합이 가역적이라는 점을 이용하여 인터페론감마 (interferon gamma; IFNγ)에 의한 글루타민-프롤린-운반RNA 연결효소 (glutamyl-prolyl-tRNA synthetase 1; EPRS1)의 방출이나, 운반RNA를 매개로 한 리보솜과 아미노산-운반RNA 연결효소 복합체의 협업과 같은 여러 자극들에 의한 복합체 내의 역동적인 구조 변화를 관찰하였다. 본 연구는 이와 같이 세포를 기반으로 한 분석법을 바탕으로 생리적 환경 (physiological condition)에서 포유동물 아미노산-운반RNA 연결효소 복합체의 골조가 유동적으로 변화하고 있음을 밝혀낼 수 있었다.

한편, 정상적이지 못한 아미노산-운반RNA 연결반응의 존재는 여러 종류의 암에서 잘 알려져 있다. 아미노산-운반RNA 연결효소는 암세포에서 과량으로 존재하며, 암이 진행되면서 늘어난 단백질 합성 요구량을 충족시킨다. 이는 대부분의 다른 단백질 합성 요소들이 암세포에서 과량으로 존재하지 않는다는 사실과 대비된다. 또한 아미노산-운반RNA 연결효소의 활성을 지속적으로 유지시키는 돌연변이는 지금까지 알려져 있지 않다. 이는 효소활성이 비정상적으로 높아진 아미노산-운반RNA 연결효소는 아미노산-운반RNA 연결효소 복합체의 형성과 유지를 저해하기 때문일 것이다. 따라서 아미노산-운반RNA 연결반응을 저해하는 치료법은 환자 개개인의 유전체 다양성 (genotype variation)에 상관없이 효과

를 낼 수 있고, 약물 저항성도 나타나지 않을 것이라 기대된다. 본 논문의 두 번째 부분에서는 고속 대량 스크리닝 플랫폼 (high-throughput screening platform)을 구축하여 포유동물 아미노산-운반RNA 연결효소의 저해제를 찾고자 하였다. 이 시스템에서 사용된 토끼의 망상적혈구 용해물 (rabbit-reticulocyte lysate) 내의 아미노산-운반RNA 연결효소들은 단독 또는 결합 구조가 인간의 효소나 그 복합체와 매우 가깝게 닮아있기 때문에 찾아낸 화합물이 인간에게 바로 적용될 수 있는 가능성을 높여준다. 이 시스템은 본 연구에서 수행된 선행 스크리닝 (pilot screening)에서 에메틴 (emetine)과 같이 잘 알려진 단백질 합성 저해제를 찾아내었을 뿐만 아니라, 훌륭한 품질관리 매개변수 (quality control parameters; QC parameters)와 결과의 반복성을 보여주었다. 따라서 이 시스템은 추후 대량 화합물 라이브러리를 타겟으로 한 고속 대량 스크리닝에 활용이 용이할 것으로 기대된다.

주요어: 아미노산-운반RNA 연결효소; 아미노산-운반RNA 연결효소 복합체; 거대분자량 복합체; 리보솜; 운반RNA; 고속 대량 스크리닝; 아미노산-운반RNA 연결반응; 단백질 합성 저해제

학번: 2013-30500